Abstract

Studies on the Performance Characteristics and System Optimization of Cascade Heat Pump

Dong Ho Kim
Department of Mechanical and Aerospace Engineering
The Graduate School
Seoul National University

In this study, the studies of cascade heat pump performance characteristics and optimization for heating and hot water supply in extremely cold region were conducted. In general, conventional heat pump water heater system shows a limited performance at low ambient temperature whereas the heating demand increases. In order to increase the water discharge temperature, multi-stage cycle was suggested and among the multi-stage cycle, cascade cycle shows the best performance at high condensing temperature condition.

In order to increase the cascade performance at low ambient temperature, R410A refrigerant which is suitable for low temperature application was

adopted in bottoming cycle. The R134a refrigerant which has a higher critical temperature was adopted in topping cycle to increase the water discharge temperature.

In order to increase the cascade system efficiency, several attempts were conducted. The determination of optimal refrigerant charge amount was studied by numerical simulation and experiment. The optimized coefficient of performance was obtained at the optimal charge amount condition and its corresponding degree of subcool at each cycle was suggested.

The intermediate temperature which determines the pressure ratio of each cycle was also optimized by numerical anaysis based on the reverse-Carnot model. The verification of optimized numerical intermediate temperature was conducted by experiment and numerical intermediate temperature well predicted the experimental optimal intermediate temperature.

The performance characteristics of cascade heat pump with water temperature lift at condenser were conducted by experiment. Despite of several advantages of heat pump than conventional boiler, slower thermal response is the weakness of heat pump water heater system. In order to increase the water discharge temperature, mass flow rate of water should be reduced. In case of decreasing water mass flow rate, the performance characteristics of cascade heat pump were obtained.

The fast response of heat pump system is the key issue for hot water supply. The optimal control logic which is suitable for cascade heat pump was designed and the verification of control logic was conducted. The optimized PI controller based on the genetic algorithm showed enhanced performance than conventional PI tuning method.

Keywords: Cascade, Heat pump, Intermediate temperature, Charge amount, PI control

***Identification Number*: 2010-31311**

Contents

List of Figures

List of Tables

Nomenclature

AWHP	air to water heat pump
COP	coefficient of performance
C	specific heat [$kJkg^{-1}K^{-1}$]
DSC	degree of subcool [K]
DSH	degree of superheat [K]
EEV	electric expansion valve
h	enthalpy [$kJkg^{-1}$]
k	control gain
$\dot{m}$	mass flow rate [kgs^{-1}]
T	temperature [K]
TXV	thermal expansion valve
u	control input
W	work [kW]
WDT	water temperature difference [K]
Q	transferred heat [kW]
x	state variable

Greek symbols

δ	temperature difference [K]
η	Carnot efficiency

Subscript

134	R134a
410	R410A
APP	approach
c	compressor
C	condenser
DIS	discharge
E	evaporator
H	heating
HS	high stage cycle
in	in
INV	inverter
INT	intermediate
LS	low stage cycle
out	out
r	refrigerant
sat	saturation
SH	superheat
w	water

Chapter 1. Introduction

1.1 Background of the study

Since the refrigeration and air-conditioning systems makes human life more comfortable and convenient, the demands for this system have increased considerably in the past couple of decades. Many attempts have been conducted to improve the heat pump system performance. In the early of stage of research, studies focused on the enhanced performance to deal with required capacity. As the usage of the heat pump system increased, the focus of researches moved to make the system work more efficiently. Furthermore, as the operating range of heat pump system has widened to meet various working conditions, it is required for the system to provide sufficient performance and satisfy the needs quite quickly for various conditions.

Air to air single stage heat pumps are widely used around the world due to their low cost and easy installation. The performance of air to air heat pump is strongly affected by the ambient temperature, since ambient temperature determines the pressure ratio of heat pump. The heating and cooling performance deteriorates as the ambient temperature decreases and increases, respectively. These heat pump characteristics induce the lack of heating and

cooling demand. For example, in the heating mode, the heating demand increases as ambient temperature decreases, whereas in the cooling mode, the cooling demand increases as ambient temperature increases. Unfortunately, climate crisis of these days require higher heating and cooling capacities since the average temperature of winter and summer gets colder and hotter.

The imbalance between heat pump performance and desired capacity can be resolved to some extent by the adoption inverter heat pump system. The variable speed compressor controls the balance between heat pump capacity and desired capacity; for example, compressor speed increases and decreases at the condition of insufficient capacity and sufficient capacity, respectively.

However, the capacity of heat pump itself is not that important in some cases. The temperature level should be considered. Originally, heat pump had been suggested to transfer heat from a heat source to a heat sink against a temperature gradient. Conventional single stage heat pump has a limitation of large temperature gradient.

Cascade system is a solution to overcome the large temperature differences between heat sink and heat source. Cascade has been widely used for various applications especially as a low-temperature refrigerating system. Low-temperature refrigeration systems are typically required in the temperature range from -30^{o}C to -100^{o}C for application in food,

pharmaceutical, chemical, and other industries, e.g., blast freezing, cold storage, liquefaction of gases such as natural gas, etc (Bansal and Jain (2007). At such low temperature, single stage compression systems are not feasible due to high pressure ratios. A high pressure ratio implies high refrigerant discharge and oil temperature and low volumetric efficiencies and, hence, low coefficient of performance value is obtained. Cascade refrigeration systems can be used to achieve low temperature, where series of single stage units are used that is thermally coupled through heat exchanger.

Recently in the EU countries, air to water heat pump (AWHP) is rapidly replacing conventional gas-fired boilers thanks to various subsidies for heat pumps in addition to their inherent energy saving and low CO_2 emission. However, there are some issues for air to water heat pump for a perfect replacement of boilers. The most important issue is the hot water discharge temperature (Park *et al*. (2010)). Gas-fired boiler heats the water above 80^{o}C whereas water discharge temperature of conventional single stage AWHP is around 50^{o}C. In order to reduce this temperature gap, there are currently possible alternatives including use of electric resistance sub heater or adoption of multi-stage cycle.

The multi-stage heat pump adopts multi compressors to make multi-stage cycle. Multi-stage vapor compression systems can be divided by three major

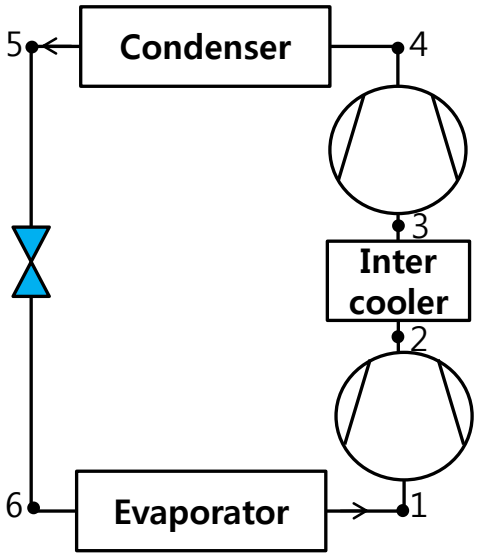

(a) Dual compression vapor compression cycle

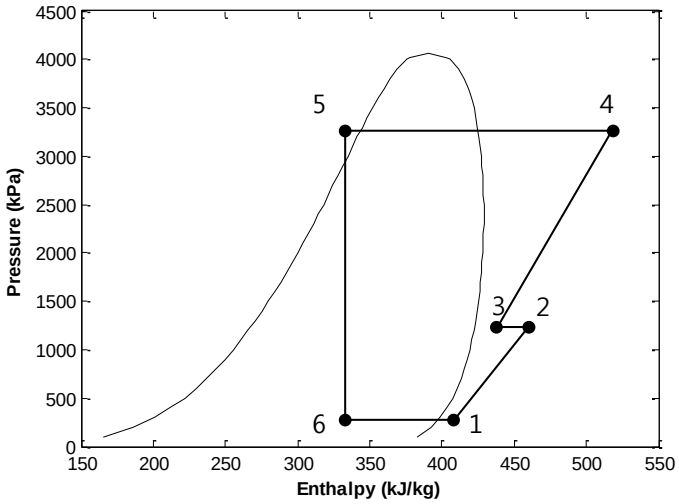

(b) P-h diagram of two dual compression cycle

Fig. 1.1 Schematics and P-h diagrams of multi stage cycles (continued)

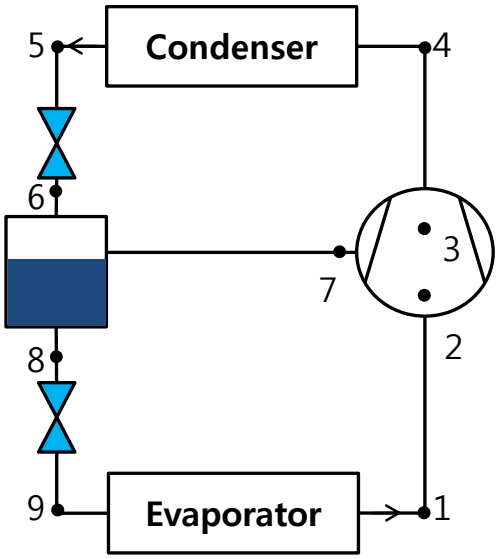

(c) Flash tank vapor injection cycle

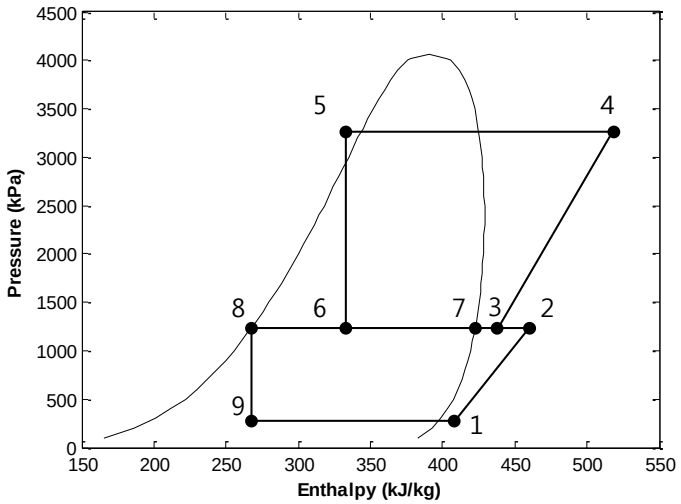

(d) P-h diagram of FTVI cycle

Fig. 1.1 Schematics and P-h diagrams of multi stage cycles (continued)

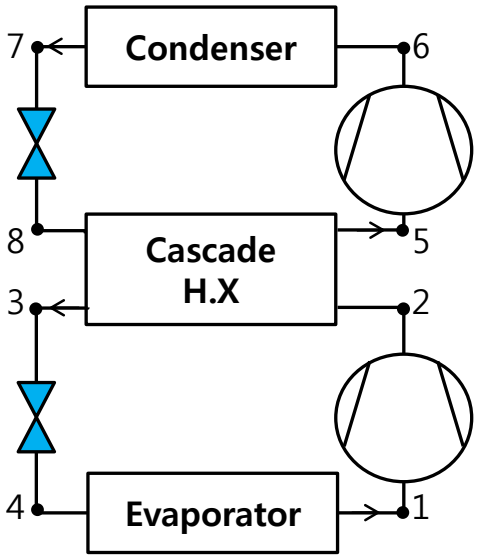

(e) Cascade cycle

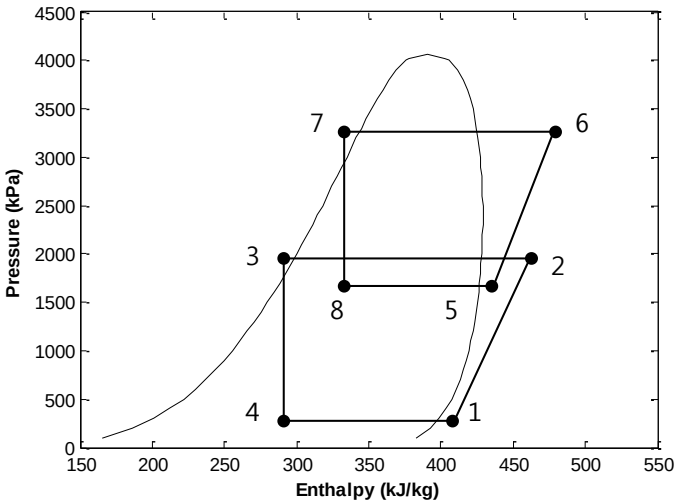

(f) P-h diagram of cascade cycle

Fig. 1.1 Schematics and P-h diagrams of multi stage cycles

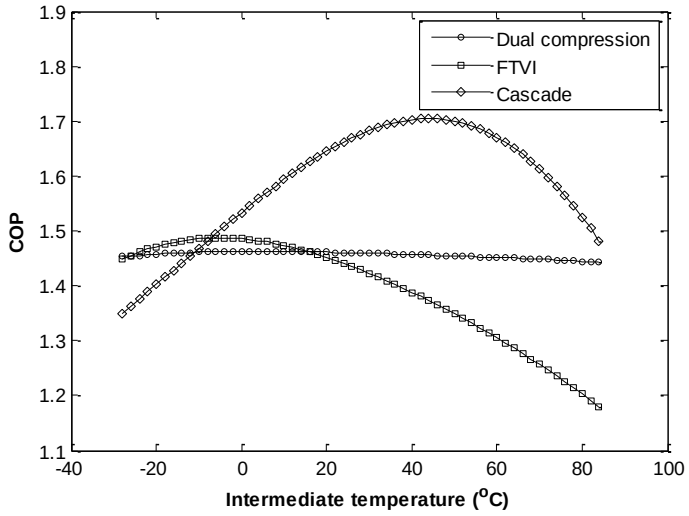

(a) Condensing temperature = 90°C, evaporating temperature = -30°C

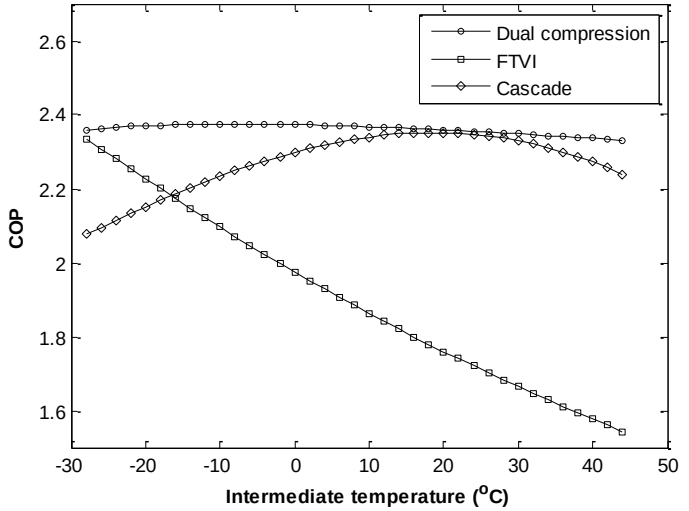

(b) Condensing temperature = 50°C, evaporating temperature = -30°C

Fig. 1.2 Performance of multi-stage cycles with respect to intermediate temperature

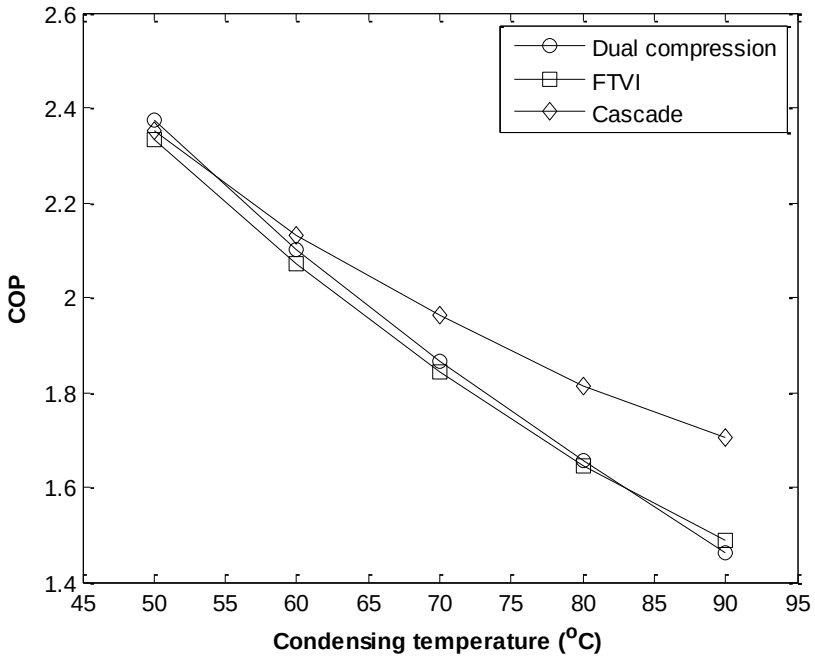

Fig. 1.3 Comparison of optimized performance with respect to condensing temperature (Evaporating temperature = -30°C)

categories; dual compression cycle, flash tank vapor injection (FTVI) cycle and cascade cycle as shown in Fig. 1.1. Each cycle adopts two compressors to lower the pressure ratio in order to enhance the compression performance. Compared to single-stage system, multi-stage has a smaller compression ratio and higher compression efficiency for each stage of compression, greater refrigeration effect, lower discharge temperature and greater flexibility (Chua *et al*. (2010)).

Fig. 1.2 shows the numerical performance comparison of two compression cycles and cascade cycle at a given condensing and evaporating temperatures with respect to intermediate temperature. For the application at extremely cold region, the evaporating temperature was assumed as -30^{o}C. The degree of subcool and superheat were assumed as 5^{o}C. Each cycle can be optimized by controlling the intermediate temperature which is the saturation temperature of state No. 2-3 (Figs. 1.1(a), (c) and (e)). The cascade cycle showed enhanced performance than two compression cycles at 90^{o}C condensing temperature condition. However, at the 50^{o}C temperature, two compression cycles showed better performance than cascade cycle. Fig. 1.3 shows the optimized coefficient of performance with respect to condensing temperature at given evaporating temperature. This demonstrates that the cascade cycle is appropriate cycle for the high water discharge at low ambient

temperature.

In this study, the cascade AWHP (R410A-R134a), which is constituted of two single cycles, was studied. There have been studies about single stage AWHP with R410A for space heating and domestic hot water applications (Park *et al*. (2010)). In order to overcome weakness of single stage AWHP, additional single stage cycle with R134a was required. The high-stage cycle with R134a as a refrigerant was used to make hot water and the low-stage cycle with R410A as a refrigerant was used to absorb heat from ambient air. The two single cycles are connected by a cascade heat exchanger, where the R134a evaporates and the R410A condenses.

Each circuit adopts a different refrigerant suitable for each temperature level. The lower temperature unit uses a refrigerant with a lower boiling point temperature, which has a higher saturation pressure at a low temperature (Bansal and Jain (2007)). High pressure at a low temperature results in a higher density of the suction line, which requires a smaller compressor. Moreover, because the critical point of R410A (344.5 K) is lower than that of R134a (374.2 K), the low-stage cycle adopts R410A.

1.2 Literature survey

Since the Montreal protocol (1987) and Kyoto protocol (1997) were established, issues regarding the reduction of refrigerant charge have drawn a great attention. Proper refrigerant charge in a heat pump system is an important subject, since the charge amount is related to the system performance. Insufficient refrigerant charge results in deteriorated performance in a heat pump system, and excessive charge also has negative effects on the performance. The optimal charge amount in a single cycle heat pump has become an important aspect of heat pump performance optimization and environmental issues. The meaning of optimal refrigerant charge itself is ambiguous, but most studies have focused its effect on the coefficient of performance (COP).

Many studies have investigated the single cycle charge optimization mostly by experiment. Cho *et al*. (2005) studied the effect of charge amount on CO_2 heat pump performance, and concluded that the CO_2 system in undercharge conditions was the most sensitive compared to other refrigerants (R22, R407C, and R410A). Kim *et al.* (2007) studied the effect of charge amount on the cycle of CO_2 and CO_2/propane mixtures. It was shown that the CO_2 refrigeration system could operate without a significant impact on its COP over a relatively wider range near the optimum charge level than the

CO_2/propane mixture system. Corberán *et al*. (2008) performed an experimental study on charge optimization with a reversible water-to-water heat pump using propane as a refrigerant. They concluded that the optimal refrigerant for heating and cooling with different flow arrangements was the same, while the optimum subcooling is 10 K for a counter-current and 5 K for a parallel flow arrangement. Corberán *et al*. (2011) studied the propane heat pump optimal subcooling temperature with respect to heat sink temperature and heat source temperature. The optimum subcooling temperature was around 5~7 K regardless of the heat sink and heat source temperatures. This optimized subcooling corresponds to the subcooling that the condenser can achieve without a significant increase in the condensing temperature. Pottker and Hrnjak (2012) experimentally proposed the optimum subcooling of R1234yf and R134a for typical AC systems. The COP was increased up to 19% for R1234yf, and to 9% for the R134a cycle.

There have also been many numerical studies of charge optimization and the distribution of refrigerant in each system component. Vjacheslav *et al*. (2001) proposed a rationally based algorithm with a physical model to evaluate the optimal mass charge. In the early stages of the charge process, a sharp rise in the COP was observed. After the optimal amount was charged, the COP showed a slight drop with further increases in the charge. Corberán *et*

al. (2008) studied the optimal subcooling by simulation and the simulation well predicted the experimental data. The optimal refrigerant mass distribution was achieved with 50% of the refrigerant in the condenser, 28.5% in the compressor, and 13.4% in the evaporator. Farzad and O'Neal (1994) simulated the charge amount with eight void fraction models to evaluate and compare the effects of void fraction models. Among the correlations, the Hughmark correlation showed the best prediction regarding heating capacity, power consumption, and COP. The Zivi (1964) correlation also showed quite a good prediction regarding superheating and subcooling. Guidelines for optimizing the charge amount in the cascade cycle are not available in the open literature to the best of the author's knowledge. Yet, to date, there has been little research conducted on the optimization of the charge amount in a cascade heat pump system.

Single-stage heat pumps are widely used around the world due to their low cost and easy installation. Nevertheless, most single-stage heat pumps have a limitation on performance; therefore, other designs are required for heat pumps to overcome the performance disadvantages, including a deteriorated heating capacity and low COP at very low ambient temperatures. Bertsch and Groll (2008) stated four main problems for single-stage air-source heat pumps. A cascade or multi-stage heat pump system was developed to

overcome the weaknesses of a single-stage heat pump. The cascade cycle has a smaller compression ratio at each cycle and exhibits a better compression efficiency compared to a single-stage cycle.

Many studies have investigated the two-stage cycle with a single refrigerant. Cho *et al*. (2009) described the operating characteristics of a two-stage CO_2 cycle with gas injection, which exhibited an enhanced COP compared to a non-injection two-stage cycle. Wang *et al*. (2005) showed that the operating characteristics of the double-stage heat pump are greatly improved over those of a single-stage heat pump. Agrawal *et al*. (2007) thermodynamically obtained the optimum inter-pressure for a two-stage CO_2 heat pump cycle. Chua *et al*. (2010) classified various types of multi-stage systems in a review article.

Lee *et al*. (2006), Alberto Dopazo *et al*. (2009), and Bingming *et al*. (2009) studied the cascade refrigeration system with NH_3 and CO_2 as working fluids in the high and low stages, respectively. Lee *et al*. (2006) determined the optimal condensing temperature of a cascade system and identified correlations with several temperature parameters. Alberto Dopazo *et al.* (2009) showed the COP and exergetic efficiency for various operating conditions and conducted an optimization study numerically. Bingming *et al*. (2009) analyzed the performance of the system experimentally and concluded that the

cascade system was very competitive in low-temperature applications. Cascade system studies have also been conducted using CO_2 and C_3H_8 as refrigerants for refrigeration. Bhattacharyya *et al*. (2008) mathematically modeled the system and developed guidelines for the user to select an intermediate temperature. Jeong and Smith (1994) showed the optimal temperature in a multi-stage cryogenic refrigeration cycle using thermodynamic approaches. The optimum temperature was obtained, which minimizes the sum of entropy generation at all stages. The optimum temperature should have the same temperature ratio at each stage of the cascade cycle, which means that the optimum temperature is the geometric mean of the condensing and evaporating temperatures.

The intermediate temperature is the most critical parameter for a multi-stage or a cascade heat pump system and affects the system efficiency because the intermediate pressure determines the compression ratio and compressor isentropic efficiency. Most studies focused on numerically determining an optimized intermediate temperature and suggested the correlations in terms of several temperature-related parameters. However, the suggested correlations cannot be adopted for other research studies and do not provide a general explanation.

Moreover, little information is available regarding experimental

optimization results because the cascade test setup is quite complex and difficult to control. Bingming *et al*. (2009) and Dopazo and Fernández-Seara (2011) provided an experimental optimum intermediate temperature in the NH_3/CO_2 cascade heat pump system. Nevertheless, these studies focused on determining a maximum COP for different heating capacities. Because the heating capacity can affect the COP directly, the optimized intermediate temperature should be obtained at a fixed heating capacity.

Issues regarding reduction of domestic energy consumption have drawn a great attention nowadays. There are generally four types of water heaters including gas, electric, solar driven and heat pump in the domestic water heater market. Water heater heat pump generally shows a high efficiency and low running cost compared to other types of water heaters. Air to water heat pump which is based on the reverse Rankine cycle absorbs heat from low temperature ambient air and transfers heat to high temperature water. Since AWHP gets energy from the environment, heat pump water heaters are called as renewable energy devices in the same way as solar water heaters (Zhang *et al*. (2007)). The most widely used AWHP which uses CO_2 as refrigerant operates above the critical point. The transcritical cycle provides a large continuous temperature glide which is favourable for heat transfer. CO_2 heat pump water heater was developed in Japan over the last decade under the

brand name Eco-cute and has been delivered about two million units.

Despite of several advantages compared to commercial gas water heater, slow thermal response of AWHP in cold weather requires the design of a large water storage tank in order to deal with the peak load (Huang *et al*. (2009)) or a control system that turns on the electric resistance backup heater (Ji *et al*. (2003)). The fast thermal response means the fast hot water temperature supply and is required at initial operation of heat pump. The urgent hot water supply can be achieved by two ways; increasing heating capacity and decreasing water mass flow rate. The former method can be accomplished by increasing the compressors speed; however, it takes a long time to reach certain water discharge temperature and the discharge temperature has a limitation. Normally, the latter method shows quite fast responses despite of low mass flow rate and low performance. Many studies have investigated the effect of water mass flow rate and water discharge temperature on heating performances. Wang *et al*. (2013) conducted CO_2 heat pump experimental research with various outlet water temperatures where inlet temperature was fixed. As water outlet temperature increases, the maximum COP decreases due to increase of discharge pressure and meanwhile the optimal discharge pressure increased. Pettersen *et al*. (1998) conducted the research to develop compact heat exchangers for CO_2 heat pump system and the temperature

approach of their heat exchanger is much lower in CO_2 gas cooler than other system condensers of equal size and capacity. Stene (2005) tested CO_2 heat pump in three different modes including space heating, hot water heating and simultaneous heating. The performance of hot water heating mode decreases as water inlet temperature increases and the COP was more sensitive to the variations in the inlet water temperature. Minetto (2011) optimized CO_2 high pressure that maximizes the COP by numerical method while the water mass flow rate was adjusted to maintain the set water temperature. Simulation results showed that high water discharge temperature leads low heating capacity and deteriorated COP and the optimal discharge pressure increases as water outlet temperature increases.

There have been many studies conducted on the effect of water flow rate or water discharge temperatures on single cycle AWHP systems, especially using CO_2 as a refrigerant. The AWHP systems based on R12 and R22 were the most common before the proposal of ozone layer protection (Zhang *et al*. (2007)). Yet, to date, there has been little research considering the effect of temperature lift on a cascade heat pump system and cascade heat pump control.

1.3 Objectives and scopes

There have been a lot of studies on the performance AWHP systems for the replacement of gas fired boiler. However, current AWHP systems have a limitation of performance compared to boiler. In order to increase the heating performance and water discharge temperature, multi-stage cycle has to be adopted. Among the multi-stage cycle system, cascade cycle showed a better performance at extremely low ambient temperature. However, due to its complexity of configuration, system irreversibility increases. Therefore, there is a chance to enhance the performance by system optimization

The objective of the present study is the optimization of cascade cycle in various ways; determination of refrigerant charge at high and low stages cycle, intermediate temperature and control logic.

In chapter two, numerical simulation and experiments are carried out for the verification of optimal refrigerant charge at cascade cycle. Since the cascade cycle is composed of separated two single stage cycle, the optimal charge amount should be obtained for each cycle. The numerical simulation which considering the charge amount was conducted and the experiment was also carried out.

In chapter three, the optimum intermediate temperature is presented by numerical model. The intermediate temperature is the key factor which

determines the pressure ratio of each cycle. Numerical optimal intermediate temperature based on the reverse-Carnot cycle was suggested and this was verified the experiments.

In chapter four, the cascade performance variation with respect to water temperature lift are carried out. Despite several advantages of AWHP compared to gas boiler, AWHP shows slow thermal response than boiler. By decreasing the water mass flow rate, high temperature of water can be obtained. This research presents the performance variation with regard to water temperature lift.

In chapter five, the optimal control of cascade heat pump is presented. Four control variables are controlled for the optimal operation of cascade heat pump. In order to optimize the controller, tuning of PI controller gain was carried out by genetic algorithm. This study presents how the optimal controller enhances the transient response.

In chapter six, conclusions are given along with the brief summarization of the results.

Chapter 2. Determination of the refrigerant charge on cascade system

2.1 Introduction

Since the Montreal protocol (1987) and Kyoto protocol (1997) were established, issues regarding the reduction of refrigerant charge have drawn a great attention. Proper refrigerant charge in a heat pump system is an important subject, since the charge amount is related to the system performance. Insufficient refrigerant charge results in deteriorated performance in a heat pump system, and excessive charge also has negative effects on the performance. Single-cycle heat pumps are widely used around the world due to their low cost and easy installation. The optimal charge amount in a single cycle heat pump has become an important aspect of heat pump performance optimization and environmental issues. The meaning of optimal refrigerant charge itself is ambiguous, but most studies have focused its effect on the coefficient of performance. There have been many studies conducted on the optimization of the charge amount or subcooling in single heat pump systems. However, most single-cycle heat pumps have limited performance in applications with very low ambient temperature. Bertsch and

Groll (2008) stated four main problems for single-stage air-source heat pumps. In order to overcome the weakness of the single-stage cycle, the cascade cycle has been suggested, which shows enhanced performance at low temperature, since the cascade cycle has a smaller compression ratio at each cycle, and it exhibits a better compression efficiency compared to a single cycle. Most of the studies conducted on cascade systems have focused on the performance and the optimum intermediate pressure (Lee *et al*. (2006), Bingming *et al*. (2009), Dopazo and Fernández-Seara (2011), Messineo and Panno (2012)).

Before optimizing the intermediate pressure, the optimal charge amount for each cycle has to be obtained. Guidelines for optimizing the charge amount in the cascade cycle are not available in the open literature to the best of the author's knowledge. Yet, to date, there has been little research conducted on the optimization of the charge amount in a cascade heat pump system. The main purpose of this research is to determine the optimum DSC (degree of subcooling) of an R410A single cycle and R134a/R410A cascade cycle, since the optimum charge amount cannot be generalized to other systems. Simulations for the single and cascade cycles were also conducted to support the basis of the experiments. Both the optimum DSC and the influences of the charge amount on the two cycles have been studied.

2.2 Single cycle charge optimization

2.2.1 System description and experimental apparatus for single cycle

The performance of a single-cycle heat pump for a hot water supply was studied numerically and experimentally. This cycle is called the AWHP (air-to-water heat pump) cycle, which absorbs heat from ambient air and heats water. The refrigerant R410A was adopted in this cycle. Figure 2.1(a) shows a schematic diagram of the test apparatus, which contains two enclosed loops for R410A and water. A scroll compressor (Copeland, ZP36KSE) was connected to an inverter in order to control the speed of the compressor. High-temperature refrigerant from the compressor flows through a plate heat exchanger (SWEP, B15H), and is expanded through an externally equalized TXV (thermal expansion valve). The expanded refrigerant enters a fin tube evaporator, which has a nominal capacity of about 6 kW. This evaporator is placed in an outdoor environmental chamber. The detailed specifications of each component are described in Table 2.1 (a). Information about the absolute pressure, differential pressure, temperature, and mass flow rate was transferred to a PC for data analysis. All of temperature sensors used in this study were T-type thermocouples, and the

saturation pressure was measured by pressure transducer (Sensotec, F. S. 1.0%). The mass flow rate of the refrigerant was measured by the Coriolis mass flow meter (Oval, F. S. 0.1%) and the mass flow rate of the water was measured by a magnetic mass flow meter (Budget meter, F. S. 0.1%). The differential pressure transmitter (Rosemount, F. S. 0.15%) was measured to examine the pressure drop through the heat exchanger. The total power including compressor and inverter was measured by the digital power meter (Yokogawa WT 1600, F. S. 0.1%)

2.2.2 Test conditions, data reduction and uncertainty of measurements

The operating conditions are listed in Table 2.2 (a). The refrigerant charge amount is one of the most important parameters, and was controlled to a range of 1.0~1.6 kg. The inverter-driven compressor speed was changed from 45 Hz to 60 Hz. The ambient temperature was set to -15, -7, and 7^{o}C, and controlled in an environmental chamber. The water temperature of 30^{o}C was quite low, because the compressor condensing temperature cannot exceed 40^{o}C when the ambient temperature is -15^{o}C.

Table 2.1 Specifications of each component for single and cascade systems

(a) Single cycle components

Refrigerant	Part	Specifications
R410A	Compressor	Scroll compressor (Copeland, ZP36KSE) Displacement : 6.0 m^3/h
	Condenser (Indoor unit)	Plate heat exchanger (Swep, B15H) Nominal capacity : 10.55 kW Plate number : 28
	Expansion valve	Danfoss, Externally equalizing TXV
	Evaporator	Tube/fin material: copper/aluminum Outer diameter of tube: 6.35 mm Rows and steps: 4 rows and 10 steps Fins per inch : 9
	Inverter	LS, SV055iG5A-4

(b) Cascade cycle components

Refrigerant	Part	Specifications
R134a	Compressor	Scroll compressor (Copeland, ZB21KSE) Displacement : 8.6 m^3/h
	Condenser (Indoor unit)	Plate heat exchanger (Swep, B25H) Nominal capacity : 17.58 kW Plate number : 26
	Expansion valve	Danfoss, Externally equalizing TXV
	Evaporator	Plate heat exchanger (Swep, B15H) Nominal capacity : 10.55 kW Plate number : 28
	Inverter	LS, SV055iG5A-4

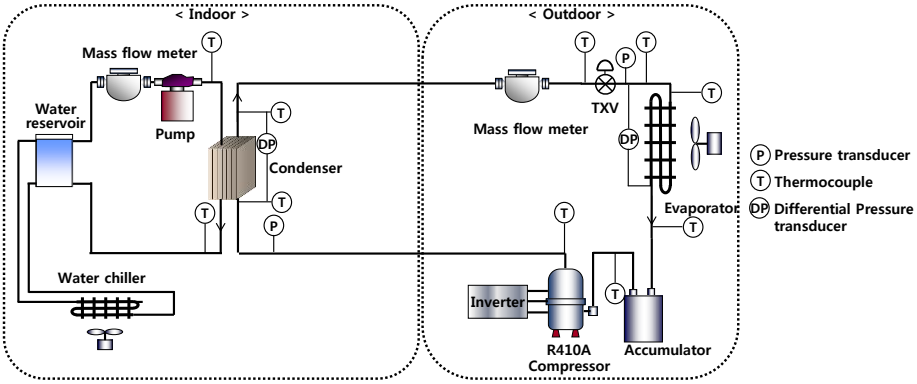

(a) Single cycle

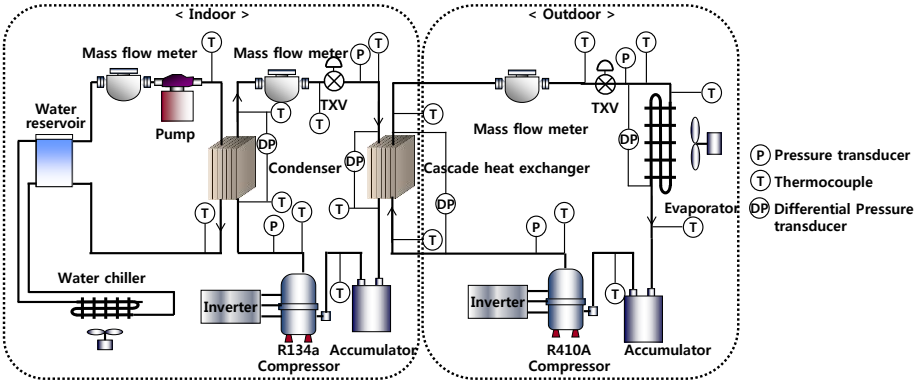

(b) Cascade cycle

Fig. 2.1 Schematic diagrams of single and cascade cycle test setup

Table 2.2 Test conditions for optimal charge amount

(a) Single cycle test conditions

Parameters	Value
Ambient temperature (^{o}C)	-15, -7, 7
Condenser water inlet temperature (^{o}C)	30
Degree of superheat (^{o}C)	10
Compressor speed (Hz)	45, 50, 55, 60
Refrigerant charge amount (kg)	1.0 ~ 1.6

(b) Cascade cycle test conditions

Parameters	Value
Ambient temperature (^{o}C)	-15, 7
Condenser water inlet temperature (^{o}C)	50
Degree of superheat at each cycle (^{o}C)	10
R134a charge amount (kg)	0.6 ~ 0.9
R410A charge amount (kg)	0.9 ~ 1.4
Compressor speed (R134a/R410A, Hz)	55/45, 50/50, 45/55

However, tests with a water inlet temperature of 50°C can be conducted with an ambient temperature of 7°C. In order to analyze the effect of ambient temperature, the water inlet temperature was fixed at 30°C. The main objective of this research is to find out the optimum refrigerant charge, which is related to the DSC. In order to neglect the effect of the DSH (degree of superheat) on the heat pump performance, the DSH was controlled to around 10 K for all test conditions. The criterion for steady state was based on the research by Kim *et al*. (2008), and the thresholds of DSH and power consumption were set as 1 K and 10 W, respectively. The actual target of the heat pump system is the heating capacity, which is defined in equation (2.1) using the mass flow rate of the secondary fluid. The heating capacity can also be obtained using the refrigerant enthalpy difference, as shown in equation (2.2). The average deviation between equations (2.1) and (2.2) is 5.38%. In this research, equation (2.1) defined the heating capacity.

$$Q_H = \dot{m}_w C_w (T_{w,out} - T_{w,in}) \tag{2.1}$$

$$Q_H = \dot{m}_r (h_{C,in} - h_{C,out}) \tag{2.2}$$

$$COP = Q_H \Big/ (W_{HS} + W_{LS} + W_{\mathrm{Inv}}) \tag{2.3}$$

The COP of this system is represented as equation 2.3, which is the ratio of the heating capacity to the power consumption, including the

inverter power. The saturation temperature was calculated by the measured pressure data using the REFPROP database (Lemmon (2007)).

The uncertainty analysis was conducted based on the method proposed by Moffat (1988). The equation of measurement uncertainty is expressed in equation (2.4), where X_i and δX_i represent the measurement variables and their uncertainties, respectively. The maximum uncertainty of the heating capacity and COP were 6.424% and 6.427%, respectively.

$$\delta R = \left\{ \sum_{i=1}^{N} \left(\frac{\delta R}{\delta X_i} \delta X_i \right)^2 \right\}^{1/2} \tag{2.4}$$

2.2.3 Test results and discussion

The condensing and evaporating pressure of a heat pump are normally related to the temperature of the secondary fluid at a given charge amount and ambient temperature. The condensing temperature is a function of the water temperature, and the evaporating temperature is a function of the ambient temperature. However, the refrigerant charge amount also determines the condensing pressure. As the charge amount increases, so does the condensing pressure. This change is related to the refrigerant density. Since a high refrigerant charge amount requires a high density at a given volume, a subcooled refrigerant with a high density is required. This is

consistent with the increased condensing temperature resulting in high subcooling. Since the difference between the condensing temperature and the temperature of the secondary fluid is high with excessive charge, the heat transfer rate is increased. The high heat transfer rate results in a highly subcooled refrigerant at the condenser exit. Fig. 2.2 shows the variation in the P-h diagram of the system with respect to the charge amount. The most noticeable change is the increase of the condensing pressure. However, there is a negligible variation at the evaporating pressure, which is also related to the refrigerant charge amount. Increasing the condensing temperature is an easy way to achieve high refrigerant density. The obvious change with the charge amount is the increase of condensing pressure. The increase of condensing pressure affects not only secondary fluid temperature difference but refrigerant degree of subcooling. The charge amount has a great influence on the subcooling. Thus, DSC is an important parameter to determine charge amount. Fig. 2.3 shows the variation of the DSC with respect to the refrigerant charge amount. The degree of subcooling increases greatly as the refrigerant charge amount increases, and the liquid refrigerant is accumulated at the exit of the condenser. The compressor speed also determines the DSC, that is higher compressor speed brings the higher degree of subcool since higher compressor speed increased the condensing

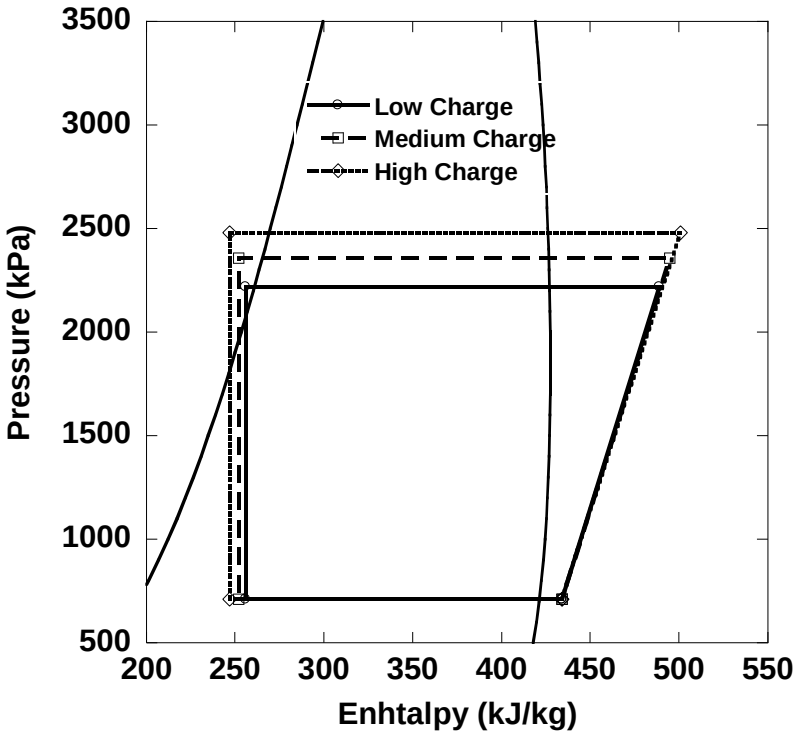

Fig. 2.2 P-h variation with respect to charge amount

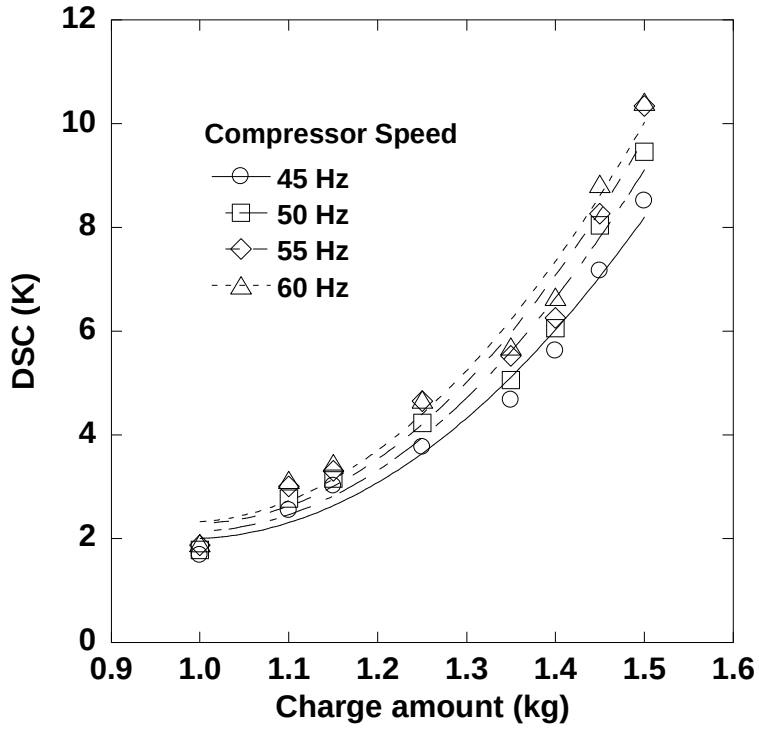

Fig. 2.3 Variation of subcooling with respect to charge amount (Ambient temperature = -7^{o}C)

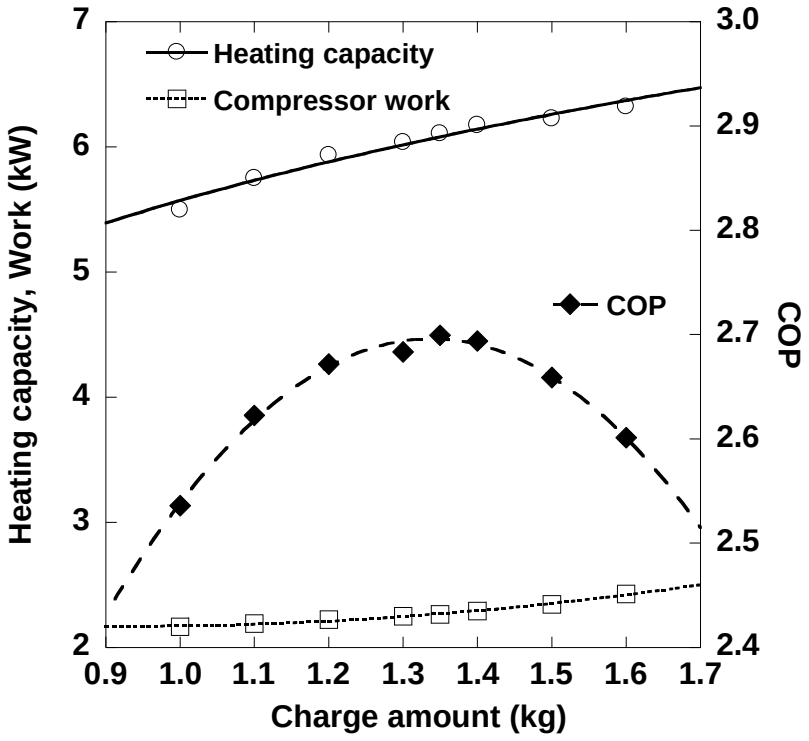

Fig. 2.4 Performance variation with respect to charge amount (Ambient temperature = 7^{o}C, Compressor speed = 45 Hz)

pressure more than that of lower compressor speed. Fig. 2.4 shows the variation in the heating capacity, compressor power, and COP with respect to the refrigerant charge amount. The heating capacity is a multiple of the mass flow rate and the enthalpy change and the enthalpy change is directly related with the heat transfer rate. The mass flow rate is slightly decrease as the pressure ratio increases. However, since the change of heat transfer rate with respect to charge amount is dominant, the heating capacity increases with the charge amount. Also, the power consumption increases due to the elevated pressure ratio. So, there should be an optimum charge amount for the COP, and finding this charge amount is the one of the goals of this research.

Fig. 2.5 shows the optimum DSC for each test condition. Since the heating capacity and compressor power increase with respect to the charge amount, there exists an inflection point in the COP that corresponds to the optimum condition. The curve of heating capacity and COP were interpolated. With a low compressor speed condition (45 Hz, Fig. 2.5 (a)), the heating capacity increased by about 14.9%, and COP increased by 6.4% compared to the minimum charge amount condition. These increases were less pronounced considering the compressor frequency change (60 Hz, Fig. 2.5 (d)), with values of 13.5% and 2.2% for the heating capacity and COP, respectively. However, the actual increase in heating capacity, not the

increment ratio, was higher at a high compressor speed than at a low compressor speed. With a compressor speed of 45 Hz, the actual increase was 1.35 kW, and 1.50 kW at a speed of 60 Hz. The same tendency at the test condition of ambient temperature of -7^{o}C and -15^{o}C was observed, where the heating capacity increment ratio was slightly decreased as the compressor speed increased, whereas the actual increment value was higher at the high speed condition than at the low speed condition. The heating capacity increment and increment ratio were great at the high ambient temperature condition. Fig. 2.5 also shows the optimal subcooling at 7^{o}C ambient condition and this optimal subcooling was in the range of 5~8 K. However, this optimal subcooling decreased slightly as the ambient temperature decreased, and the optimal subcooling at -15^{o}C was about 3~4 K.

Fig. 2.6 presents the optimized heating capacity and COP with respect to the ambient temperature, where the water inlet temperature was constant. The optimized heating capacity increases as the ambient temperature and the compressor speed increase and the optimized COP also increased as the ambient temperature increased. Normally, the maximum COP is observed at 50 Hz condition except for 7^{o}C ambient condition. Since the compressor in this research was fixed speed compressor (50 Hz), the COP is maximized at the speed of 50 Hz. However, the maximum COP was 45 Hz for the 7^{o}C

ambient condition. The error of COP at 45 Hz and 50 Hz was about 3% which is the range of the uncertainty of COP.

2.2.4 Simulation results for single cycle and discussion

A numerical simulation has been conducted to support the experimental data. The simulation was conducted using MATLAB code. All the heat exchangers in this simulation were modeled under the assumption of uniform mass distribution and the heat transfer area were divided by 500 elements in this 1D simulation. The property of R410A was calculated using REFPROP Matlab code. The specifications of the components are the same as those shown in Table 2.1(a). The compressor discharge temperature was simulated using the isentropic efficiency, and the mass flow rate was modeled using the volumetric efficiency. The plate heat exchanger was modeled using a finite volume method, and the TXV was simulated with the assumption of isenthalpic expansion. The fin tube heat exchanger was also simulated using the effectiveness-NTU method. The correlation of condensing heat transfer coefficient for the plate heat exchanger and the evaporating heat transfer coefficient for the fin tube heat exchanger are described in Table 2.3(a). On the air side, uniform air velocity and

temperature and fully dry conditions were assumed. A flow chart of the simulation is shown in Fig. 2.7 (a). In this simulation, the DSH at the inlet of the compressor was assumed to be 10 K. The evaporating pressure was iterated until the assumed DSH was met, after which the refrigerant chargeamount was calculated. The refrigerant charge amount with two phases was calculated using the Zivi (1979) correlation, which provides the void fraction of the two-phase state. In order to calculate the charge amount in the two-phase state, the saturated density and the volume that the two-phase refrigerants occupy are required. The single-phase charge amount was calculated using the density information and a given volume, and the condensing pressure was iterated until the charge amount restriction was met.

Fig. 2.8 shows a comparison of the simulation results and the experimental results with respect to charge amount. The simulation results quite well predicted the experimental data and the average error of heating capacity were 7.2% and 4.4% in Figs. 2.8 (a) and (b), respectively. Simulation predicted the higher heating capacity than actual value, since simulation assumed that enthalpy change of refrigerant was totally transferred to the water.

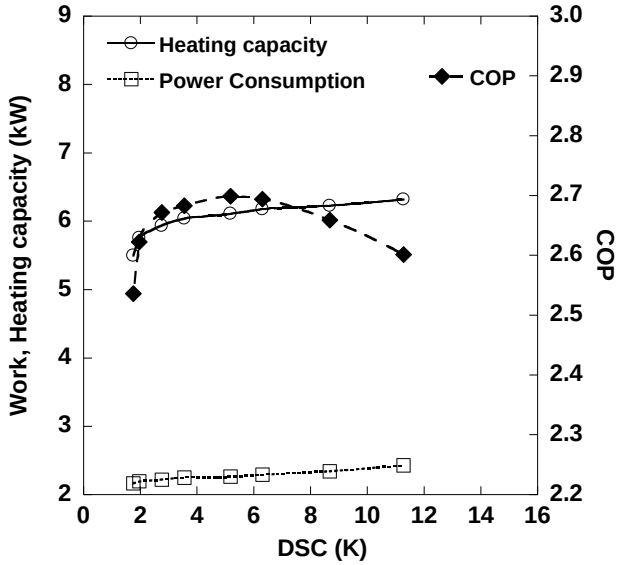

(a) 45 Hz

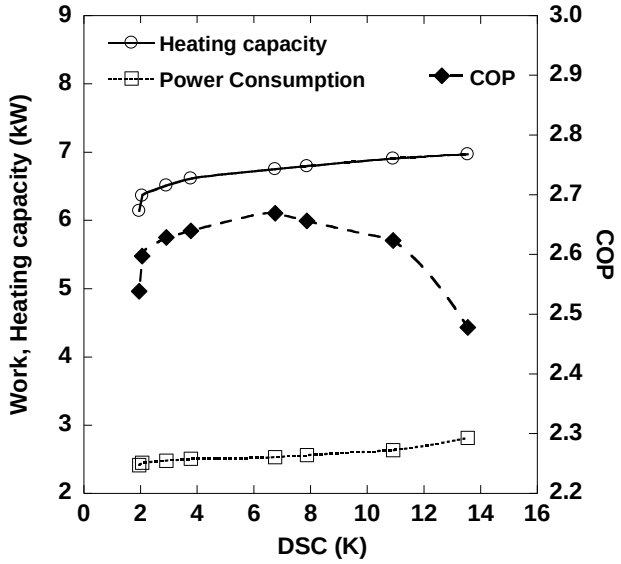

(b) 50 Hz

Fig. 2.5 Performance variation with respect to degree of subcooling (Ambient temperature = 7°C, continued)

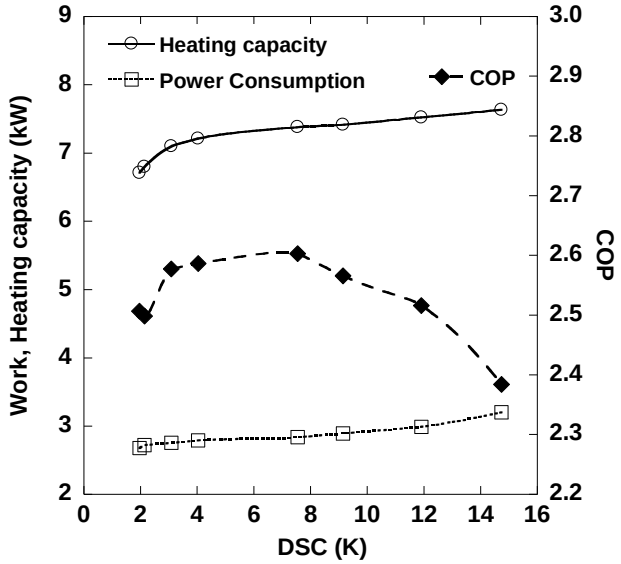

(c) 55 Hz

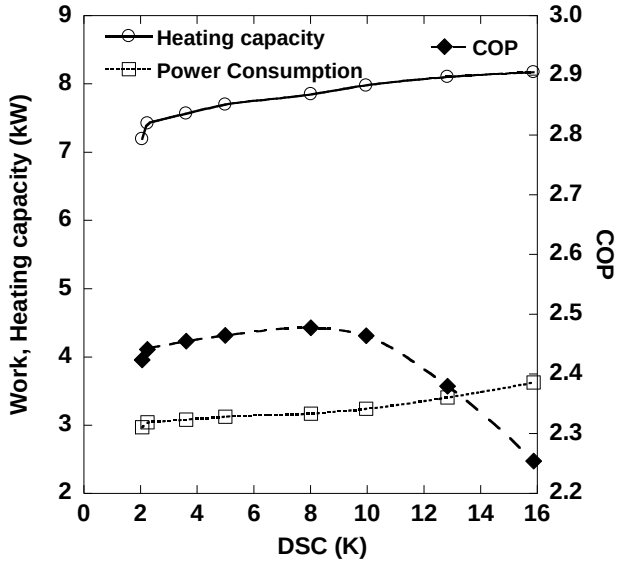

(d) 60 Hz

Fig. 2.5 Performance variation with respect to degree of subcooling (Ambient temperature = 7°C)

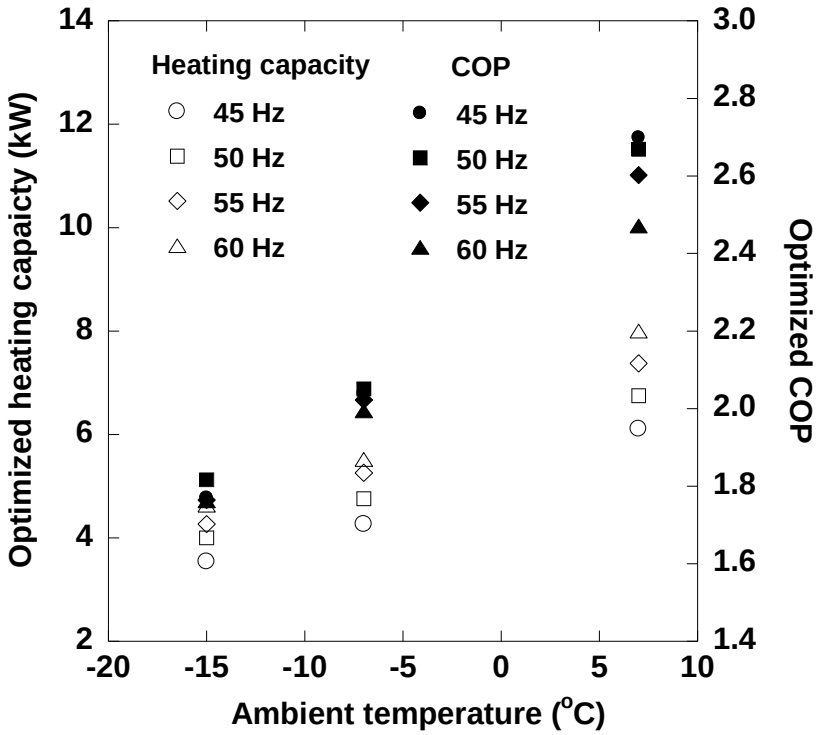

Fig. 2.6 Optimized heating capacity and COP of single cycle

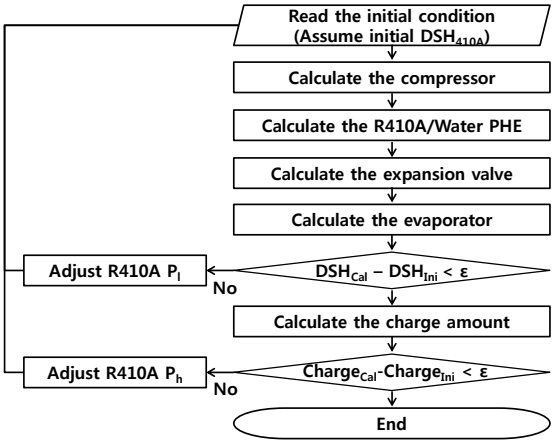

(a) Single cycle simulation

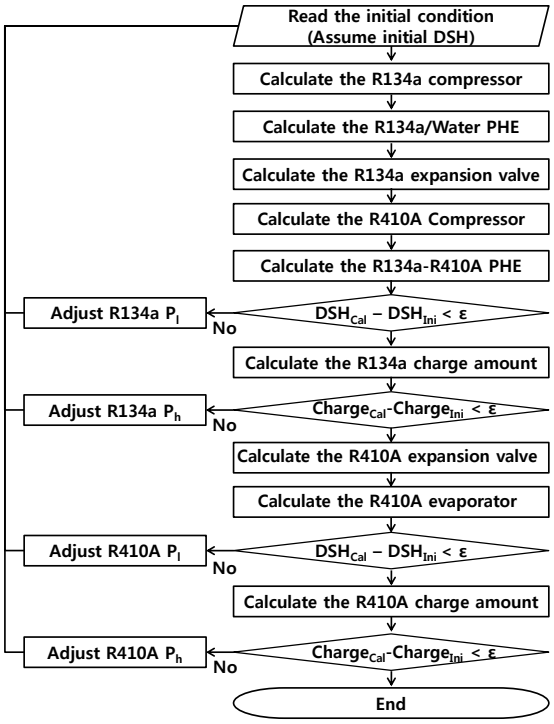

(b) Cascade cycle simulation

Fig. 2.7 Flow chart of single and cascade cycle simulation

Table 2.3 Simulation conditions and correlations for single and cascade cycles modeling

(a) Single cycle (R410A)

Part	Specifications
Compressor (Indoor unit)	Isentropic efficiency = 0.55 (Compressor discharge temperature) Volumetric efficiency (Mass flow rate of compressor)
Condenser (Indoor unit)	Finite volume method R410A condensing HTC in plate heat exchanger : Longo, G.A. (2009) Water HTC in plate heat exchanger : Longo, G.A. (2009)
TXV	Isenthalpic assumption
Evaporator (outdoor unit)	Finite volume method & Effectiveness-NTU method R410A evaporating HTC : Gungor, K.E. and Winterton R.H.S. (1986) Air HTC : Wang, C.C. and Chi, K.Y. (2000) Uniform inlet velocity and temperature assumption
Charge amount	Zivi correlation (1964)

(b) Cascade cycle (R134a)

Part	Specifications
Compressor (Indoor unit)	Isentropic efficiency = 0.55 (Compressor discharge temperature) Volumetric efficiency (Mass flow rate of compressor)
Condenser (Indoor unit)	Finite volume method R134a condensing HTC in plate heat exchanger : Yan, Y.Y. *et* al. (1999) Water HTC in plate heat exchanger : Longo, G.A. (2009)
TXV	Isenthalpic assumption
Evaporator (outdoor unit)	Finite volume method R134a evaporating HTC in plate heat exchanger : Yan, Y.Y. and Lin, T.F. (1999)
Charge amount	Zivi correlation (1964)

* The simulation method and the correlation for cascade low cycle (R410A) is the same as Table 2.3 (a)

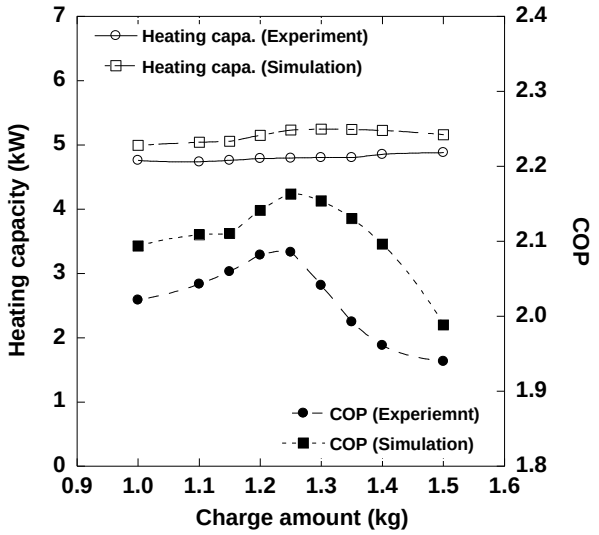

(a) Ambient temperature = -7°C

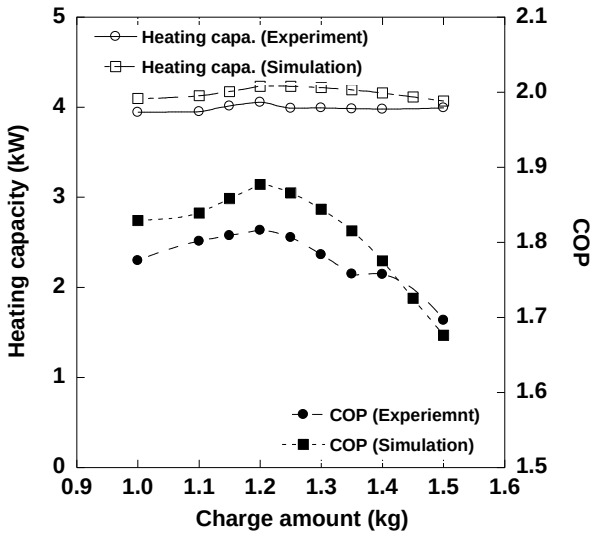

(b) Ambient temperature = -15°C

Fig. 2.8 System performance comparison of simulation and experiment results (Compressor speed = 50 Hz)

However, in actual operation, the energy of refrigerant is transferred to ambient air. This error is related to the difference of equation (2.1) and (2.2). Due to the error of heating capacity, the simulation also predicted the higher COP than experimental data and the error of COP were 4.2% and 2.3% in Figs. 2.8 (a) and (b). The simulation also showed the inflection point of COP since the compressor work increases as charge amount increases. The optimum charge amount of simulation and test results showed same value and the trend of optimum DSC with respect to ambient temperature will be discussed. Fig. 2.9 shows the variation of heating capacity and COP of simulation and experiment results. The heating capacity increases slightly with respect to charge amount at 7^{o}C ambient condition. However, this increment decreases as ambient temperature decreases. This analysis showed similar trend to experimental results, however, heating capacity decreases at overcharge condition of low ambient temperature. This is considered that low ambient temperature brings a low refrigerant mass flow rate, the overcharge condition at this low ambient condition deteriorates the mass flow rate because overcharge condition requires high pressure ratio. Due to the decrease of this mass flow rate, heating capacity decreases. However, the decrement is not that significant. In the numerical analysis, the heating capacity is based on the enthalpy difference of refrigerant.

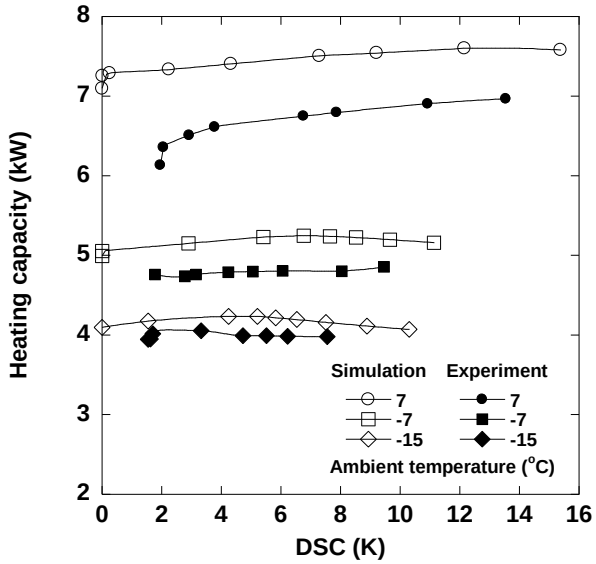

(a) Heating capacity variation

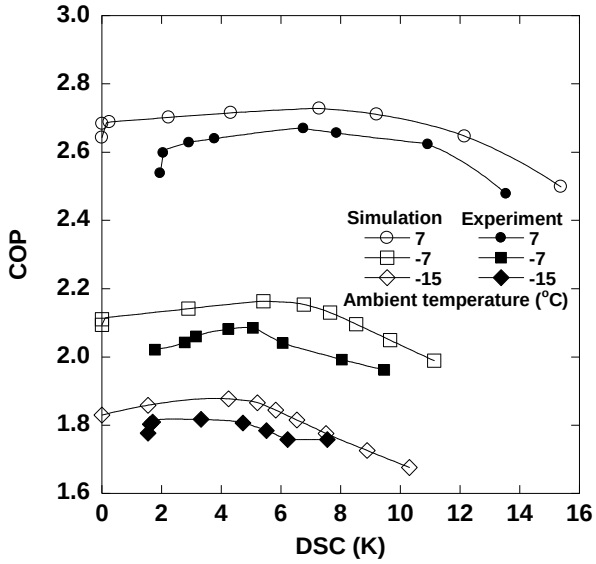

(b) COP variation

Fig. 2.9 Simulation results of heating capacity and COP with degree of subcooling (Compressor speed = 50 Hz)

Since the simulation didn't assumed the heat loses to ambient, the heating capacity of simulation is about 7% higher than experimental results. The maximum error of heating capacity was observed at the condition of low charge amount at 7°C ambient condition. Fig. 2.9 (b) shows the variation of COP and due to the error of heating capacity, simulation estimated higher value than experiment about 3.3%. COP increases to some extent with the increase of degree of subcooling and decreases after optimal DSC. The simulation of the optimal DSC at 7°C ambient temperature was also about 7~8 K and this is consistent with the experimental data shown at Fig. 2.5 (b). The optimal DSC decreases as ambient temperature decreases, and the optimum DSC at -7°C and -15°C was about 5~6 K and 4~5 K, respectively. As ambient temperature increases, the increment of condensing temperature with charge amount increases. The condensing temperature increments with charge amount were about 5 K and 3 K at the ambient temperature of 7°C and -15°C, respectively. Also, as charge amount increases, the enthalpy of condenser outlet decreases. Then, the DSH at compressor inlet decreases and TXV decreases the opening to maintain the target DSH. As a results, the mass flow rate decreases. The decrements of mass flow rate with charge amount were about 4.8% and 7.2% at the ambient 7°C and -15°C condition. As a result, the increasing rate of heating capacity with charge amount

increases at high ambient temperature condition. This is consistent that the optimal DSC decreases as ambient temperature decreases since the increasing rate of heating capacity with charge amount decreases as ambient temperature decreases.

2.3 Cascade cycle charge optimization

2.3.1 System description and experimental apparatus for cascade cycle

The performance of the cascade cycle, which comprises two single cycles, was studied numerically and experimentally. In order to overcome the limitations of the single-cycle performance at low temperature, the cascade cycle was suggested, and showed better performance than the single cycle. Since the cascade cycle has a smaller compression ratio at each compressor, it exhibits good efficiency, even at very low temperature. Fig. 2.1 (b) shows a schematic diagram of the cascade test apparatus, which contains three enclosed loops for R410A, R134a, and water. The R410A cycle absorbs the heat from the ambient air, and transfers it to the R134a cycle. The component specifications of the R410A cycle, including a scroll compressor, plate heat exchanger, TXV, and fin-tube evaporator, are the

same as those shown in Table 2.1 (a). The additional R134a cycle requires a scroll compressor (Copeland, ZB21KCE) with an inverter, a refrigerant-water plate heat exchanger, (SWEP, B25H), and a TXV. The detailed specifications of the components for R134a are shown in Table 2.1 (b). The information of absolute pressure, differential pressure, temperature, and mass flow rate were used for data analysis and the specifications of sensors are the same as described in section 2.2.1.

2.3.2 Test conditions, data reduction and uncertainty of measurements

The operating test conditions are listed in Table 2.2 (b). The refrigerant charge amount for each cycle is one of the most important parameters. The ambient temperature was set to -15 and 7^{o}C, and the water inlet temperature was 50^{o}C. The compressor condensing temperature can exceed 60^{o}C when the evaporating temperature is above -5^{o}C. This demonstrates the strength of the cascade cycle; that is even at an ambient temperature of about -15^{o}C, cascade cycle can heat water to about 60~70^{o}C, whereas the single cycle is limited to 40^{o}C at an ambient temperature of -15^{o}C. The speed of the inverter-driven compressor for each cycle was varied from 45 Hz to 55 Hz. The difference of the compressor speed for each cycle is related to the

intermediate pressure, which can also be the subject of cascade cycle research. The main objective of this research is to find out the optimum refrigerant charge for each cycle, which is related to the DSC for each cycle. Since there has been little research conducted on the effect of the refrigerant charge on a cascade system, the effect of each cycle charge amount on the heat pump performance is also the subject of this research. In order to neglect the effect of DSH on the heat pump performance, the DSH was controlled to around 10 K for each cycle. The heating capacity of the cascade cycle is defined by equation (1). The heating capacity can also be obtained using the refrigerant enthalpy difference, as shown in equation (2). The average deviation between equations (1) and (2) was 5.81%. The uncertainty analysis was conducted based on the method proposed by Moffat (1988). The maximum uncertainty of the heating capacity and COP were 3.527% and 3.529%, respectively.

2.3.3 Test results and discussion

At a given test condition, the condensing pressure of the high stage (R134a cycle) and the evaporating pressure of the low stage (R410A cycle) are related to the water inlet temperature and the ambient temperature, respectively. In the investigation of the single-cycle charge amount, the

refrigerant charge amount affects the condensing pressure. However, the effect of the charge amount in each cycle on the cascade cycle performance is hard to forecast, since the low stage cycle affects the high stage cycle.

Fig. 2.10 shows the variation of P-h variation of the cascade heat pump with regard to charge amount at each cycle. Fig. 2.10 (a) shows the variation of the cycle with the increase of R134a charge amount at given R410A charge amount. There is an obvious increase at R134a condensing pressure while the variations of other pressures are negligible. Fig. 2.10 (b) shows the P-h diagram with respect to R410A charge amount where R134a charge amount was fixed. The noticeable change was observed at R410A condensing pressure and R134a evaporating pressure. Since the R134a evaporator is connected with R410A condenser at refrigerant-refrigerant heat exchanger, evaporating temperature of R134a affected by R410A condensing temperature. As R410A condensing pressure increases, heat transfer at cascade heat exchanger increases since the refrigerant-refrigerant temperature difference is increased. That is, R134a evaporates well and have a high DSH. Then R134a TXV increases the opening to reduce the DSH. As a results, R134a evaporating pressure increases. Fig. 2.11 (a) shows the change of the R134a pressure ratio at ambient temperature of 7^{o}C with respect to the charge amount in each cycle. As the high stage charge amount

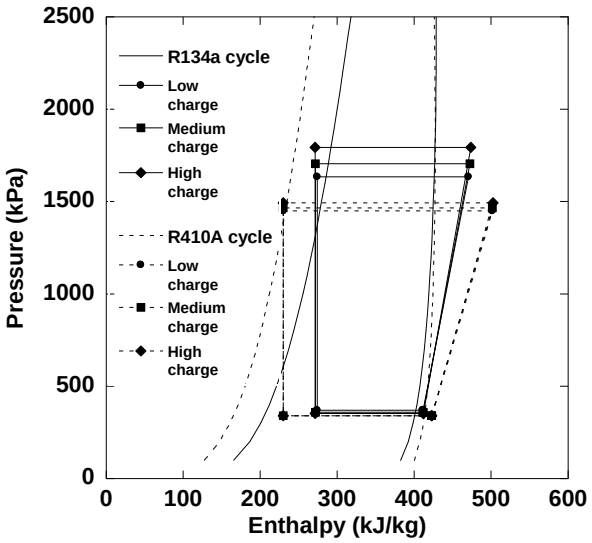

(a) R134a charge effect on cascade cycle P-h diagram

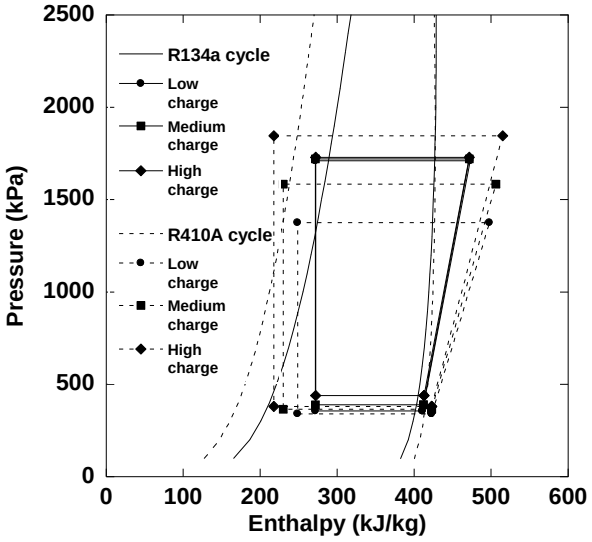

(b) R410A charge effect on cascade cycle P-h diagram

Fig. 2.10 Variation of P-h diagram with respect to charge amount at each cycle (Ambient= -15^{o}C, Water inlet =50^{o}C)

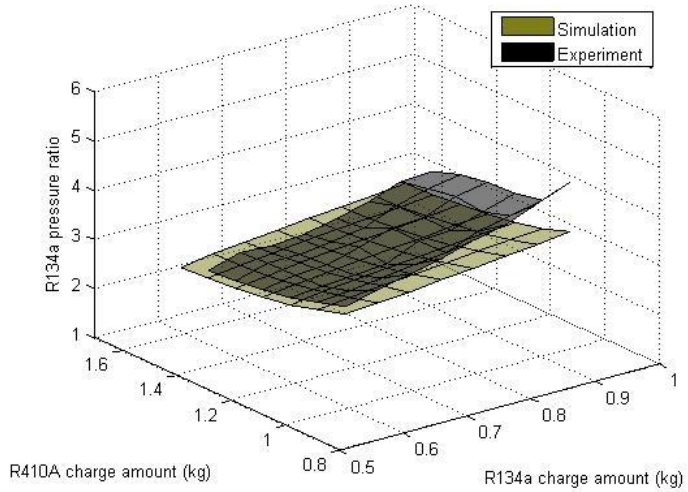

(a) Pressure ratio of R134a

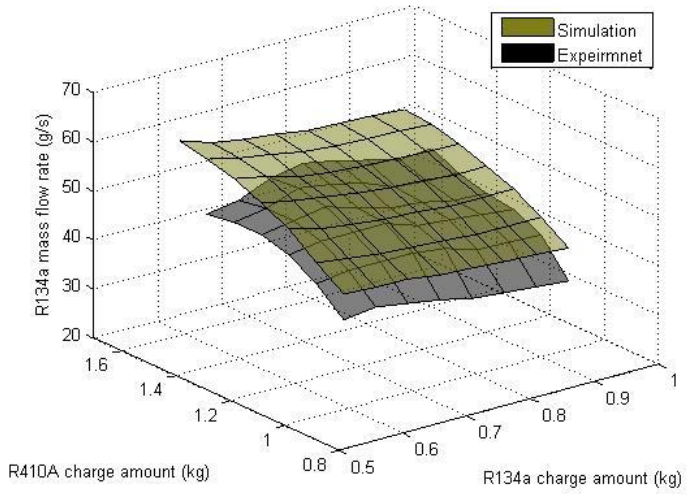

(b) Mass flow rate of R134a

Fig. 2.11 Mass flow rate and pressure ratio variation with respect to charge amount (Ambient= 7^{o}C, Water inlet = 50^{o}C, R134a/R410A compressor speed = 50/50 Hz, continued)

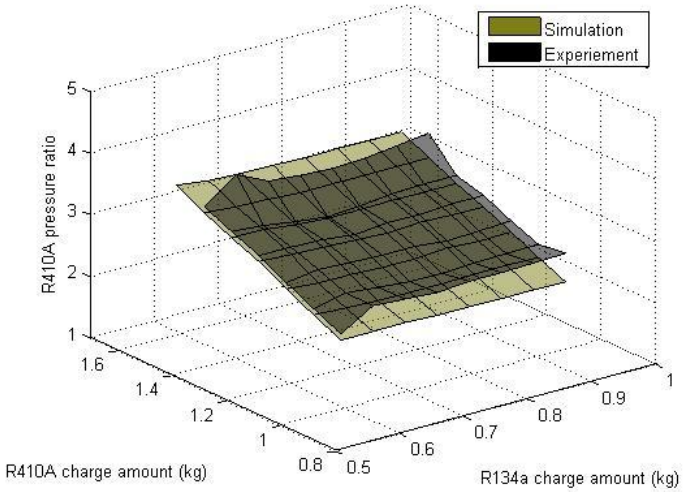

(c) Pressure ratio of 410A

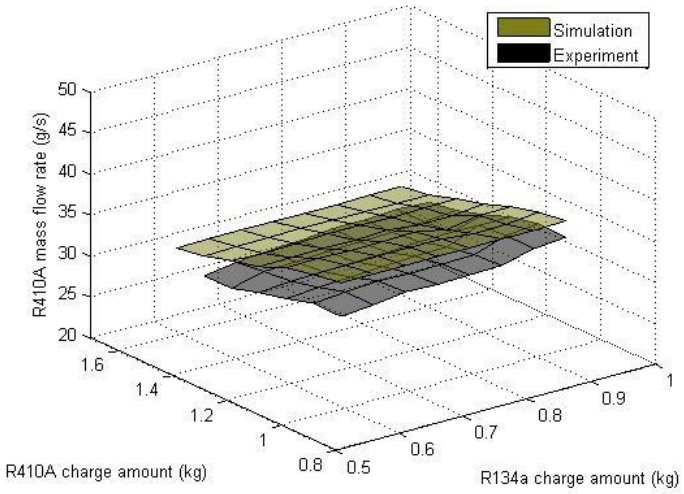

(d) Pressure ratio of R410A

Fig. 2.11 Mass flow rate and pressure ratio variation with respect to charge amount (Ambient= 7^{o}C, Water inlet = 50^{o}C, R134a/R410A compressor speed = 50/50 Hz)

increases, the high stage condensing pressure increases, whereas the evaporating pressure is kept almost constant. As the low stage charge amount increases, the increase in the evaporating pressure of the high stage is slightly higher than that of the condensing pressure at the high stage. As a result, the high pressure ratio was observed under conditions of high stage overcharge and low stage undercharge. On the other hand, a low pressure ratio was discovered under conditions of high stage undercharge and low stage overcharge. The same tendency was observed at the ambient temperature of -15^{o}C, however, the pressure ratio was in the range of 4.0 to 5.5 which was higher than that of 7^{o}C condition. Fig. 2.11 (b) shows the variation of the R134a mass flow rate, which showed a trend counter to that of the pressure ratio. As the pressure ratio increases, the volumetric efficiency decreases, and mass flow rate decreases at a given compressor suction inlet condition. In most cases, the DSH of high stage was controlled in the range of 10 K, however, in case of high stage undercharge and low stage overcharge condition, the high stage DSH showed about 20 K. Since the high DSH means the low vapor density, the mass flow rate of high stage showed a decrease trend at high stage undercharge and low stage overcharge condition.

Fig. 2.11 (c) shows the change of the R410A pressure ratio under

various refrigerant charge amounts in each cycle. There is no notable variation of the pressure ratio with respect to the R134a charge amount. The low stage charge amounts affect the evaporating pressure of the high stage, though the effect of the high stage charge amount on the low stage condensing pressure seems to be small. There is a clear tendency with the R410A charge amount, where an increase of the low stage charge amount leads to an increase of the pressure ratio of the low stage, since the evaporating pressure of R410A showed less variation. The pressure ratio of R410A cycle at ambient temperature of -15^{o}C was in the range of 4.5 to 5.6, which also showed higher value than that for 7^{o}C ambient condition. Fig. 2.11 (d) shows the change of the mass flow rate. The tendency can be interpreted in the same way as the description of the R134a mass flow rate. The mass flow rate showed a counter trend to that of pressure ratio.

Fig. 2.12 (a) shows the variation of the R134a DSC for various charge amounts. The DSC is determined as a consequence of the increased condensing pressure, and is strongly affected by the R134a charge amount, as expected. The effect of the R410A charge amount on the R134a DSC is quite hard to define, since the DSC is a function of temperature difference of refrigerant-water and the mass flow rate. Under conditions of R134a overcharge, the DSC of R134a increases with respect to R410A charge. In

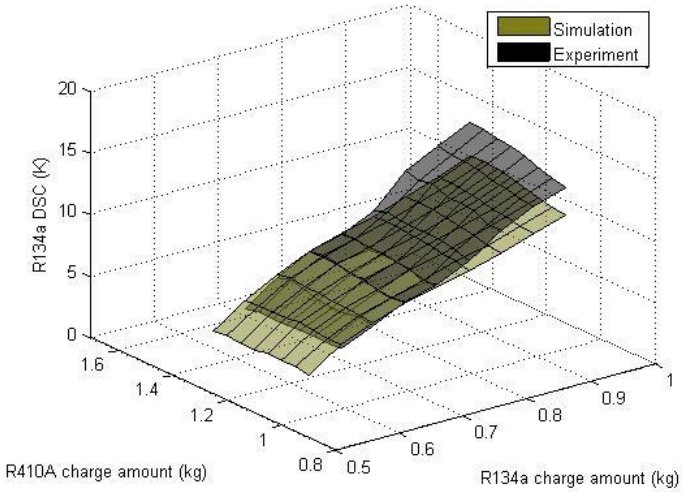

(a) R134a DSC

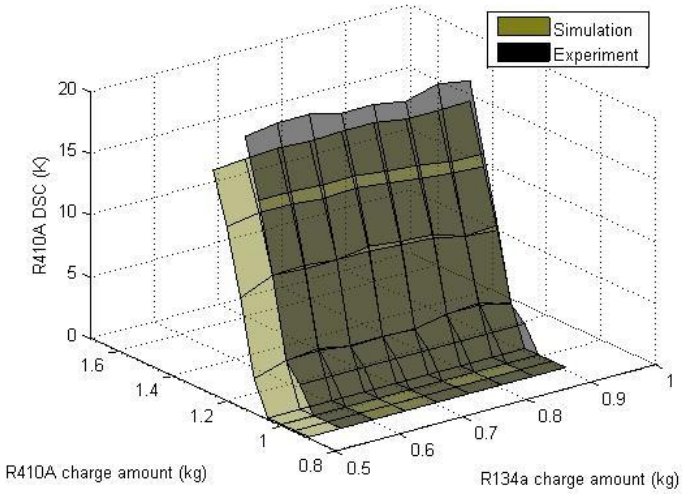

(b) R410A DSC

Fig. 2.12 Variation of system performances with respect to charge amount (Ambient= -15°C, Water inlet =50°C, R134a/R410A compressor speed = 50/50 Hz, continued)

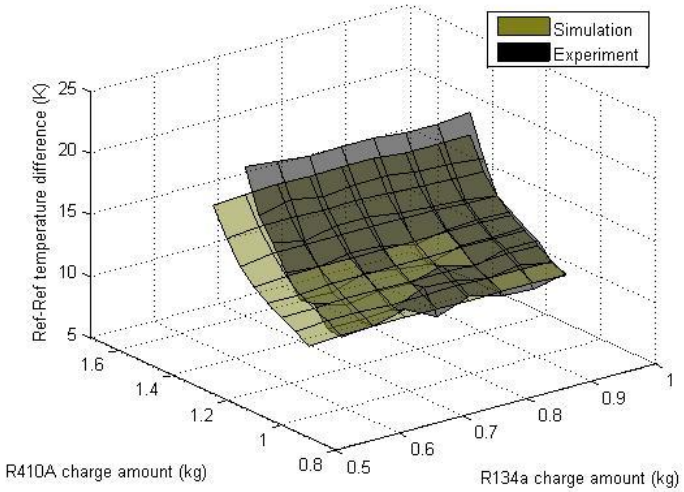

(c) Ref-Ref temperature difference

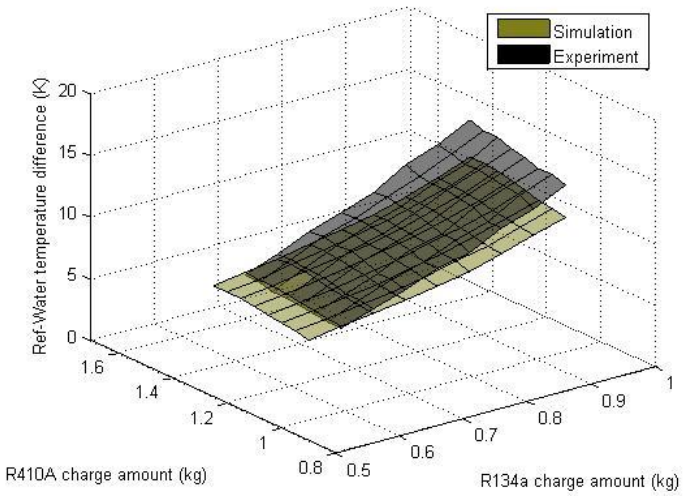

(d) Ref-Water temperature difference

Fig. 2.12 Variation of system performances with respect to charge amount (Ambient= -15^{o}C, Water inlet =50^{o}C, R134a/R410A compressor speed = 50/50 Hz)

R134a undercharge conditions, the DSC decreases as the R410A charge amount increases. Fig. 2.12 (b) shows the variation of the DSC of R410A, which increases with the charge amount of R410A. The DSC also increases with the R134a charge amount, the reason for which can be explained by the temperature difference between the refrigerants at the cascade heat exchanger, as shown in Fig. 2.12 (c). High temperature difference at cascade heat exchanger leads to an enhanced low stage DSC. Fig. 2.12 (d) shows the temperature difference of the refrigerant and water. This temperature difference is strongly affected by the R134a charge amount due to the elevated condensing pressure of R134a. The R410A charge amount also affects this temperature difference, since the R410A charge amount elevated the evaporating temperature of the high stage cycle. Figs. 2.13 (a), 2.14 (a) shows the heating capacity variation with respect to each cycle charge amount. In the study on the single-cycle charge amount, the heating capacity increases with the charge amount. A similar tendency was shown in the cascade cycle, with the maximum heating capacity being observed at the maximum charge amount in each cycle. The heating capacity is a function of the mass flow rate of R134a and the heat transfer rate, and the heat transfer rate is proportional to the refrigerant-water temperature difference. The effect of the R410A charge amount on the heating capacity seems to be

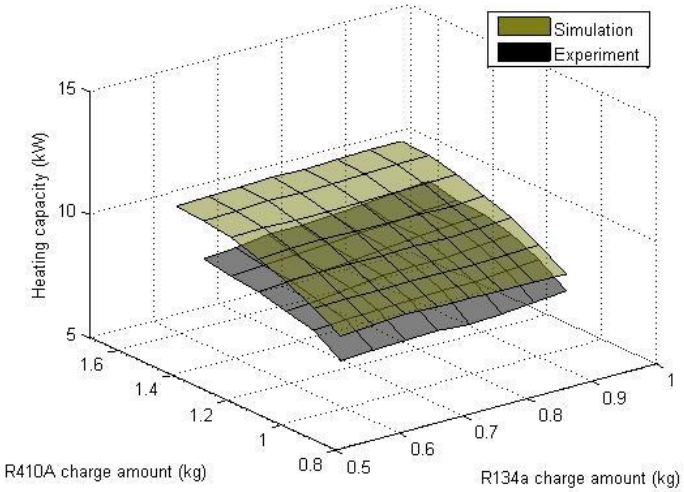

(a) Heating capacity

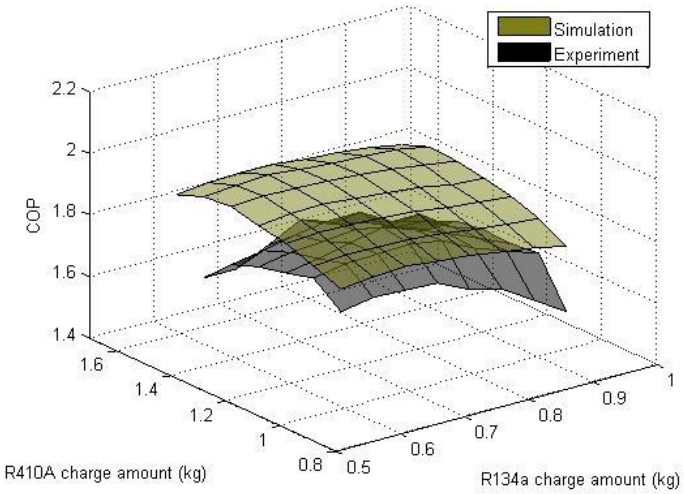

(b) COP

Fig. 2.13 Variation of heating capacity and COP (Ambient= 7^{o}C, Water inlet =50^{o}C, R134a/R410A compressor speed = 50/50 Hz)

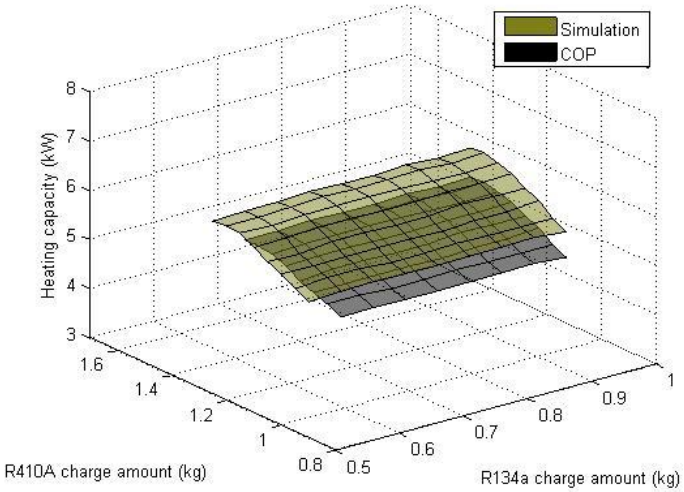

(a) Heating capacity

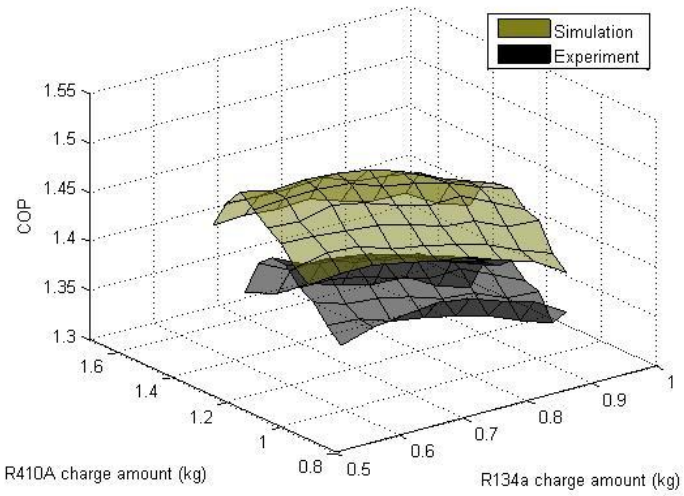

(b) COP

Fig. 2.14 Variation of heating capacity and COP (Ambient= -15^{o}C, Water inlet =50^{o}C, R134a/R410A compressor speed = 50/50 Hz)

stronger than that of the R134a charge amount. This can be interpreted as the effect of the mass flow rate is more influential than that of the temperature difference of the refrigerant and water. Actually, the average increase of R134a mass flow rate of due to the increase of charge amount of R410A was 33%, whereas the average decrease of enthalpy difference of R134a due to the increase of R134a charge amount was 8%. As R410A charge amount increases, R134a evaporating temperature increases. As mentioned previously, due to the increase of R410A condensing temperature, heat transfer at cascade heat exchanger increases. So, the R134a evaporates well and the DSH of R134a increases than expected. In order to reduce the DSH, the TXV increases the opening and as a results, evaporating temperature of R134a increases. High evaporating temperature means not only low pressure ratio but also high compressor inlet density. So, the effect of R410A charge amount on heating capacity is stronger than that of R134a charge amount. Figs. 2.13 (b), 2.14 (b) show the COP variation of the system. There is an optimum charge condition that maximizes the COP. The total compressor work shows similar trend to the heating capacity curve, however, there is an optimum point. The maximum heating capacities are occurred at high charge condition for each cycle, and are about 10 kW and 6 kW at ambient temperature of 7^{o}C and -15^{o}C, respectively. However, the optimal COP at

7^{o}C ambient temperature corresponds to the condition of the DSC at the high stage in the range of 7~8 K, and the DSC at the low stage in the range of 5~6 K, and the optimal high and low stage DSC of -15^{o}C ambient condition showed 4~5 K and 5~6 K, respectively. As ambient temperature decreases, the optimal DSC at high stage is decreased.

2.3.4 Simulation results for cascade cycle and discussion

A numerical simulation of the cascade cycle performance has been conducted to support the experimental data. The cascade cycle simulation involves calculation that is quite complex, since there are many restrictions to meet. Normally, two energy balances and two mass balances are required in a cascade cycle simulation. Since the calculation is complex, the simulation merits further research. Gunawardane and Bansal (2011) proposed a low temperature evaporator model using NTU-effectiveness model; however, it did not considered the whole system. The properties of R410A and R134a were calculated using REFPROP Matlab code. The compressor discharge temperature for each cycle was simulated using isentropic efficiency, and the mass flow rate was modeled using the volumetric efficiency. The plate heat exchangers for R134a-water and

R134a-R410A were modeled using a finite volume method. The fin tube heat exchanger was also simulated using the effectiveness-NTU method. The condensing and evaporating heat transfer coefficients of R134a for the plate heat exchangers are required, and are described in Table 2.3 (b). The other assumptions are the same as in section 2.2.4. A flow chart of the simulation is shown in Fig. 2.7 (b). As mentioned previously, a total of four iterations are required including two energy balances and two mass balances. The R134a evaporating pressure was iterated until the assumed DSH was met, and the R134a condensing pressure was varied until the refrigerant charge amount was met, which was also done for R410A.

Figs. 2.11 (a) and (c) show the pressure ratio of each cycle. The simulation effectively predicted the tendency of the pressure ratio, but simulation under-predicted the pressure ratio of R134a, especially at R134a high charge condition. The pressure ratio of R134a and R410A cycles at 7^{o}C ambient condition were in the range of 2.7~3.8 and 2.4~3.7, respectively. The evaporating pressure of the high stage showed similar values to the experimental data, but the condensing pressure of high stage lower predicted than experiment. It is considered that the error of simulation volume and real volume at plate heat exchanger and the volume of the whole system. For instance; when simulation predicted the higher volume than experimental

volume, numerical condensing pressure is lower than that of experimental condensing pressure to meet the charge amount. And the error could be also occurred due to the error of void fraction equation. That is, when the void correlation predicted the lower value than its real value, the condensing pressure is lower than experimental condensing pressure. Generally, this numerical simulation predicted the R410A saturation pressure well. The average error of pressure ratio was about 6.78%, which is derived from the error of R410A condensing pressure. And, in case of -15^{o}C ambient condition, the pressure ratio of R134a and R410A were in the range of 4.0~5.0 and 4.0~5.5, respectively. Since the -15^{o}C ambient condition requires greater pressure ratio at each cycle, the value was higher than that in the 7^{o}C ambient condition.

Figs. 2.11 (b) and (d) represent the mass flow rate of each cycle. Simulation showed higher value compared to the experimental data, the average error were 8.26% and 6.65% for R134a and R410A respectively. Due to the error of the condensing pressure and pressure ratio at high stage, the mass flow rate of R134a was predicted higher than the experiment data and the average deviation was about 8.26%. The maximum error of R134a mass flow rate was shown at R134a low charge amount and R410A high charge amount. In this charge amount, the opening of R134a TXV could not

be increased more, so the experimental DSH showed higher value. However, the error of R410A mass flow rate showed less error about 6.65%. Since the simulation well predicted the compressor inlet condition and pressure ratio, the error was less than that of R134a. And, in case of -15^{o}C ambient condition, since the pressure ratio of R134a and R410A were higher than that of 7^{o}C ambient condition, the mass flow rate of R134a at -15^{o}C condition was in the range of 28~34 g/s whereas the mass flow rate of R410A was in the range of 15.5~17.5 g/s.

Figs. 2.12 (a) and (b) show the DSC of R134a and R410A at -15^{o}C ambient temperature, respectively, and the trend seems quite similar to those of experimental data. However, the simulation R134a DSC predicted lower than experimental data, this is considered that the error of R134a condensing pressure error. In case of 7^{o}C ambient temperature condition, the R134a DSC is higher than that of -15^{o}C condition since the temperature difference of refrigerant-water showed higher value. The DSC of R410A at -15^{o}C condition showed higher value than that at 7^{o}C condition, and this is because decreased mass flow rate was easily affected by the charge amount. Figs. 2.12 (c) and (d) show the temperature differences between the two refrigerants, and those for the refrigerant and water, respectively. The refrigerant-refrigerant temperature difference at the cascade heat exchanger

is related to the low stage DSC and the refrigerant-water temperature difference at the condenser affects the high stage DSC. Simulation R134a refrigerant-water temperature difference showed less value than the experiments, this is related the error estimation of R134a condensing pressure and this is quite related the error of R134a DSC. The refrigerant-water temperature difference at -15^{o}C condition was in the range of 8~14 K whereas the temperature difference was in the range of 10~20 K at 7^{o}C ambient condition.

The Fig. 2.13 shows the heating capacity of the cascade system and COP at 7^{o}C ambient condition. The simulation average error of heating capacity and COP were 11.4% and 7.28%. Due to the error of mass flow rate and definition of heating capacity for experiment and simulation results, there showed an error of heating capacity and COP. The maximum heating capacity was about 11.2 kW and was observed at the high stage and low stage overcharge conditions. The maximum COP was about 1.97 and the optimal charge amount was observed at 0.6 kg and 1.4 kg at high and low stage, which corresponding to a DSC for R134a of 8~9 K and that for R410A of 7~8 K, respectively. Fig. 2.14 shows the variation of heating capacity and COP at -15^{o}C ambient condition. The maximum heating capacity and COP was about 6.6 kW and 1.52, respectively, and the

optimized DSC at high and low stage was 4~5 K and 7~8 K. The optimized subcooling of high stage was decreased as ambient temperature decreases, and this is consistent with experimental analysis. The optimal subcooling for cascade system should be focused on the high stage refrigerant rather than low stage refrigerant. The optimal subcooling for high stage cycle decreases as ambient temperature decreases whereas low stage optimal subcooling was quite constant.

2.4 Conclusion

The optimal degree of subcooling for the single cycle and cascade cycle was investigated experimentally and numerically. The single-stage experiment with R410A was conducted under various ambient temperatures and charge amounts. The maximum heating capacity was observed at the maximum charge condition, but the maximum COP was observed at DSCs of 3~7 K with various ambient temperatures. The simulation considering the charge amount was also conducted, and the simulation effectively predicted the system variables, including saturation pressure and performance. The simulation also predicted the DSC at 3~7 K with various ambient temperatures.

An experiment for the cascade cycle with R134a/R410A was conducted, and the variation of the mass flow rate, pressure ratio, temperature difference at the heat exchanger, and system performance was studied. The maximum heating capacity of the cascade cycle was also found at the maximum charge amount at each cycle, but the optimal COP condition was shown at DSCs of 4~8 K and 5~6 K for high and low stages, respectively. The simulation for the cascade cycle effectively predicted the tendency of the system variables, and the optimum COPs were shown at the R134a DSC of 4~9 K and the R410A DSC of 7~8 K. Both the optimized subcoolings of single and cascade high stage cycle decrease as ambient temperature decreases, however, the subcooling of cascade low stage cycle was quite constant. So, the optimal degree of subcooling should be focused on the high stage rather than low stage.

Chapter 3. Optimal intermediate temperature on cascade system

3.1 Introduction

The intermediate temperature is the most critical parameter for a multi-stage or a cascade heat pump system and affects the system efficiency because the intermediate pressure determines the compression ratio and compressor isentropic efficiency. Most studies focused on numerically determining an optimized intermediate temperature and suggested the correlations in terms of several temperature-related parameters. However, the suggested correlations cannot be adopted for other research studies and do not provide a general explanation.

Moreover, little information is available regarding experimental optimization results because the cascade test setup is quite complex and difficult to control. Bingming *et al*. (2009) and Dopazo and Fernández-Seara (2011) provided an experimental optimum intermediate temperature in the NH_3/CO_2 cascade heat pump system. Nevertheless, these studies focused on determining a maximum COP for different heating capacities. Because the heating capacity can affect the COP directly, the optimized intermediate

temperature should be obtained at a fixed heating capacity.

The main purpose of this research was to determine the optimum temperature of an R134a/R410A cascade heat pump system by experiment and compared with numerical analysis. The numerical solution was obtained by adopting the concept of a Carnot cycle efficiency and minimum total compressor work. The experiments were conducted at a given operating condition (e.g., water inlet temperature and ambient temperature) and fixed heating capacity. The optimum intermediate temperature was experimentally obtained and compared with the numerical analysis results.

3.2 System description and experimental apparatus

3.2.1 System description

In this study, the performance of an AWHP (air-to-water heat pump), which is constituted of two single cycles, was studied numerically and experimentally. There have been studies (Park *et al*. (2010)) about single stage AWHP with R410A for space heating and domestic hot water applications. In low temperature or high water temperature applications, however, there were heat pump performance limitations. In order to overcome these limitations, additional single stage cycle with R134a was

required. The high-stage cycle with R134a as a refrigerant was used to make hot water and the low-stage cycle with R410A as a refrigerant was used to absorb heat from ambient air. A schematic diagram of the R134a/R410A cascade system is the same as shown in Fig. 2.1. The two single cycles are connected by a cascade heat exchanger, where the R134a evaporates and the R410A condenses. The refrigerant in the low-stage cycle evaporates by absorbing heat from ambient air and is compressed and condensed by the cascade heat exchanger. The refrigerant in the high-stage cycle evaporates while the refrigerant in the low-stage cycle condenses, and is then compressed and condensed during the water heating.

Each circuit adopts a different refrigerant suitable for each temperature level. The lower temperature unit uses a refrigerant with a lower boiling point temperature, which has a higher saturation pressure at a low temperature (Bansal and Jain (2007)). High pressure at a low temperature results in a higher density of the suction line, which requires a smaller compressor. Moreover, because the critical point of R410A (344.5 K) is lower than that of R134a (374.2 K), the low-stage cycle adopts R410A. The difference between the low-stage condensing temperature and high-stage evaporating temperature is an important parameter. The proper temperature difference in the cascade heat exchanger is required for proper operation of

the system, and the temperature difference can significantly affect the heat pump performance. In this study, the temperature difference between the condensation of R410A and the evaporation of R134a was maintained in the range of 8–10 K.

3.2.2 Experimental apparatus and test procedure

As shown in Fig. 2.1, the three enclosed loops—R134a, R410A, and water loops—are completely separated. The outdoor unit (R410A) was placed in an environmental chamber to keep the ambient temperature constant. The R410A evaporator, which has a nominal cooling capacity of 14 kW, was a fin tube heat exchanger with 2 rows and 64 steps. A hermetic twin rotary compressor with an inverter was used in each cycle to control the compressor speed. The R134a condenser and cascade heat exchanger were plate heat exchangers. Each single-stage cycle used an EEV (electronic expansion valve) as an expansion valve, which controls the degree of superheat by varying the valve opening. Hot water from the R134a condenser entered the water reservoir, and a water chiller cooled the hot water, which allowed the system to remain in a steady state. The detailed specifications of each component are described in Table 3.1.

The measurement data of temperature, pressure, and mass flow rate were transferred to a personal computer for data analysis. All the temperature sensors used in this research were T-type thermocouples and the saturation pressure was measured by pressure transducers (Saginomiya, F.S. 2.5%). The mass flow rate of the hot water was measured by a magnetic mass flow meter (Badget meter, F.S. 0.1%). The detailed uncertainty of measurement is described in section 3.2.3.

The main objective of this research was to find the highest COP for a given heating capacity and operation condition. In order to maintain the heating capacity, the compressor speeds in each stage were precisely controlled. By increasing the compressor speed in the high-stage cycle and decreasing the compressor speed in the low cycle, the heating capacity was maintained at a desired value. The DSH (degree of superheat) is an important parameter because a large DSH decreases the heating capacity and a small DSH may cause a durability problem for the compressor. In order to exclude the effect of the DSH on the system performance, each cycle's DSH was maintained below 5 K by controlling the opening of the expansion valve.

Table 3.1 Specifications of each component for optimum temperature test

Part	Specifications
Compressor (Indoor,R134a)	Inverter driven hermetic twin rotary compressor (LG electronics), Displacement : 52.5 cm^3/rev
Compressor (Outdoor, R410A)	Inverter driven hermetic twin rotary compressor (LG electronics), Displacement : 42.5 cm^3/rev
Condenser (Indoor unit)	Plate heat exchanger (Alfa laval, Brazed type, Plate number : 48)
Cascade heat exchanger (Indoor unit)	Plate heat exchanger (Alfa laval, Brazed type, Plate number : 70)
Evaporator (outdoor unit)	outer diameter of tube: 7.32 mm rows and steps: 2 rows and 64 steps
Expansion valve	Type: electronic expansion valve (Fuzikoki, 500 Stage Valve Element)

Table 3.2 Test conditions for optimum temperature test

Parameters	Value
Ambient temperature (^{o}C)	-7, -2, 7
Heating capacity (kW)	9, 12, 15
Water flow rate (LPM)	18
Condenser water inlet temperature (^{o}C)	25, 40, 55
Degree of superheat* (^{o}C)	~5

* DSH of each cycle was controlled by the opening of EEV

The steady state of the system was judged by two parameters, DSH and electric power consumption, which are very sensitive parameters. The steady state judgment was based on research by Kim *et al*. (2008), and the threshold of the DSH and electric power were selected as 1 K and 10 W, respectively.

3.2.3 Test conditions, data reduction and uncertainty of measurements

The operating test conditions are listed in Table 3.2. The ambient temperature and inlet water temperature are the most important parameters, which determine the performance of the AWHP. The ambient temperature was controlled by an environmental chamber, and the water inlet temperature was adjusted by controlling the water chiller. The ambient temperature seems quiet higher than that of its real application; however, this research deals the high water temperature conditions. The heating capacity was controlled by each compressor frequency. For each test condition, there are several data points which have a different intermediate temperature and the explanation is in section 3.4.1.

The evaluation of the heat pump performance, including the heating capacity and COP, was conducted with measured data. The heating capacity

of the cascade system, which is the actual target of the heat pump system, was calculated by equation (3.1) using the mass flow rate of secondary fluid.

$$Q_H = \dot{m}_w C_w (T_{w,out} - T_{w,in}) \tag{3.1}$$

The heating capacity was also obtained using the R134a enthalpy difference as shown in equation (3.2). The maximum deviation between equations (3.1) and (3.2) was less than 3.2%. In this research, equation (3.1) defined the heating capacity of the cascade system.

$$Q_H = \dot{m}_r (h_{C,in} - h_{C,out}) \tag{3.2}$$

The overall COP of this system was defined by equation (3.3), which is the ratio of the heating capacity to the total power consumption including fan power.

$$COP = Q_H \Big/ \left(W_{HS} + W_{LS} + W_{\mathrm{Inv}}\right) \tag{3.3}$$

The intermediate temperature was calculated by equation (3.4), which is the average of the evaporating temperature of R134a and the condensing temperature of R410A. The saturation temperature was calculated by the measured pressure data using the REFPROP database (Lemmon (2007)).

$$T_{INT} = \frac{\left(T_{E,134} + T_{C,410}\right)}{2} \tag{3.4}$$

The measurement uncertainty was calculated by the method proposed by Moffat (1988). The basic equation of measurement uncertainty is

expressed in equation (3.5), where X_i and δX_i represent the measurement variables and their uncertainty, respectively. The measurement of uncertainties for the COP and heating capacity were obtained, and the maximum uncertainty of the COP and heating capacity were 3.772 and 3.778%, respectively.

$$\delta R = \left\{ \sum_{i=1}^{N} \left(\frac{\delta R}{\delta X_i} \delta X_i \right)^2 \right\}^{1/2} \tag{3.5}$$

In this study, the performance of an AWHP (air-to-water heat pump), which is constituted of two single cycles, was studied numerically and experimentally. There have been studies (Park *et al*. (2010)) about single stage AWHP with R410A for space heating and domestic hot water applications. In low temperature or high water temperature applications, however, there were heat pump performance limitations. In order to overcome these limitations, additional single stage cycle with R134a was required. The high-stage cycle with R134a as a refrigerant was used to make hot water and the low-stage cycle with R410A as a refrigerant was used to absorb heat from ambient air.

3.3 Numerical analysis of optimum intermediate temperature

Jeong and Smith (1994) reported the optimum temperature at each cycle in a multi-stage cryogenic system using a theory for minimizing entropy generation. By introducing the first and second laws of thermodynamics, the best intermediate temperature was determined to have the same high to low temperature ratio at each stage of the system. Specifically, the intermediate temperature was found to be the geometric mean of the condensing and evaporating temperatures ($\sqrt{T_{C,134}T_{E,410}}$). While this optimum intermediate temperature calculation seems very simple, the results provide insight for operating the cascade system, and the actual value may not differ from the ideal value by more than 10% (Bansal and Jain (2007)). In this research, a similar process was conducted that minimized the total compressor work. Because the objective of this research was to determine the maximum COP at a given heating capacity, the maximum COP was obtained to minimize the total compressor work. Fig. 3.1 shows the concept of the two-stage heat pump cycle.

By the first law of thermodynamics,

$$\begin{aligned} Q_H &= Q_{INT} + W_{HS} \\ Q_{INT} &= Q_L + W_{LS} \end{aligned} \tag{3.6}$$

By the second law of thermodynamics,

$$W_{Carnot,HS} = Q_{INT}\left(\frac{T_{C,134}}{T_{INT}-\delta}-1\right)$$

$$W_{Carnot,LS} = Q_{LS}\left(\frac{T_{INT}+\delta}{T_{E,410}}-1\right) \tag{3.7}$$

$$\eta = \frac{W_{Carnot}}{W_{Actual}}$$

Where η is the ratio of Carnot work to actual compressor work at each stage, which represents the efficiency of each stage. The minimized total work is in which the derivative of total compressor work is zero, and the maximum COP was obtained by equation (3.8).

$$\frac{\partial\left(W_{HS}+W_{LS}\right)}{\partial T_{INT}} = 0$$

$$\frac{\partial\left(W_{HS}+W_{LS}\right)}{\partial T_{INT}} = \frac{Q_{LS}}{\eta_{HS}}\left(1+\frac{1}{\eta_{LS}}\left(\frac{T_{INT}+\delta}{T_{E,410}}-1\right)\right)\left(\frac{T_{C,134}}{T_{INT}-\delta}-1\right)+\frac{1}{\eta_{LS}}Q_{LS}\left(\frac{T_{INT}+\delta}{T_{E,410}}-1\right)=0$$

$$\frac{\partial\left(W_{HS}+W_{LS}\right)}{\partial T_{INT}} = \frac{Q_L}{\eta_{LS}\eta_{HS}}\left[\frac{-\eta_L T_{C,134}}{(T_{INT}-\delta)^2}-\frac{T_{C,134}(T_{INT}+\delta)}{(T_{INT}-\delta)^2 T_{E,410}}+\frac{T_{C,134}}{(T_{INT}-\delta)^2}+\frac{T_{C,134}}{(T_{INT}-\delta)T_{E,410}}-\frac{1}{T_{E,410}}+\frac{\eta_{HS}}{T_{E,410}}\right]=0$$

$$(T_{INT}-\delta)^2\left(\eta_{HS}-1\right)\frac{1}{T_{E,410}}+\frac{T_{C,134}}{T_{E,410}}(T_{INT}-\delta)-\frac{T_{C,134}}{T_{E,410}}(T_{INT}+\delta)+T_{c,134}(1-\eta_{LS})=0$$

$$(T_{INT}-\delta)^2 = T_{C,134}(\eta_{LS}-1+\frac{2\delta}{T_{E,410}})T_{E,410}\frac{1}{\left(\eta_{HS}-1\right)}$$

$$(T_{INT}-\delta)^2 = T_{C,134}T_{E,410}\frac{(\eta_{LS}-1+\frac{2\delta}{T_{E,410}})}{\left(\eta_{HS}-1\right)}$$

$$\therefore T_{INT} = \sqrt{T_{C,134}T_{E,410}\frac{(\eta_{LS}-1+\frac{2\delta}{T_{E,410}})}{\left(\eta_{HS}-1\right)}}+\delta \tag{3.8}$$

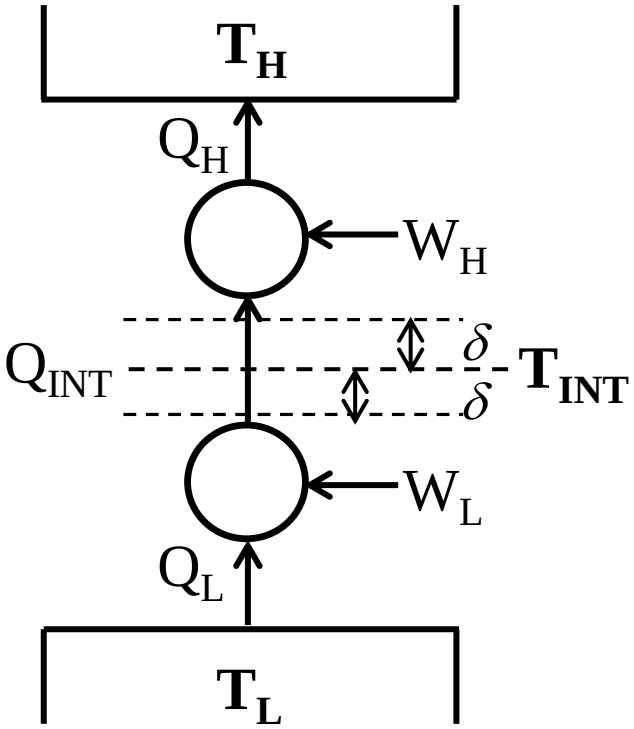

Fig. 3.1 Concept of numerical analysis

The optimum intermediate temperature can be calculated explicitly with five parameters: high-stage condensing temperature, low-stage evaporating temperature, high and low stage efficiencies, and temperature difference. If the equalities $\eta_{LS} = \eta_{HS}$ and $\delta = 0$ are true, the optimum intermediate temperature is the geometric mean of the high-stage condensing temperature and low-stage evaporating temperature ($\sqrt{T_{c,134} T_{E,410}}$). This result is similar to that of Jeong and Smith (1994) research, in which the efficiency of each cycle is the same. However, Jeong and Smith (1994) did not consider the temperature difference in the heat exchanger and the difference in efficiency of the high- and low-stage cycles. As condensing temperature of high stage and evaporating temperature of low stage increases, the optimal intermediate temperature increases. This is quite instinctive knowledge that each temperature could affect the optiaml intermediate temperature. In case of high stage carnot efficiency is higher than that of low stage, the optimal intermediate temperature increases compared to the same carnot efficiency condition, that means that pressure ratio at high stage is lower than that of low stage. Therefore, the intermediate temperature is increased. In case of low stage carnot efficiency is higer than that of high stage, the optimal intermediate temperature decrease. The effect of temperature difference on optimal intermediate temperature is quite complex. As temperature

difference at refrigerant-refrigerant increases, carnot efficiency increases at given temperature. Since this temperature difference is coupled with carnot efficiency, the trend with respect to temperature difference is quite complex to predict. However, when the carnot effieicny and temperature difference is get from experiment, the optimal intermediate temperature is easy to calculate.

3.4 Experimental analysis of optimum intermediate temperature

3.4.1 Characteristics of cascade system

In this section, the characteristics of the cascade heat pump system are depicted, specifically regarding each compressor. Fig. 3.2 (a) shows the saturation pressure variation of each cycle and the pressure ratio with respect to the R134a compressor frequency. The R134a condensing pressure and R410A evaporating pressure were kept almost constant while the R134a compressor frequency varied, whereas both the R134a evaporating and R410A condensing pressures decreased. Because the high-stage condenser pressure is normally related to the water inlet temperature and the low-stage evaporator pressure is related to the air source temperature, no notable

pressure variation occurred during the compressor frequency change. Therefore, the pressure ratio of R134a increased, whereas that of R410A decreased. Fig. 3.2 (b) shows the variation of the heating capacity, power consumption, and COP. The variation of the power consumption at each cycle was due to pressure variations; the high-stage compressor required more electricity due to the increase of the pressure ratio. The heating capacity for the high-stage condenser was slightly enhanced because the mass flow rate of the high-stage cycle increased. Because the increase in heating capacity and the increase in total power consumption were not significantly different, the COP was approximately the same. The temperature difference for the cascade heat exchanger was maintained in the range of 8~10 K, which is not a range critical to the performance.

A similar behavior was exhibited by the R410A compressor frequency. The pressure change was minimal for the high-stage cycle condenser and low-stage cycle evaporator, as previously mentioned. The heating capacity was also enhanced as the R410A compressor frequency increased, and the degree of enhancement was larger than that for the R134a compressor frequency. Since the heating capacity is normally related to compressor speed, the heating capacity of cascade cycle can be controlled by increasing one compressor frequency and decreasing the other compressor frequency.

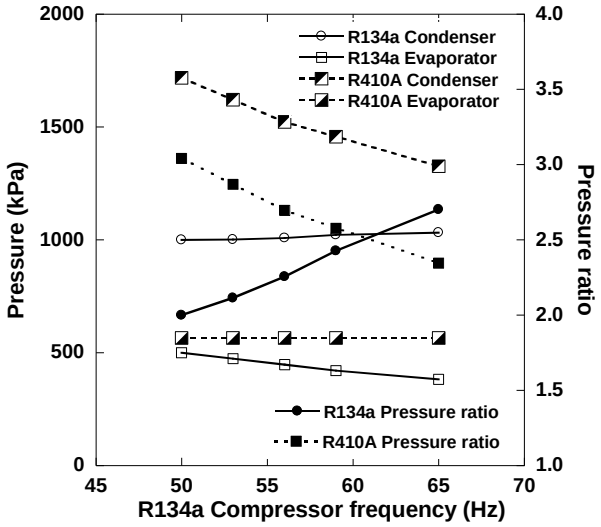

(a) Pressure variation

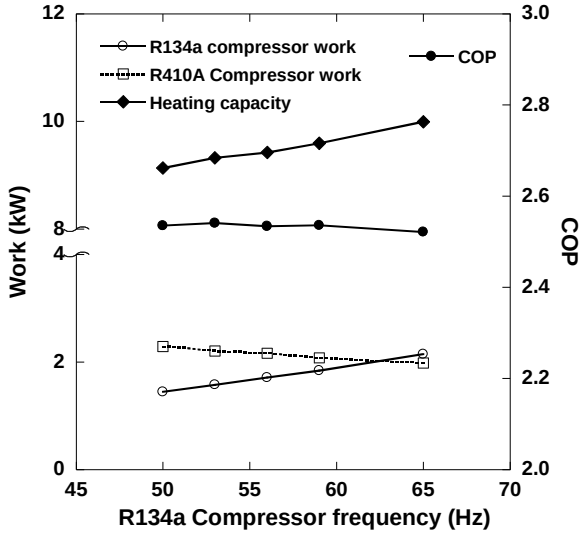

(b) Performance variation

Fig. 3.2 System variation with respect to compressor frequency (Fixed R410A compressor frequency = 50 Hz, Water temperature = 25^{o}C, Ambient temperature = -2^{o}C)

Fig. 3.3 shows how the heating capacity was controlled in this research. There are 3 data sets which have a different heating capacity. The same heating capacity could be obtained by controlling the R134a compressor frequency increasing and decreasing the R410A compressor frequency and the heating capacity deviations are in the range of 2%. Although each data sets show same heating capacities, they have different intermediate temperature. The detailed explanation will be described in Fig. 3.4.

Fig. 3.4 shows the different system states at given operating conditions for the same heating capacity. There are 10 data points at Fig. 3.4, however, each data points have different intermediate temperature. Every points was obtained from same test conditions. State 1 is the state in which the high-stage cycle pressure ratio is much larger than that of the low-stage cycle, which indicates that the high-stage compressor requires more work than the low-stage compressor. State 2 is the state in which the low-stage compressor requires more work than the high-stage compressor. State 1 and state 2 are called high-stage overworking and low-stage overworking, respectively. As the system state changed from state 1 to 2, the intermediate temperature increased and the minimum point for the total compressor work was approximately 293 K, which maximized the COP at the given heating capacity of 15 kW.

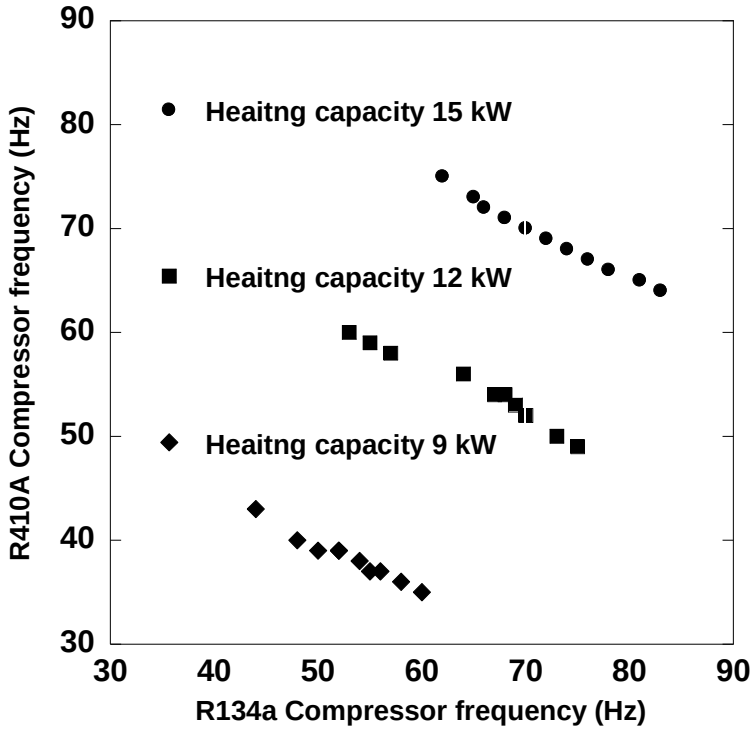

Fig. 3.3 Heating capacity control by varying each compressor frequency (Water temperature = 25°C, Ambient temperature = -2°C)

3.4.2 Experimental results for heating capacity change

Fig. 3.5 shows the COP variation with respect to the heating capacity at a given water inlet temperature and ambient temperature. As the heating capacity increased, the optimal intermediate temperature also increased. Because a high heating capacity required a greater pressure ratio compared to that of a small heating capacity, the optimal intermediate temperature increased. A higher heating capacity caused an increase in the R134a condensing temperature and a decrease in the R410A evaporating temperature, and the increase of the high-stage temperature was greater than the low-stage temperature decrease. Thus, the optimal intermediate temperature increased. Fig. 3.5 contains the information of the COP at the ambient temperatures of -7℃ and 7℃ with respect to different heating capacities, and the water inlet temperature was 25℃ for all data sets. The data sets were fitted with second polynomials and each point had the same heating capacity. The lower intermediate temperature indicated the R134a overworking conditions and the high intermediate temperature indicated the R410A overworking conditions. As shown in Fig. 3.5, the optimal temperature for the ambient temperature of 7℃ is greater than that for the ambient temperature of -7℃ because the R410A evaporating temperature is greater than the ambient temperature of -7℃. The optimal temperature for

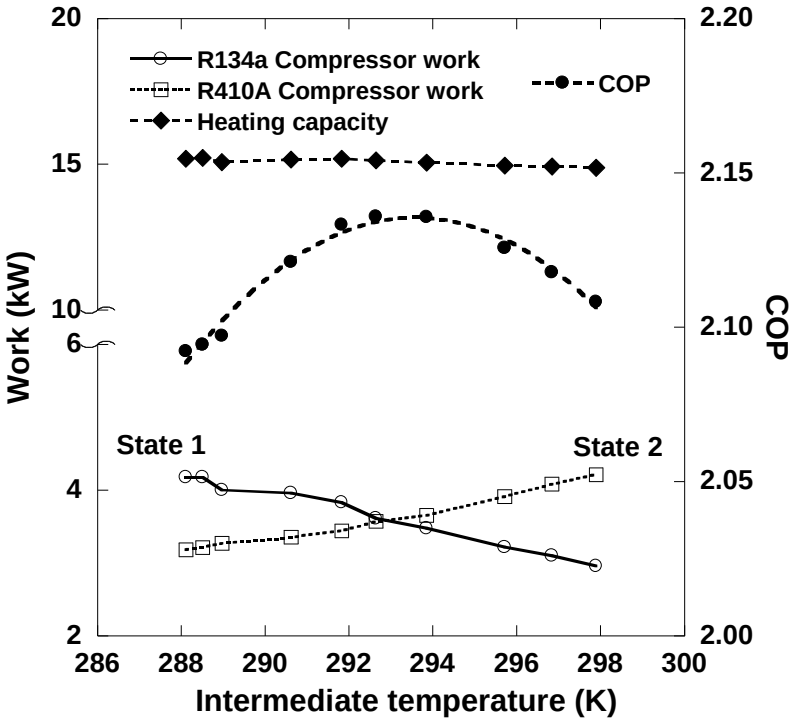

Fig. 3.4 Optimal intermediate temperature and system variation (Heating capacity = 15 kW, Water temperature = 40^{o}C, Ambient temperature = -7^{o}C)

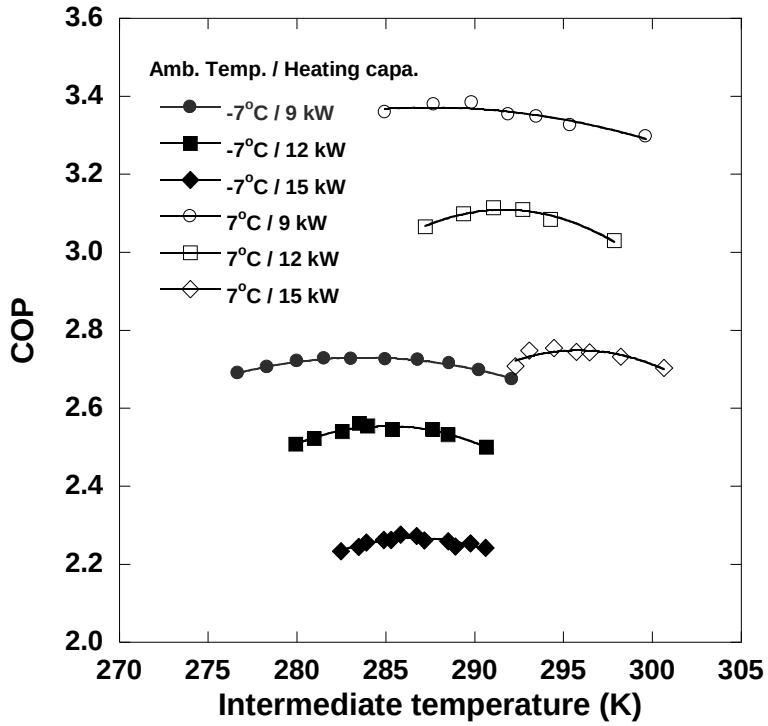

Fig. 3.5 Optimum intermediate temperature variation with respect to heating capacity (Water temperature = 25°C)

the ambient temperature of -2℃ was between -7℃ and 7℃. From these results, the optimal temperature was found to be related to the R134a condensing temperature and R410A evaporating temperature. The COP was found to have a close relationship with the heating capacity; a large heating capacity lead to a higher compression ratio, which reduced the COP. Actually, the COP variation at each curve was not significant because each data point had the same capacity; however, the behavior was quite evident.

3.4.3 Experimental results for water inlet temperature change

Fig. 3.6 shows the COP variation with respect to the water inlet temperature at a given heating capacity and ambient temperature. As the water inlet temperature increased, the optimal intermediate temperature also increased. A high water inlet temperature affected the condensing temperature of R134a, whereas the R410A evaporating temperature was almost constant because the ambient temperature was stabilized. Because the water inlet temperature strongly affected the high-stage condensing temperature, a higher water temperature caused the intermediate temperature to increase. Comparing the effect of the heating capacity and water inlet temperature on the optimal intermediate temperature is ambiguous. However,

the water inlet temperature, rather than the heating capacity, significantly affects the optimal temperature. Specifically, the increase of the high-stage condensing temperature is much greater than that of the heating capacity variation. This information is important because the water inlet temperature varies with time in actual situations.

Fig. 3.6 contains the information of the COP at the ambient temperatures of -7℃ and -2℃ with respect to the water inlet temperature, and all data sets had a heating capacity of 15 kW. As expected, a higher condenser water inlet temperature caused a decrease in the heat pump performance. In the case of the inlet temperature of 55℃, the COP decreased below 2, and this decrease is serious at a low ambient temperature. The decrease with respect to the ambient temperature is also shown in Fig. 3.6. The data for the ambient temperature of -2℃ exhibited a higher optimal intermediate temperature than that of the ambient temperature of -7℃ due to the high evaporating temperature of R410A. This phenomenon was consistent with the previous discussion, where the optimal temperature is related to the R134a condensing temperature and R410A evaporating temperature.

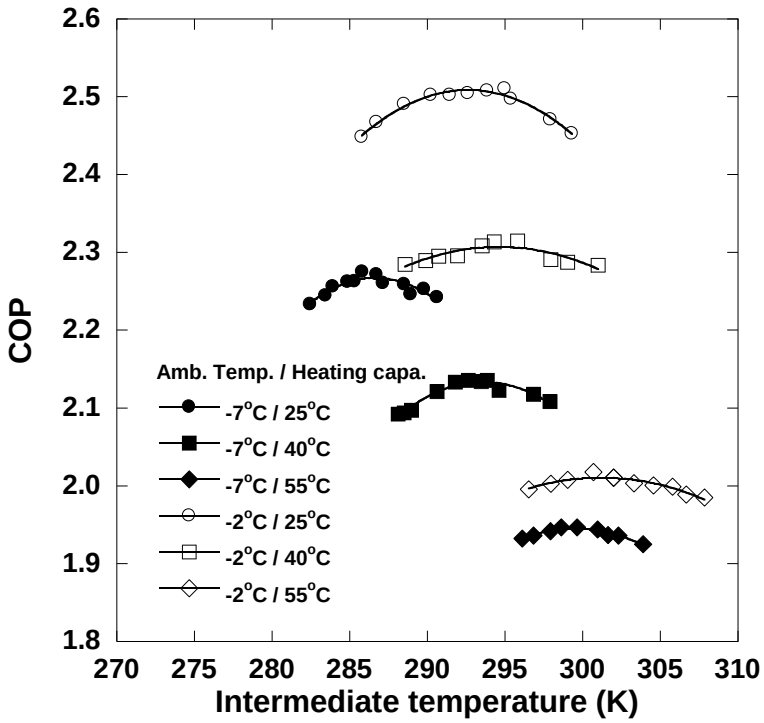

Fig. 3.6 Optimum intermediate temperature variation with respect to water inlet temperature (Heating capacity = 15kW)

3.4.4 Experimental results for ambient temperature change

Fig. 3.7 shows the COP variation with respect to the ambient temperature at a given water inlet temperature and heating capacity. As shown in Fig. 3.7, the optimal temperature increases with the ambient temperature increase. As previously mentioned, the ambient temperature affected the evaporating temperature of the low-stage cycle, which induced an increase of the optimal temperature as the ambient temperature increases. This is consistent with the conclusion that the optimal temperature is related to the evaporating temperature of the low-stage cycle and the condensing temperature of the high-stage cycle. The effect of the ambient temperature on the optimal temperature is also significant, as shown in Fig. 3.7. The COP decreased significantly with the ambient temperature. Because the low ambient temperature required a higher compression ratio for the low cycle, the COP was reduced at the low ambient temperature, which is a common tendency of an air source heat pump system. In Figs. 3.5 to 3.7, the variation of the intermediate temperature is limited; operating the system at very low and high intermediate temperatures is difficult due to limitations of the compressor operation and EEV opening range.

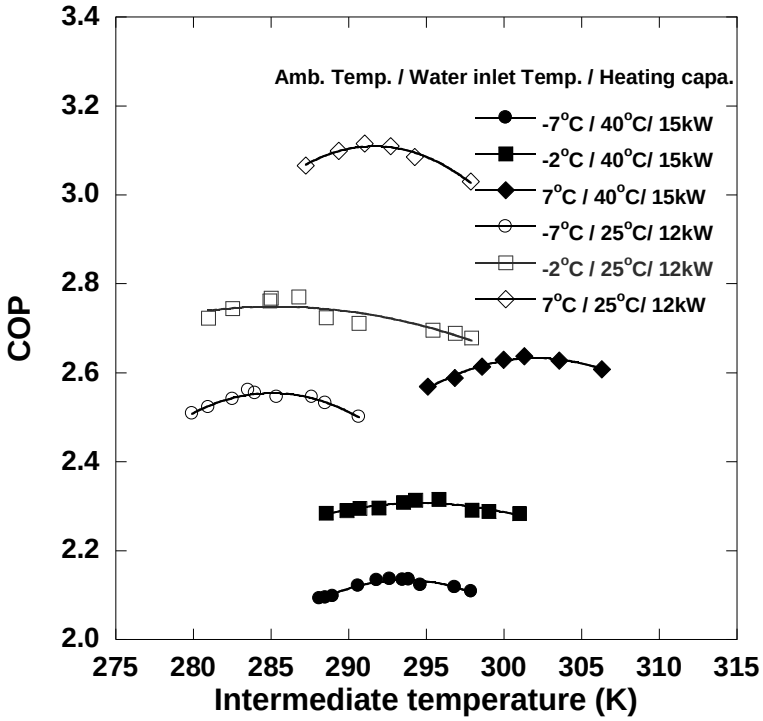

Fig. 3.7 Optimum intermediate temperature variation with respect to ambient temperature

3.4.5 Validation of numerical analysis

The results of the numerical and experimental analyses were compared. From the experiment, the optimal intermediate temperature was found to be strongly related to the condenser water inlet temperature and ambient temperature, and the effect of the heating capacity was also important. Fig. 3.8 shows the deviation of each cycle efficiency from equation 3.7. The high-stage exhibited a slightly higher efficiency value than the low-stage for most cases; however, the difference was not significant. The mean values of the high and low stages were 0.4798 and 0.4553, respectively. This mean value was adopted in the explicit solution equation; Fig. 3.9 shows the deviation of the experimental optimum temperature and explicit solution. The explicit solution accurately predicted the parameter to be approximately 5 K in most cases, and the RMSE (root mean squared error) was 2.760.

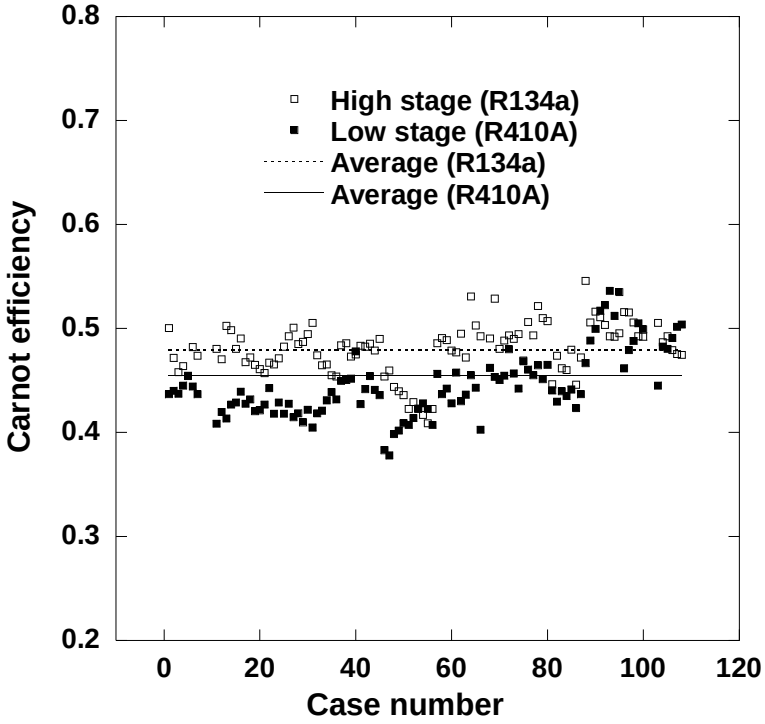

Fig. 3.8 Carnot efficiency of each cycle and mean value

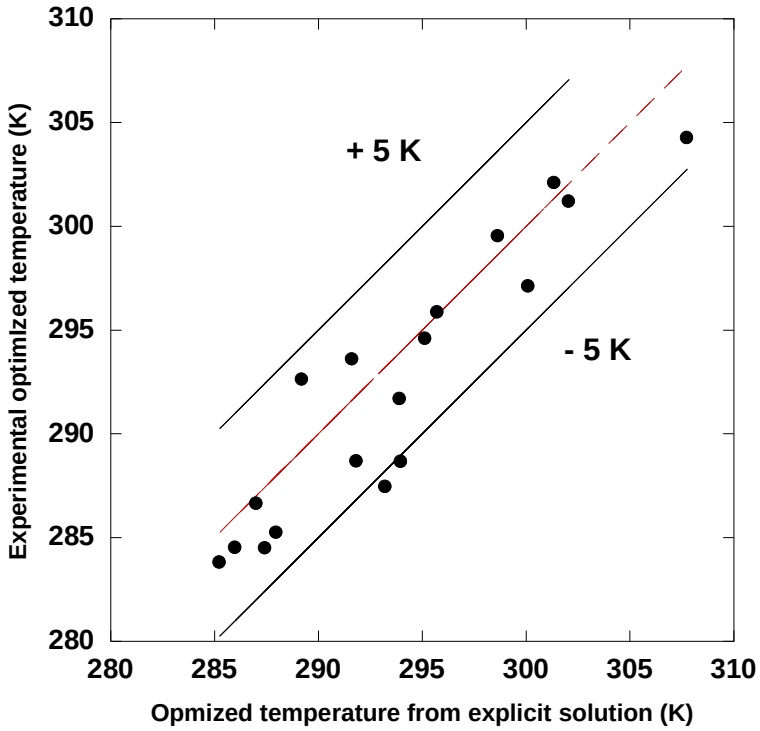

Fig. 3.9 Comparison of explicit solution and experimental results

3.5 Conclusion

The optimal intermediate temperature for the AWHP cascade system was studied experimentally and numerically. The numerical analysis was conducted: an explicit method. The explicit method was developed using an analysis of the minimum total compressor work, and the explicit solution was obtained as a function of five parameters considering the temperature difference and system efficiency. The AWHP performance is known to be reduced at a high water inlet temperature and low ambient temperature. These parameters affected not only the optimal intermediate temperature but also the COP. In other words, the AWHP performances decreased at a high water inlet temperature and low ambient temperature. The optimal intermediate temperature increased as the ambient temperature, water inlet temperature, and heating capacity increased. These phenomena were explained by the differences between the high-stage condenser temperature and low-stage evaporator temperature. Numerical solution exhibited good prediction of the experimental results, and the RMSE was about 2.760 K.

Chapter 4. Performance characteristics of cascade heat pump with regard to water temperature lift

4.1 Introduction

Despite of several advantages compared to commercial gas water heater, slow thermal response of AWHP in cold weather requires the design of a large water storage tank in order to deal with the peak load (Huang *et al*. (2009)) or a control system that turns on the electric resistance backup heater (Ji *et al*. (2003)). The fast thermal response means the fast hot water temperature supply and is required at initial operation of heat pump. The urgent hot water supply can be achieved by two ways; increasing heating capacity and decreasing water mass flow rate. The former method can be accomplished by increasing the compressors speed; however, it takes a long time to reach certain water discharge temperature and the discharge temperature has a limitation. Normally, the latter method shows quite fast responses despite of low mass flow rate and low performance. Yet, to date, there has been little research considering the effect of temperature lift on a cascade heat pump system and cascade heat pump control. This study was

conducted to verify the effect of the water temperature lift in terms of pressure and performance change. Also, the optimal intermediate temperature of cascade cycle with respect to temperature lift was studied and this temperature was adopted for a heat pump transient operation.

4.2 Performance of cascade heat pump performance with water temperature lift

4.2.1 System description and experimental apparatus

The heat pump test performance with regard to mass flow rate of water was studied experimentally. Fig. 2.1 shows a schematic diagram of the cascade heat pump test apparatus which consisted of two single stage cycles and this cascade heat pump is called AWHP (air to water heat pump). An actuator valve (Tootech, JCVU-01B) controlled the mass flow rate of hot water in the range of 15 g/s to 500 g/s by valve opening and the mass flow rate of hot water was measured by a magnetic flow meter (Badger meter, DN-6). R410A scroll compressor (Copeland, ZP36KSE) and R134a scroll compressor (Copeland, ZB21KSE) were connected with inverter (LS, SV055iG5A-4) in order to control the speed of compressor. The mass flow rate of refrigerant was measured by the Coriolis mass flow meter (Oval, CN-

010). The fin-tube heat exchanger which has a nominal capacity of 6 kW is placed in an outdoor environmental chamber and two plate heat exchangers are placed in an indoor chamber, one for cascade heat exchanger (SWEP, B15H) and the other for R134a condenser (SWEP, B25H). Electronic expansion valves (Sanhua, DPF) were used for each cycle to expand the refrigerant from condenser outlet and were connected with control drivers (Dotech, EVC10B) to control the DSH (degree of superheat). The compressor inverter and EEV (electronic expansion valve) control drivers are linked to the PC in order to communicate by RS-485 standard. Experimental data of absolute pressure, differential pressure, temperature, mass flow rate was transferred to a PC for data analysis. All of temperature sensors used in this study were T-type thermocouples, and the saturation pressure was measured by pressure transducer (Sensotec, FP-2000). The differential pressure transmitter (Emerson, Rosemount 3051) was measured to examine the pressure drop through the heat exchanger. The total power including compressor and inverter was measured by the digital power meter (Yokogawa, WT 1600). The detailed specifications of components are presented in Table 4.1.

4.2.2 Test conditions, data reduction and uncertainty of measurements

Table 4.1 Specification of each component for performance test with WDT

(a) R410A components

Refrigerant	Part	Specifications
R410A	Compressor	Scroll compressor (Copeland, ZP36KSE) Displacement : 6.0 m^3/h Gain (P, I, D) : 0.360, 0.0267, 1.122
	Condenser (Indoor unit)	Plate heat exchanger (Swep, B15H) Nominal capacity : 10.55 kW Plate number : 28
	Expansion valve (EEV)	Sanhua, DPF O series, 5.28 kW
	Evaporator	Tube/fin material: copper/aluminum Outer diameter of tube: 6.35 mm Rows and steps: 4 rows and 10 steps Fins per inch : 9
	Inverter	LS, SV055iG5A-4

(b) R134a components

Refrigerant	Part	Specifications
R134a	Compressor	Scroll compressor (Copeland, ZB21KSE) Displacement : 8.6 m^3/h Gain (P, I, D) : 0.275, 0.0254, 0.742
	Condenser (Indoor unit)	Plate heat exchanger (Swep, B25H) Nominal capacity : 17.58 kW Plate number : 26
	Expansion valve (EEV)	Sanhua, DPF O series, 17.6 kW
	Evaporator	Plate heat exchanger (Swep, B15H) Nominal capacity : 10.55 kW Plate number : 28
	Inverter	LS, SV055iG5A-4

Table 4.2 Test conditions for performance test with WDT

(a) Performance test with regard to WDT

Parameters	Value
Ambient temperature (^{o}C)	-15, -7, 7
Condenser water inlet temperature (^{o}C)	40, 50, 60
Water temperature difference (K)	5, 10, 15, 20, 25, 30
Water flow rate (g/s)	54 ~ 410
Compressor speed (high / low, Hz)	50 / 50
DSH (high / low, K)	5 / 5
Refrigerant Charge amount (high / low, kg)	0.8 / 1.1

(b) Optimum intermediate temperature test with regard to WDT

Parameters	Value
Ambient temperature (^{o}C)	-15
Condenser water inlet temperature (^{o}C)	30, 40, 50
Water temperature difference (K)	5, 15
Water flow rate (g/s)	95~280
Compressor speed (high / low, Hz)	40~60 / 40~60
DSH (high / low, K)	5 / 5
Refrigerant Charge amount (high / low, kg)	0.8 / 1.1

(c) Transient operation with regard to WDT

Parameters	Value
Ambient temperature (^{o}C)	-15
Water reservoir temperature (^{o}C)	30 to 60
Water temperature difference (K)	5, 10, 15
Target heating capacity (kW)	6
DSH (high / low, K)	5 / 5
Refrigerant Charge amount (high / low, kg)	0.8 / 1.1

The operating conditions are listed in Table 4.2 (a). The temperatures of ambient air and water inlet are important parameters which determine the performance of AWHP. The ambient temperature was controlled in an environmental chamber and its value was -15, -7, and 7^{o}C. The water inlet temperature was varied in the range of 40 to 60^{o}C. The water temperature difference (WDT) at condenser was varied 5 to 30 K by controlling the mass flow rate of water and the maximum water discharge temperature was 70^{o}C due to the limitation of R134a compressor's condensing temperature (75^{o}C). The water mass flow rate was controlled by an actuator valve which is actuated by input signal of 4-20 mA. The speeds of high and low stage compressor were fixed in this experiment by the value of 50 Hz for each cycle. In order to neglect the effect of the DSH on the cascade heat pump performance, the DSH was controlled to 5 K for high and low stage cycles. The EEV control drivers conduct PID control by the opening of EEV to maintain target DSHs. The measured data was saved at PC by the criterion of steady state and this was based on the research (Kim *et al*. (2008)), and the thresholds of DSHs and total power consumption were set as 1 K and 10 W, respectively.

The heating capacity that is the actual performance of cascade heat pump is defined by the equation (4.1) using the mass flow rate of the

secondary fluid. However, the heating capacity can also be obtained by the refrigerant enthalpy difference, as shown in equation (4.2). The average deviation between equations (4.1) and (4.2) is 5.4%. In this research, equation (4.11) defined the heating capacity.

$$Q_H = \dot{m}_w C_w (T_{w,out} - T_{w,in}) \tag{4.1}$$

$$Q_H = \dot{m}_r (h_{C,in} - h_{C,out}) \tag{4.2}$$

The COP of this system is represented as equation (4.3), which is the ratio of the heating capacity to the power consumption, including the inverter power. The average power consumption of compressor inverter was about 90 W for each cycle. The saturation temperature was calculated by the measured pressure data using the REFPROP database (Lemmon (2007)).

$$COP = Q_H \Big/ \left(W_{HS} + W_{LS} + W_{\text{Inv}}\right) \tag{4.3}$$

The measurement uncertainty analysis was conducted based on the research proposed by Moffat (1988). The equation of measurement uncertainty is expressed in equation (4.4), where X_i and δX_i represent the measurement variables and their uncertainties, respectively. The maximum uncertainty of the heating capacity and COP were 5.7% and 5.8%, respectively.

$$\delta R = \left\{ \sum_{i=1}^{N} \left(\frac{\delta R}{\delta X_i} \delta X_i \right)^2 \right\}^{1/2} \tag{4.4}$$

4.2.3 Test results and discussion

The temperatures of high stage condenser and low stage evaporator are related to the temperatures of water inlet and ambient air, respectively. However, the flow rate of secondary fluid also affects not only condensing temperature of low stage but evaporating temperature of high stage. Fig. 4.1 shows the change of pressure-enthalpy (P-h) diagram of cascade cycle with regard to the variation of WDT. The R410A evaporation temperature was almost kept constant with the increase of WDT, while there were the increases of R134a evaporation and R410A condensing temperature. Both temperatures increased about 4 K as the WDT varied from 5 K to 30 K. The significant increase was observed at the R134a condenser, and the value was about 17 K. The increase of WDT strongly affected the R134a condensing pressure. As expected, the pressure ratio of each cycle was increased. Fig. 4.2 (a) shows the variation of pressure ratio with respect to ambient temperature. The increase of R134a pressure ratio with regard to WDT is higher than that of R410A. The pressure ratio increases linearly with WDT and the maximum pressure ratio occurred at low ambient temperature and high WDT condition and the pressure ratio of R134a and R410A were 5.18 and 4.69, respectively. The increase of R410A pressure ratio is derived from the increase of R410A condensing pressure.

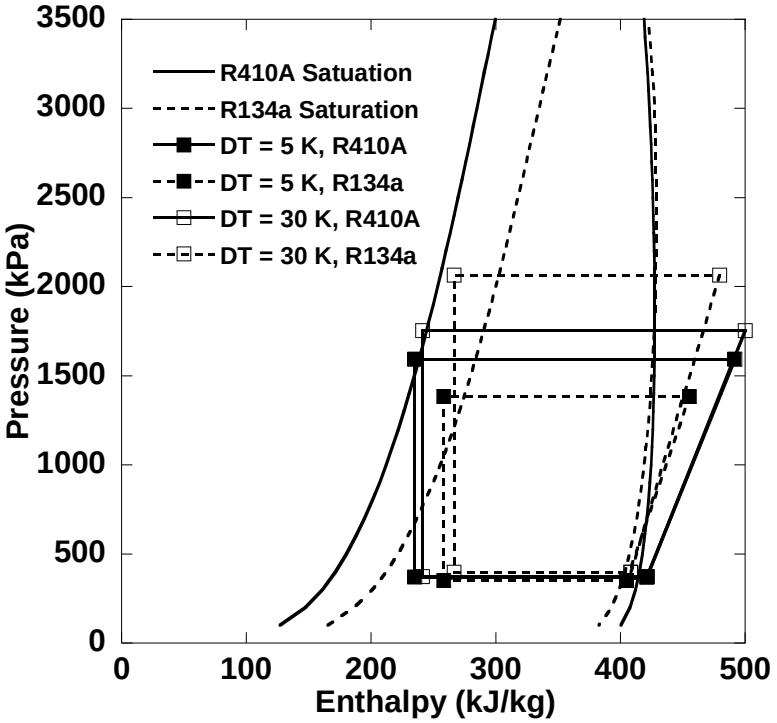

Fig. 4.1 P-h variation with respect to WDT (Ambient temperature = -15^{o}C, Water inlet temperature = 40^{o}C)

The R410A evaporating pressures are almost constant with variation of WDT since the ambient temperature was kept constant. The increase of R134a pressure ratio is caused by the significant increase of condensing pressure which is higher than that of evaporating pressure. The high pressure ratio results in high discharge temperature, and Fig. 4.2 (b) shows the temperature of refrigerant at the exit of compressor. Since the condensing pressures of R134a and R410A increases, discharge temperature increases. The increase of high stage discharge temperature is much higher than that of low stage cycle. This points out that the increase rate of R134a pressure ratio and R134a evaporating temperature with WDT are higher than that of R410A. And as ambient temperature decreases, refrigerant compressor discharge temperature was increased. Even though, the condensing pressure of low ambient temperature is lower than that of high ambient temperature, the compressor discharge temperature increases as ambient temperature decreases. The discharge temperature is determined by the compressor refrigerant inlet properties, pressure ratio and isentropic efficiency and the isentropic efficiency is the determined by the pressure ratio. High pressure ratio deteriorates the isentropic efficiency and as a result, compressor discharge temperature increases at low ambient temperature condition. In this study, the R134a isentropic efficiencies are in the range of 0.49~0.64

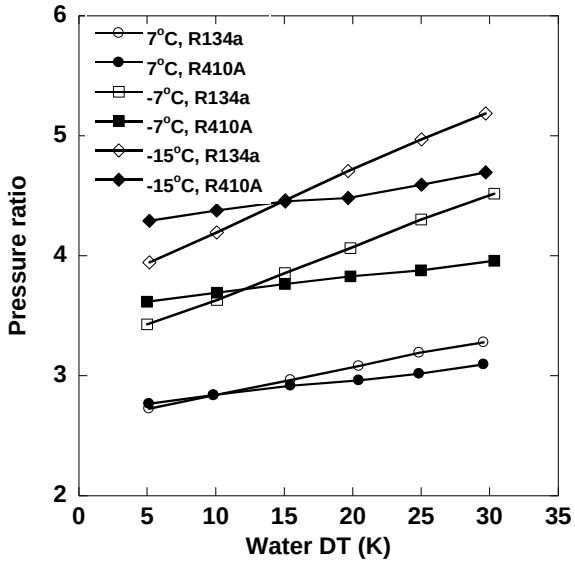

(a) Pressure ratio

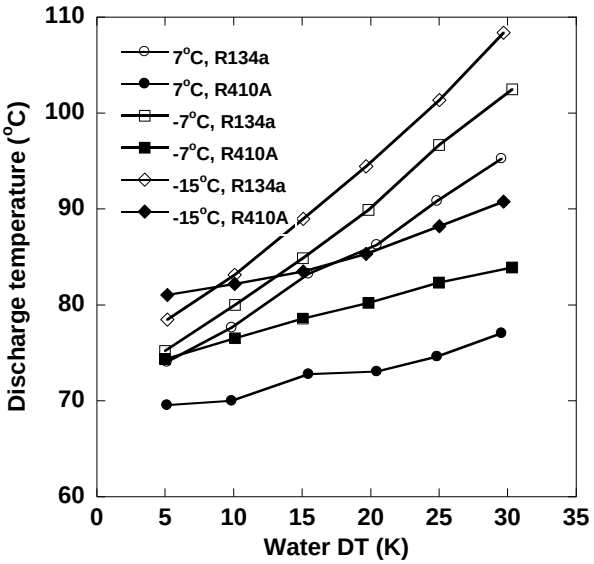

(b) Discharge temperature

Fig. 4.2 Variation of heat pump performances with respect to WDT (Ambient temperature = -15°C, Water inlet temperature = 40°C)

when the pressure ratios are in the range of 2.72~5.18. The isentropic efficiencies of R410A are in the range of 0.55~0.61 where the pressure ratios are between 2.77~4.92. Fig. 4.3 (a) shows the variation of R134a mass flow rate and the refrigerant compressor inlet density. As R134a WDT increases, evaporating temperature increases. In case of higher evaporating temperature, the compressor inlet density becomes higher. As a result, the refrigerant mass flow rate increases as WDT increases. There was a remarkable effect of WDT on R134a mass flow increment rate at the high ambient temperature condition. At the ambient temperature of 7^{o}C condition, the R134a evaporating temperature was increased from 17.7^{o}C to 23.9^{o}C and the compressor inlet density increased about 20% with the increase of WDT of 5 to 30 K. However, increment of density was about 13% at the condition of -15^{o}C temperature and the R134a evaporating temperature was increased about 5^{o}C to 8.7^{o}C with the increase of WDT of 5 to 30 K. Fig. 4.3 (b) shows the specific enthalpy differences at the condenser. The value of specific enthalpy difference is high at the -15^{o}C ambient temperature condition, and this means that low mass flow rate refrigerant is strongly affected by the secondary fluid. As a result, the condenser inlet enthalpy increases whereas the condenser outlet enthalpy decreases as ambient temperature decreases. And, there is a noticeable change of specific enthalpy with respect to WDT.

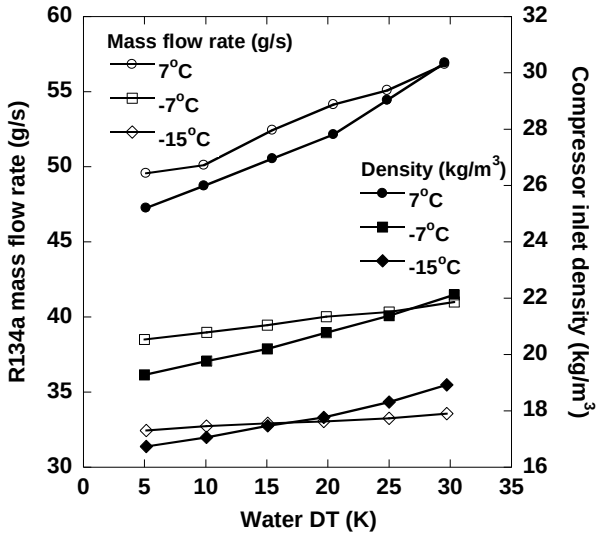

(a) R134a mass flow rate and compressor inlet density (Ambient temperature = -15°C, Water inlet temperature = 40°C)

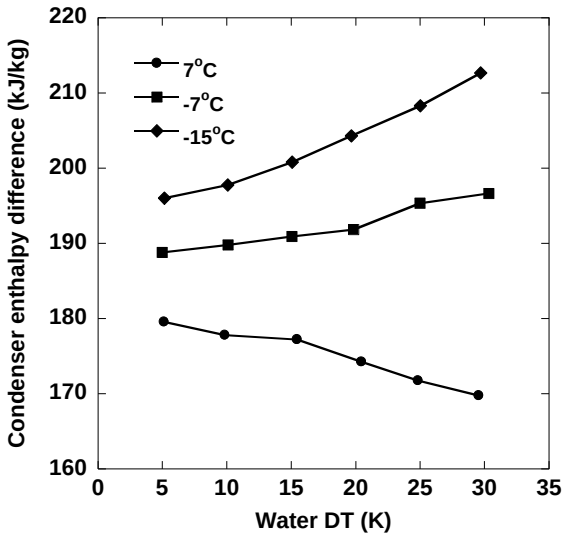

(b) R134a specific enthalpy differences (Ambient temperature = -15°C, Water inlet temperature = 40°C)

Fig. 4.3 Variation of R134a mass flow rate and enthalpy differences with respect to WDT (contined)

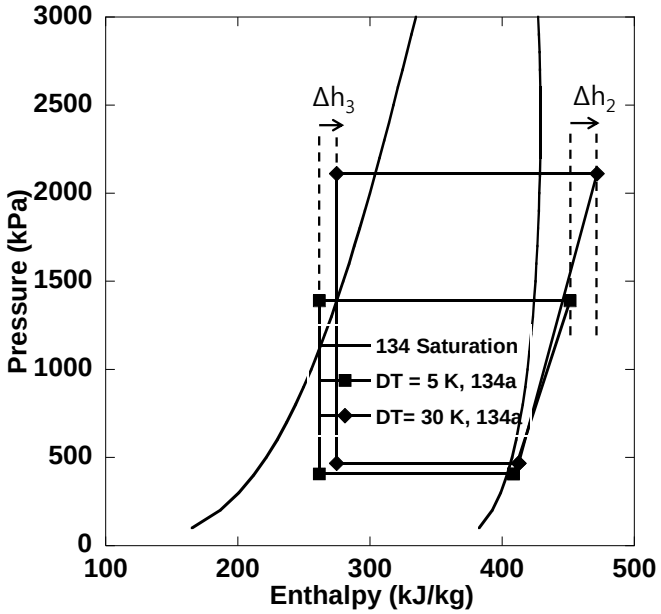

(c) R134a specific enthalpy variation (Ambient temperature = -7^{o}C, Water inlet temperature = 40^{o}C)

Fig. 4.3 Variation of R134a mass flow rate and enthalpy differences with respect to WDT

The specific enthalpy difference increases with WDT at the condition of low ambient condition whereas the specific enthalpy difference decreases with WDT at the condition of high ambient condition. Fig. 4.3 (c) shows the enthalpy variation with regard to WDT. As WDT increases, the condenser inlet and outlet enthalpy increases. However, the increase rates are different with ambient temperature. At low ambient temperature, the increment of condenser inlet enthalpy ($\Delta h2$) with WDT is much higher than that condenser outlet enthalpy increment ($\Delta h3$). As ambient temperature increases, the increment rate shows opposite trend; that is the increment of condenser outlet enthalpy ($\Delta h3$) is much higher than condenser inlet enthalpy increment ($\Delta h2$). As a result, the specific enthalpy difference with WDT increases at the low temperature and decreases at the high ambient temperature. Fig. 4.4 shows heating capacity and COP variation with regard to WDT. The refrigerant heating capacity is the product of mass flow rate and enthalpy differences as shown in Eq. 4.2. The heating capacity increases with the increase of WDT. The increase at the high ambient temperature condition is considered due to the increase of mass flow rate whereas the increase of low ambient condition is due to the increase of mass flow rate and specific enthalpy differences. As WDT increases, the high pressure ratio of each cycle brings out high compressor work for each cycle.

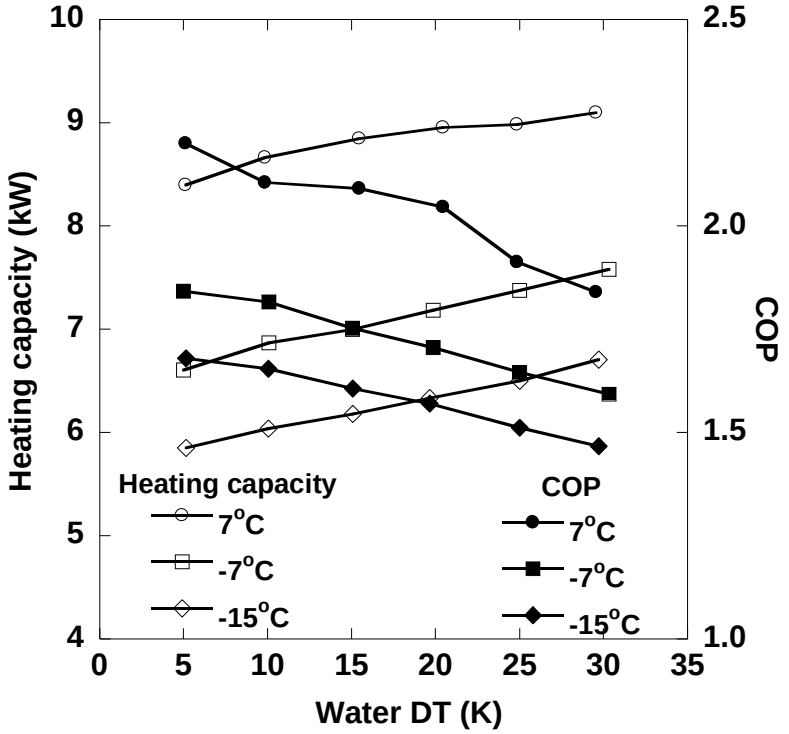

Fig. 4.4 Performance of heat pump with respect to WDT (Water inlet temperature = 40°C)

COP deteriorates as WDT increases; this is because the increase of total compressor work is larger than the increase of heating capacity. Fig. 4.5 shows the variation of approach temperature and discharge superheat with regard to WDT. The definitions of approach temperature and discharge superheat are presented in the equations (4.5) to (4.6) and shown in Fig. 4.5 (a).

$$T_{APP} = T_{r,C,out} - T_{w,C,in} \tag{4.5}$$

$$T_{Dis,SH} = T_{r,c,in} - T_{r,c,sat} \tag{4.6}$$

The approach temperature is the difference of refrigerant condenser inlet and water inlet temperature. The importance of small approach temperature has been reported from many studies (Pettersen *et al*. (1998), Nekså *et al*. (1998)). The high approach temperature brings pinch temperature which results in small temperature difference at heat exchanger. As shown in Fig. 4.5 (b), this approach temperature increases with the increase of WDT since the R134a condensing pressure increases. The smallest approach temperature was obtained at the condition of WDT 5 K which showed the highest COP. And this approach temperature increase as ambient temperature increases. This is thought that the temperature of condenser outlet at high ambient condition is higher than that of low ambient condition. However, the approach temperature showed almost the same

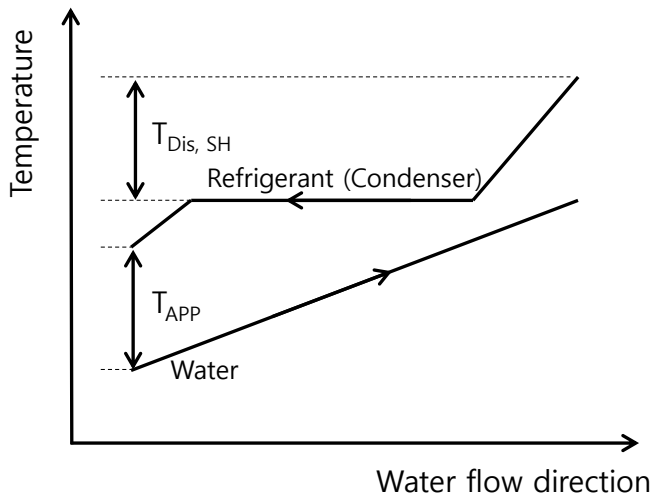

(a) Definition of approach temperature and discharge superheat

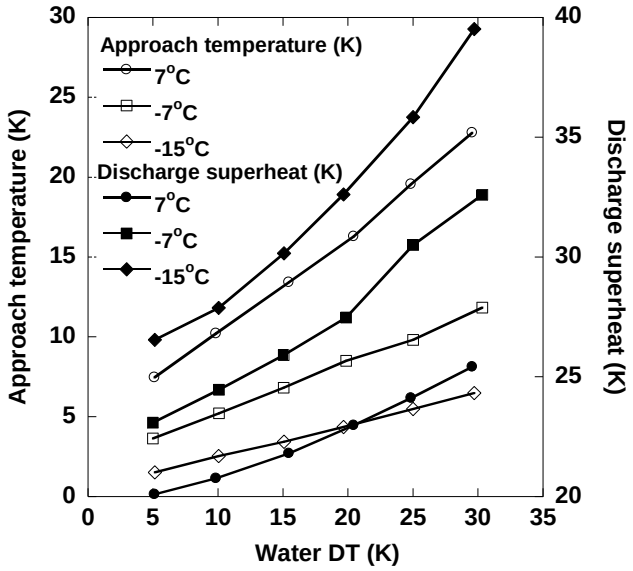

(b) Variation of approach temperature and discharge superheat

Fig. 4.5 Variation of approach temperature and discharge superheat (Water inlet temperature = 40°C)

value with respect to water inlet temperature at given WDT condition. Discharge superheat temperatures are also shown in Fig. 4.5 (b). The discharge superheat is the difference of condenser inlet and condensing saturation temperature. It is considered that high discharge superheat deteriorates the heat pump performance. The refrigerant specific heat of vapor phase decreases as discharge temperature increases that is unfavorable for heat transfer. This discharge superheat increases as ambient temperature decreases since the compressor discharge temperature increases at low ambient temperature. Figs. 4.6 (a) and (b) show the variation of heating capacity and COP with discharge water temperature at given water inlet temperatures. Heating capacity linearly increases as discharge temperature increases and this is due to the increase of mass flow rate at given ambient temperature as mentioned previously. There is not a significant variation with water inlet temperature; however, there is distinguishable variation with ambient temperature. The COP falls linearly with discharge water temperature. There is an obvious reduction in high water discharge temperature, high water inlet temperature and low ambient temperature conditions. The reason of performance reduction with high discharge temperature is the rapid rise of total compressor work. As water discharge temperature increases, increase rate of total compressor work is much higher

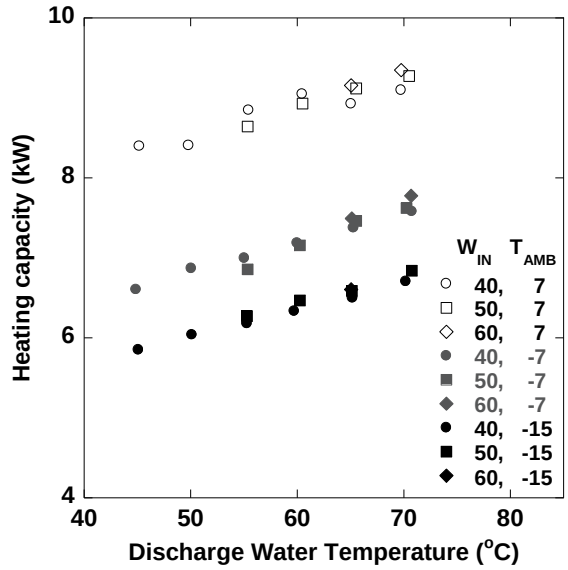

(a) Heating capacity

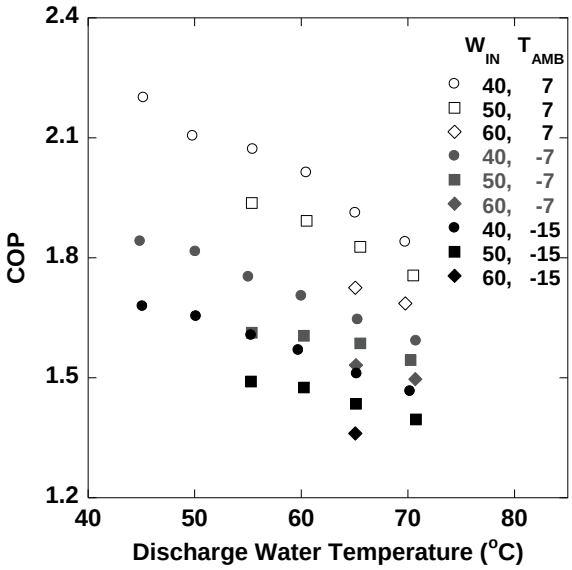

(b) COP

Fig. 4.6 The performance of heat pump with regard to water discharge temperature

than that of heating capacity. The high water inlet temperature also deteriorates the COP due to the increase of power consumption at each cycle. The same water discharge temperature condition, higher water inlet temperature requires higher power consumption at R134a cycle. For example, at the same water discharge temperature of 75^{o}C, the R134a compressor work of 40^{o}C water was 2.47 kW whereas that of 60^{o}C was 2.85 kW. The ambient temperature also affects the COP since ambient temperature determines the pressure ratio and compressor work. The total compressor work was the highest at the 7^{o}C ambient condition due to the highest mass flow rate; however, specific compressor work was the highest at the -15^{o}C condition. The specific compressor works was about 47 kJ/kg and 73 kJ/kg at the conditions of 7^{o}C and -15^{o}C ambient condition, respectively.

4.3 Effect of water temperature lift on optimum intermediate temperature

4.3.1 Optimum intermediate temperature and test conditions

In case of single cycle, the heating capacity can be controlled by two ways; controlling the compressor speed and controlling the expansion valve

opening. Both ways are in charge of controlling the heating capacity by adjusting the mass flow rate of refrigerant. However, the latter method cannot control the DSH accurately since the mass flow rate was focused on the control of heating capacity. Yet, to date, there has been little research about what and how to control the cascade heat pump. Since the cascade heat pump contains two compressors and two expansion valves at each topping and bottoming cycle, it is normally recommended that each expansion valve takes charge of controlling the DSH at each cycle and the high stage (R134a) compressor is in charge of controlling the heating capacity. And the low stage compressor (R410A) is then, in charge of optimal operation. The cascade optimal operation can be achieved by intermediate temperature which refers to the low stage (R410A) condensing temperature. The optimum intermediate temperature which minimizes total compressor work at a given test condition exists since it determines the pressure ratio at each cycle. The higher R410A condensing temperature results in higher pressure ratio of R410A whereas lower pressure ratio of R134a. On the contrary to this, the lower R410A condensing temperature results in lower pressure ratio of R410A and higher pressure ratio of R134a. Since the isentropic efficiency decreases rapidly after certain pressure ratio, the optimal intermediate temperature is the variable that maximizes the

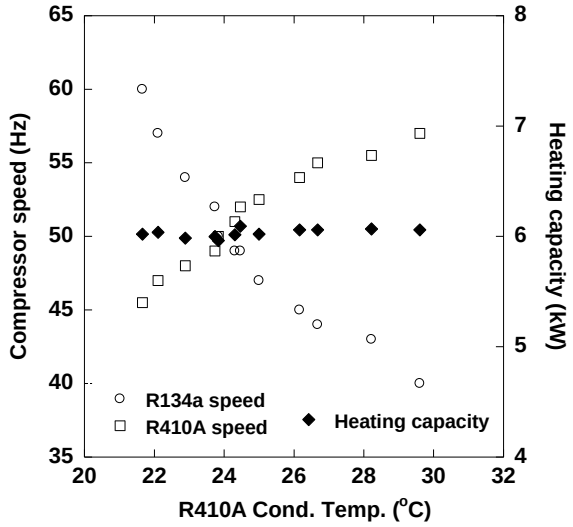

(a) Determination of heating capacity and R410A condensing temperature by compressor speed change

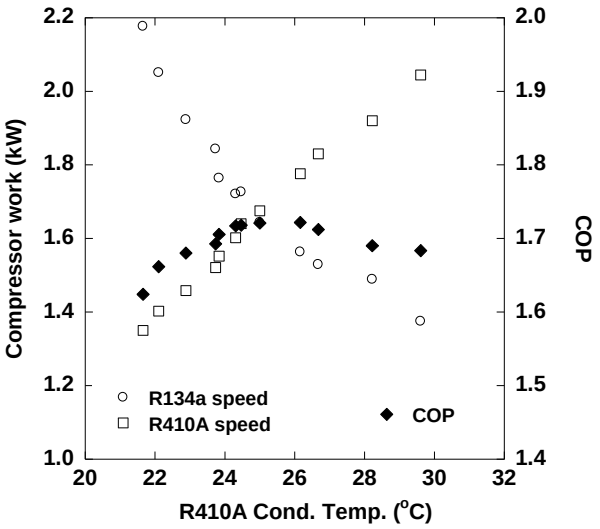

(b) Compressor work and COP variation with respect to R410A condensing temperature

Fig. 4.7 Performance variation with respect to intermediate temperature (WDT = 5 K, Water inlet temperature = 40°C)

isentropic efficiency of compressor at each cycle. In order to investigate optimal intermediate temperature with regard to WDT, several tests has been conducted. Experimental apparatus are the same as previous test that was mentioned in section 4.2; however, test conditions are different. Test conditions for optimum intermediate temperature are described in Table 4.2 (b). In order to vary the R410A condensing temperature, R410A compressor speed was controlled and in order to maintain the heating capacity, R134a compressor speed was controlled. Fig. 4.7 (a) shows how to achieve different intermediate temperature while keeping constant heating capacity. As mentioned previously, R410A condensing temperature increases as R410A compressors speed increases. Meanwhile, the R134a compressor speed was decreased to keep the same heating capacity. For example, to maintain heating capacity of 6 kW and R410A condensing temperature of 29.5^{o}C, R134a and R410A compressor speed was set as 57 and 40 Hz, respectively. Fig. 4.7 (b) shows the variation of compressor power consumption at each cycle and total system COP. As R410A condensing temperature increases, R134a compressor work decreases while R410A compressor work decreases. And, there is an optimum R410A condensing temperature which maximizes the COP. The optimal intermediate temperature is about 25^{o}C and the COP decreases rapidly after the optimal

temperature. The objective of this research is to investigate the optimal intermediate temperature with respect to WDT and water inlet temperature. The obtained optimal temperature is adopted at transient optimal operation which will be discussed in the next chapter.

4.3.2 Test results and discussion

Fig. 4.8 shows the variation of performances with respect to R410A condensing temperature. Figs. 4.8 (a) and (b) shows the test results for WDT 5 K and 15 K conditions, respectively. The COP variation shows as quadratic curve and there is an optimal intermediate temperature. The noticeable trend is that the optimal intermediate temperature increases with water inlet temperature. This is considered that increased R134a condensing pressure affected the optimal intermediate temperature. Since the R410A evaporating temperature was almost kept constant in this test conditions, the optimal R410A condensing temperature should be increased with increase of R134a condensing temperature to meet the appropriate pressure ratio at each cycle. The optimal COP also decreases as water inlet temperature increases. This is also regarded as the increase of R134a and R410A power consumption due to high pressure ratio at high water inlet temperature. Fig. 4.8 (b) shows the

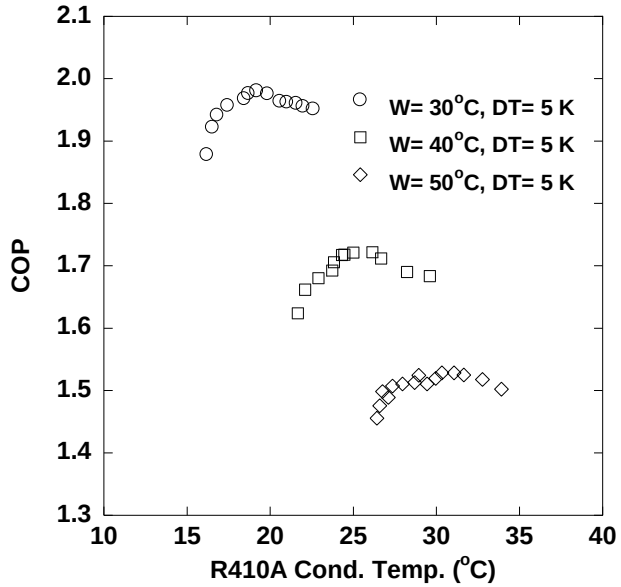

(a) Optimal intermediate temperature of WDT = 5 K condition

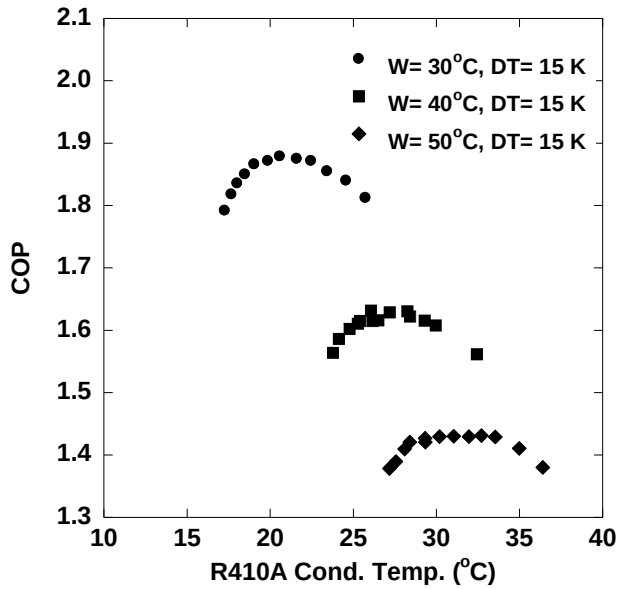

(b) Optimal intermediate temperature of WDT = 15 K condition

Fig. 4.8 Optimal intermediate temperature with regard to water inlet temperature

variation of COP at high WDT condition. As shown in Fig. 4.8 (a), optimal R410A condensing temperature increases with the increase of water inlet temperature whereas optimal COP decreases with the water inlet temperature. The higher WDT (15 K) showed lower COP at the same water inlet condition. The reason can be inferred from the previous test result that performance decreases as WDT increases. Compared to lower WDT (5 K) condition, the optimal temperature of higher WDT increased about 2~3K for the same water inlet temperature. This is also attributed to the increased optimal intermediate temperature due to the increased condensing temperature of R134a. The optimum intermediate temperature of cascade cycle has been studied from many studies (Lee *et al*. (2006), Bingming *et al*. (2009), Bhattacharyya *et al*. (2008)) and the optimal temperature has been suggested as empirical correlations or numerical equations. Most of empirical correlations and numerical equations are suggested with the variables which are the high stage condensing temperature, low stage evaporating temperature and the temperature difference between cascade heat exchanger. Though those equations do not consider the effect of water flow rate, the effect of WDT on optimal temperature is reflected in the highs stage condensing temperature. Thus, the optimal R410A temperature was compared to previous research (Eq. (3.8)).

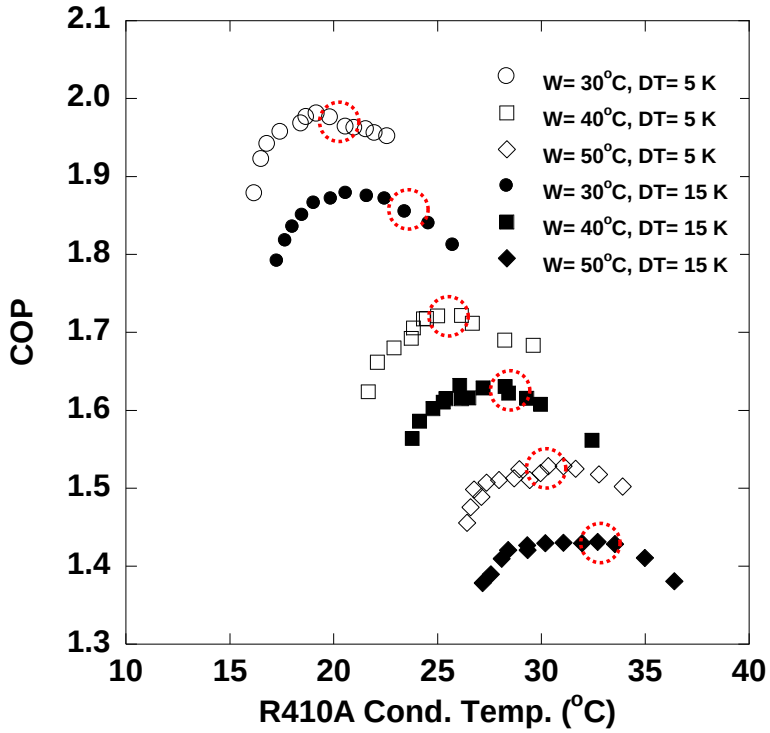

Fig. 4.9 Comparison of optimal R410A condensing temperature with previous research (Ambient= -15°C, Water inlet = 50°C)

Fig. 4.9 shows the comparison of optimal intermediate temperature with previous research. The equation predicted well the optimal temperature in six test cases, and the root mean squared error and maximum error were 0.46 K and 2.18 K, respectively. The Carnot efficiencies for each cycle were obtained by the average value during tests and the values were 0.408 and 0.357 for high and low stage, respectively. Since the previous optimum intermediate temperature equation well predicted the test results, this equation is adopted to optimal R410A control for transient heat pump performance test.

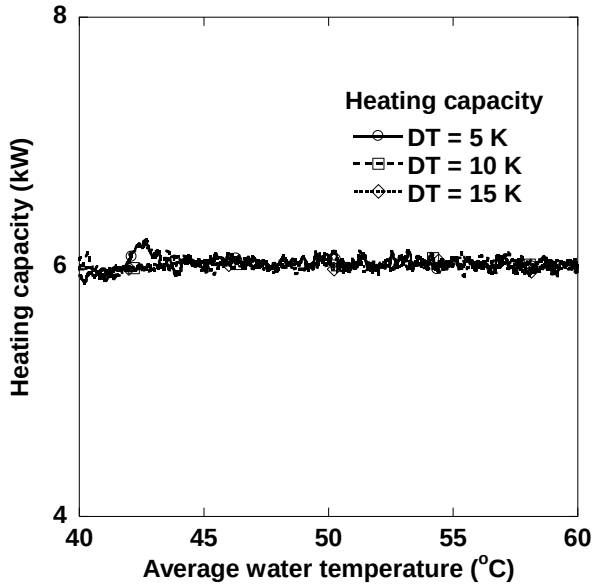

(a) Heating capacity control

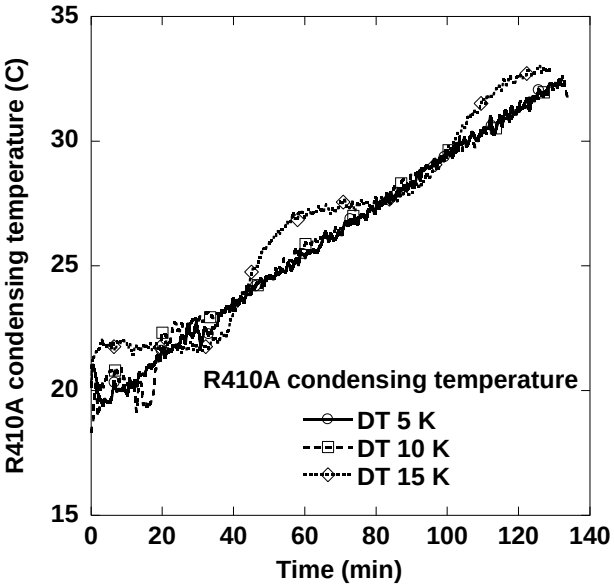

(b) R410A condensing temperature control

Fig. 4.10 Control of heating capacity and R410A condensing temperature

4.4 Effect of water temperature lift on transient performance

4.4.1 Transient heat pump performance and test conditions

As mentioned previously, there has been little information about which variables to control heating capacity and optimal operation. It is normally suggested that high stage compressor is in charge of heating capacity control and low stage compressor is in charge of optimal operation by controlling R410A condensing temperature. In this study, in order to verify the effect of WDT on heat pump transient performance during hot water charging, heating capacity and optimal R410A condensing temperature were controlled. Both heating capacity and intermediate temperature are adjusted by compressor PID controller. The controller gain is obtained by Ziegler-Nichols tuning method. Both R134a and R410A compressor controller PID gains are written in Table 4.1. Table 4.2 (c) shows the test condition and heat pump was operated at the -15^{o}C ambient temperature until the average water reservoir temperature reaches to 60^{o}C. The 5 T-types thermocouples were attached along the vertical location of water reservoir and were labelled from 1 to 5, with 1 being the lowest vertical direction. In real application of water heater heat pump, hot water from condenser enters

the top of water reservoir and cold city water is charged at the bottom of reservoir in order to maintain water stratification (Fernandez *et al*. (2010)). The heating capacity and R410A condensing temperature were controlled to keep 6 kW and Eq. (3.8), respectively and the speed of each compressor was kept in the range of 40 Hz to 60 Hz.

4.4.2 Test results and discussion

Fig. 4.10 shows the heating capacity and R410A condensing temperature variation. The R134a compressor kept heating capacities constant for each test conditions of 6 kW and the R410A compressor also controlled the target condensing temperature very well. The target intermediate temperatures are different with various WDT condition due to the difference of water inlet temperatures during hot water charging operation. Since the intermediate temperature depends on the high stage condensing temperature, the target intermediate temperature varies with water inlet temperature. The water inlet temperature varies with regard to WDT in stratified water reservoir. Fig. 4.11 shows the temperature stratification in water reservoir with WDT. In case of WDT 5 K condition, the average vertical temperatures difference (T_5-T_1) was only 0.57 K that

means the stratification is not achieved. The temperatures along the vertical direction affected by the heat transfer by water flow, heat conduction and heat loss from the tank surface (Yokoyama *et al*. (2007)). Since the water mass flow rate for WDT 5 K is high, heat transfer along the vertical direction is high and that disturbs the thermal stratification. As a result, the condenser water inlet temperature increases linearly with time and the target intermediate temperature increases linearly shown in Fig. 4.10 (b). However, stratification well occurred at the condition of WDT equal to 15 K and the vertical temperature difference (T_5-T_1) was about 10 K. Since the heat transfer by the water flow is low, the heat propagation along the vertical direction was negligible. The stratification affects the condenser water inlet temperature behavior that is kept constant to some extent then increases and this behavior recurred during hot water charging. As a result, the R410A target condensing temperature shows similar trend with water inlet temperature. And the inlet temperature behavior also affects the heat pump transient performances.

Fig. 4.12 shows the transient performance during hot water charging from 30^{o}C to 60^{o}C. Fig. 4.12 (a) shows the variation of COP with time and COP deteriorates as water temperature increases. The COP variation for WDT of 5 K and WDT of 10 K is similar since the water inlet temperature

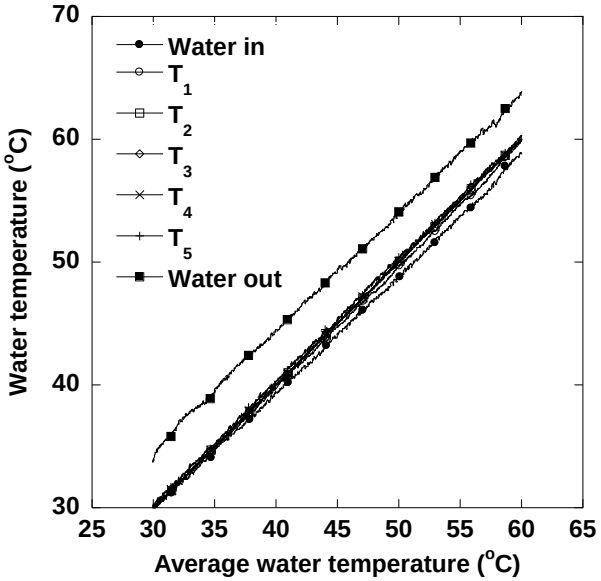

(a) WDT=5 K

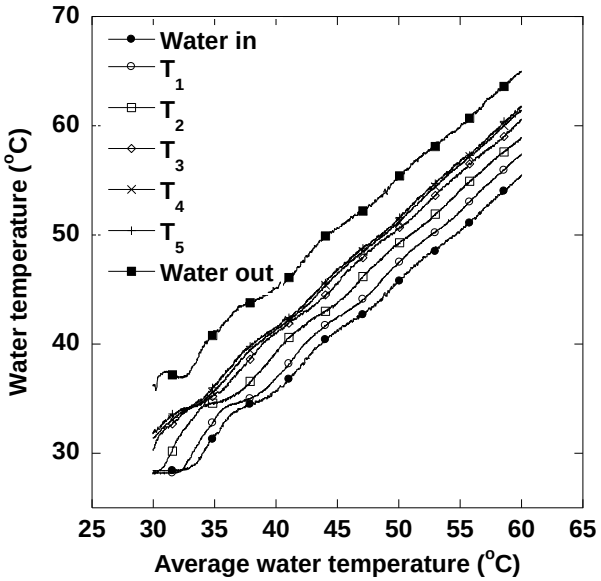

(b) WDT=10 K

Fig. 4.11 Water temperature profile with regard to different WDT (continued)

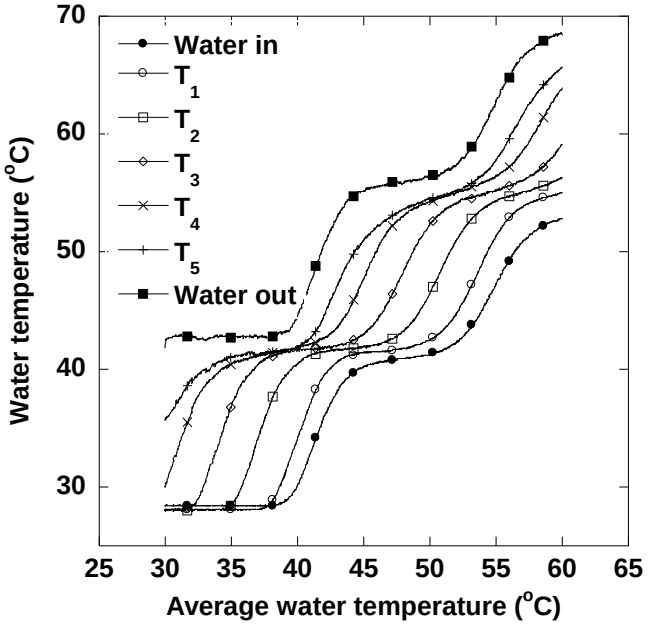

(c) WDT=10 K

Fig. 4.11 Water temperature profile with regard to different WDT

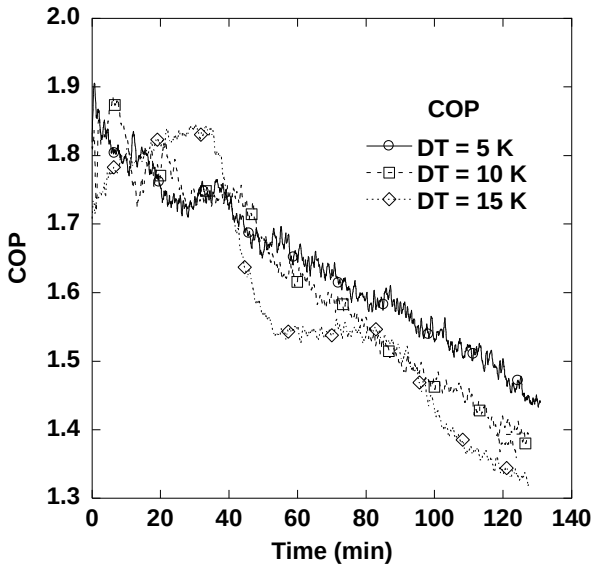

(a) WDT=5 K

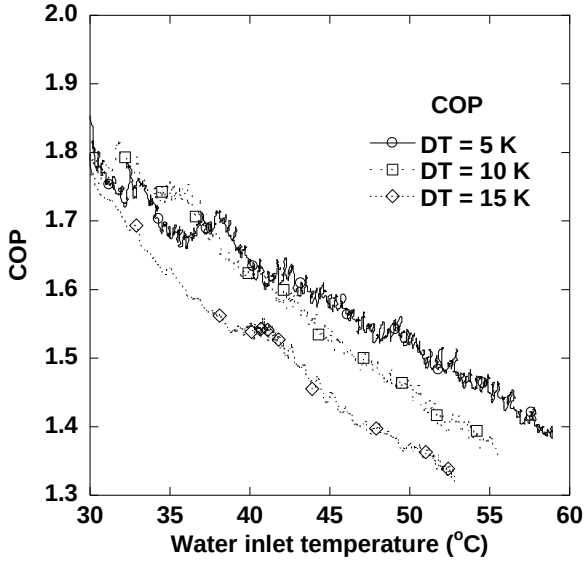

(b) WDT=10 K

Fig. 4.12 Variation of transient performance with various WDT conditions

profile showed similar tendency shown in Figs. 4.11 (a) and (b). The COP decreases linearly as time goes by and this is due to the increase of compressor power consumption at given ambient temperature. The COP variation for WDT of 15 K is quite interesting since COP increases to some extent and decreases rapidly. This is due to the variation of condenser water inlet temperature which is shown in Fig. 4.11 (c). Condenser water inlet temperature which is the temperature of water out in Fig. 4.11 was kept constant to some extent and increases. Fig. 4.12 (b) shows the variation of performance with respect to water inlet temperature and the effect of WDT on transient performance. There showed a significant effect of WDT at the same water inlet temperature and this is due to the increase of high and low stage power consumption.

4.5 Conclusion

The rapid hot water supply is required for the heat pump initial operation and the high water discharge temperature can be obtained by controlling the mass flow rate of water. The effect of water mass flow rate on cascade heat pump in terms of pressure and temperature variation was dealt in this study. There were increases of saturation temperatures with regard to

WDT except for low stage evaporating temperature. In contrast with single stage cycle characteristics, the evaporating temperature of high stage increases as WDT increases. High evaporating temperature leads high compressor inlet density of R134a and the mass flow rate of R134a increases with water temperature lift. As a results, heating capacity increases with regard to water temperature lift. However, due to the increases of discharge temperature, discharge superheat and pressure ratio, COP deteriorates. The cascade cycle can be optimized by controlling R410A condensing temperature which determines the pressure ratio at each cycle. The optimal R410A condensing temperature variation with regard to water temperature lift also conducted in this study. The experimental optimal temperature was compared with correlation and showed good accordance with correlation. The obtained optimal temperature was adopted for transient water charging operation and the effect of water temperature lift on transient performance was studied. The water temperature lift affected the thermal distribution of water reservoir and thermal distribution determined the transient COP.

Chapter 5. Cascade heat pump control

5.1 Introduction

The recent advance of a variable speed compressor technology opened up new possibilities for improving system performance and energy efficiency. The compressor speed and expansion valve openings can be continuously adjusted in order to obtain a desired capacity and high coefficient of performance. For high performance and efficiency, proper methods of operation of the driving units have been investigated by many researchers. Several attempts have been made to apply modern linear control theory to the heat pump systems.

Ohgata *et al.* (1997) constructed a robust controller for an absorption heat pump system. They linearized the nonlinear system equation at each step. Shah *et al.* (2004) applied a multivariable adaptive control strategy to a typical automotive air conditioning system. An experimentally validated the physical model was presented and recursive identification was carried out to obtain an equivalent discrete-time state space model of the system. Linear quadratic regulator (LQR) design was implemented with the objectives of reference tracking and disturbance rejection.

The proper identification of nonlinear system is the key factor for developing a controller through linear theories since the unknown dynamics of linear model may make the system repose unstable (Makila and Partington, 2003). Because heat pump system is highly nonlinear system, a lot of approximation methods were developed to simplify the system dynamics by integrating the governing equations or assuming the temperature disturbances. Experimental methods were also developed which consider the system as a black box and find the system model by input/output data. Albert *et al.* (1995) developed a new controller based on the system identification. A simulation model for a practical air-handling system was developed and its behaviors under a conventional system of PID controllers and new controller were studied. Sousa *et al.* (1997) presented a method of designing a nonlinear predictive controller based on a fuzzy model. The Takagi-Sugeno fuzzy model was used for representing nonlinear dynamics of system. The fuzzy model was incorporated as a predictor in a nonlinear model-based predictive controller, using the internal model control scheme to compensate for disturbance and modeling errors. The conventional controller of the heat pump system consists of two independent single-input single-output (SISO) controller; one is for the desired capacity and the other is for a high COP. Lee (2006) made a controller with optimized

fuzzy controller with genetic algorithm, where controller was consisted of two independent loops. Expansion valve was modulated by expansion valve using fuzzy control, and compressor speed was modulated by PID controller. Degree of superheat at the compressor discharge and outlet temperature of secondary fluid in evaporator were selected as control variables.

In this study, for the control optimization of cascade heat pump which has two compressors and two expansion valves has been suggested. System model was generated through system identification, and pseudo-random binary sequences (PRBS) were used as an input signal. Genetic algorithm was selected for the optimization method of controller. Optimized PI controller was constructed and verified conventional controller.

5.2 System identification

To evaluate and construct an optimal controller, system identification should be carried out. By the system identification, the transient characteristics required to build mathematical models of dynamic systems are obtained based on measured data from the systems. The techniques of system identification for diverse dynamic systems have a wide application area.

5.2.1 Input signal for the system identification

The design of an identification method includes several choices; which singnals to measure, when to measure them, which signals to manipulate, and how to manipulate them. It also includes some more practical aspects, such as how to generate the signal before sampling and how to process them afterwards. The pseudo-random binary sequences (PRBS), also called as a M-sequences, have a wide variety of application in system identification field. A pseudo-random is not random, as the name implies, however, it has many properties of a random sequence. The pseudo-random binary sequences have the following properties.

(a) The signal is periodic, with period T, and can take on only values +a or –a. Changes between values +a and –a take place only at interger fractions of T.

(b) The difference in the number of +a and –a states does not exceed one.

The pseudo-random binary sequence is generate using a linear feedback shift register. The m-element shift register is initially loaded with ‘1’ and produces an output sequence. The modulo-2 addition changes the input sequences as a function of the current shift-register value. Many different sequences are possible depending on which of the feedback elements are fed

back to the input. The maximum length of the output, N, is 2^m-1. Fig. 5.1 and Fig. 5.2 show a pseudo random sequence generator and its example for a 3-element case.

Digital data which consists of ‘1’ and ‘0’ are line-coded into a pulse train according to a signaling scheme. The most widely used scheme is polar signaling in which a positive pulse is transmitted for a ‘1’ and negative pulse for a ‘0’. The number of element, m, is determined by maximum length of signal, N. Rasmussen *et al.* (2005) derived 11th-order nonlinear dynamic model for a transcritical vapor compression system. Then, the model is reduced to the 5th-order dynamic model for the multivariable controller design. Since there are four inputs, which are two compressor speeds for each cycle and two expansion valve openings for each cycles are used in the system, the minimum value of element becomes ‘6’ in this study. The sampling time is 5 seconds

The system variations by the PRBS signal input are presented in Figure 5.3. The inlet temperature and mass flow rate of water were fixed during the experiment. The corresponding value of R410A expansion valve input for ‘1’ is 60 and for ‘0’ is 15. The corresponding value of R134a expansion valve input for ‘1’ is 11.5 and for ‘0’ is 9.5. The input speed of compressor for each cycle is shifted between 45 and 55 Hz.

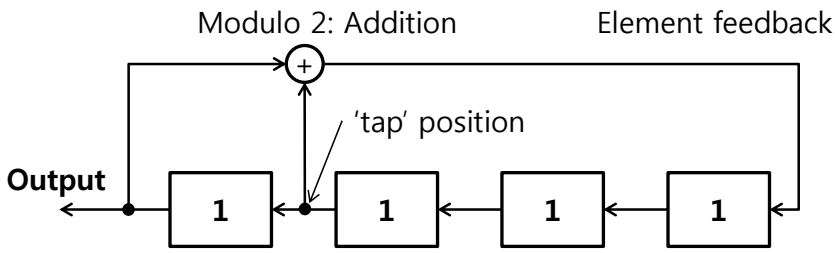

Fig. 5.1 The example of pseudo random binary sequence (PRBS) generator

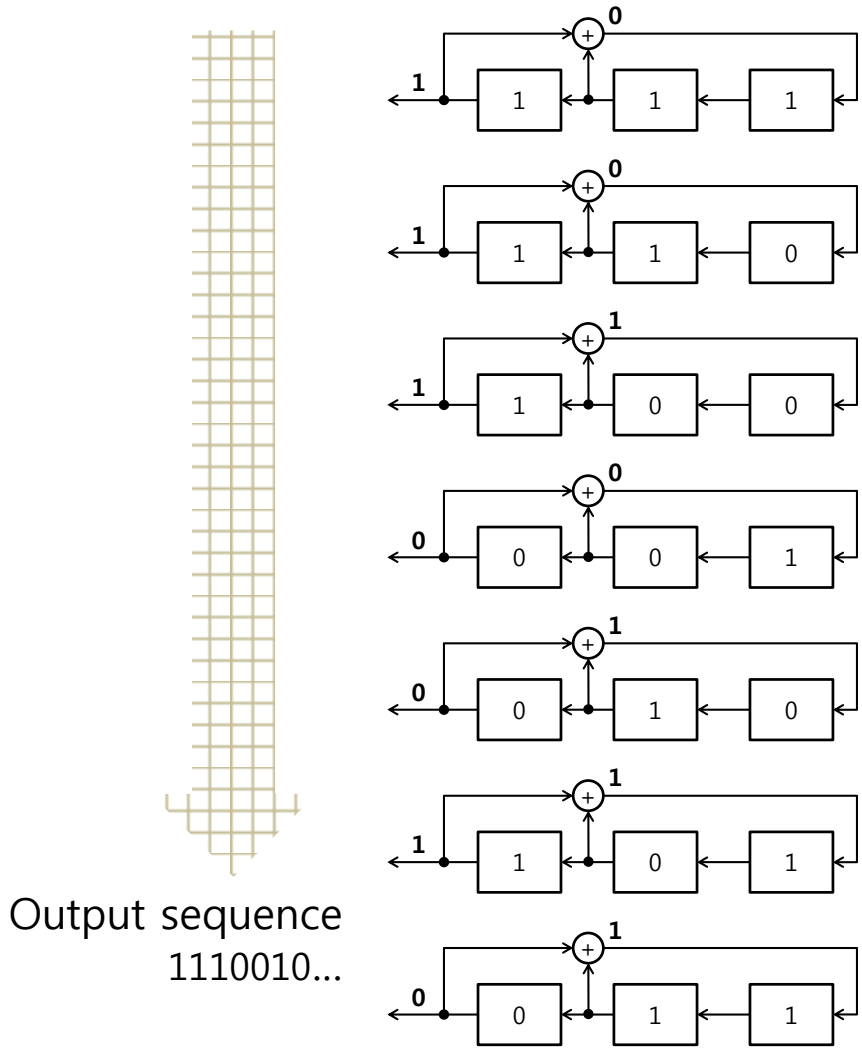

Fig. 5.2 The example of signal generation process for 3-element case

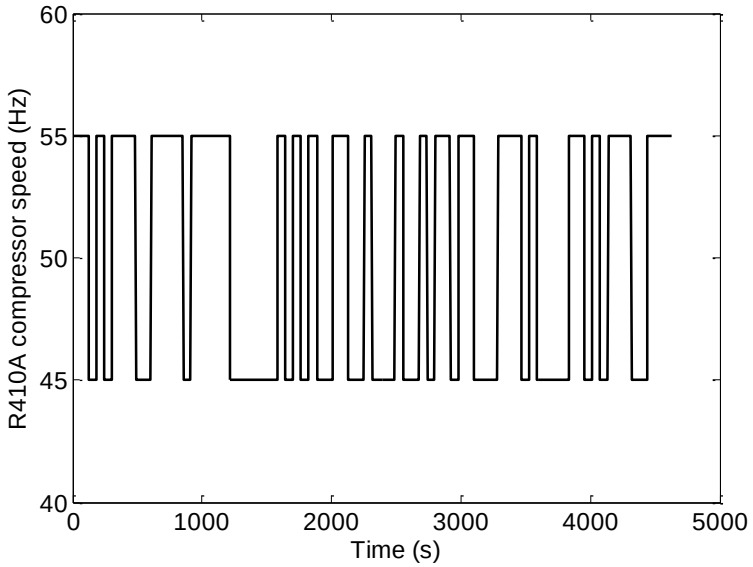

(a) Input signal to R410A compressor

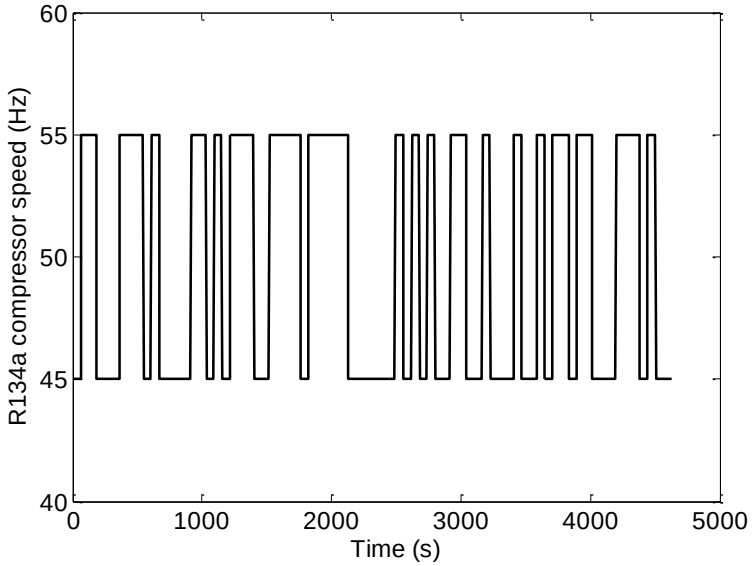

(b) Input signal to R134a compressor

Fig. 5.3 System variables variation when the input signals are changed according to PRBS (continued)

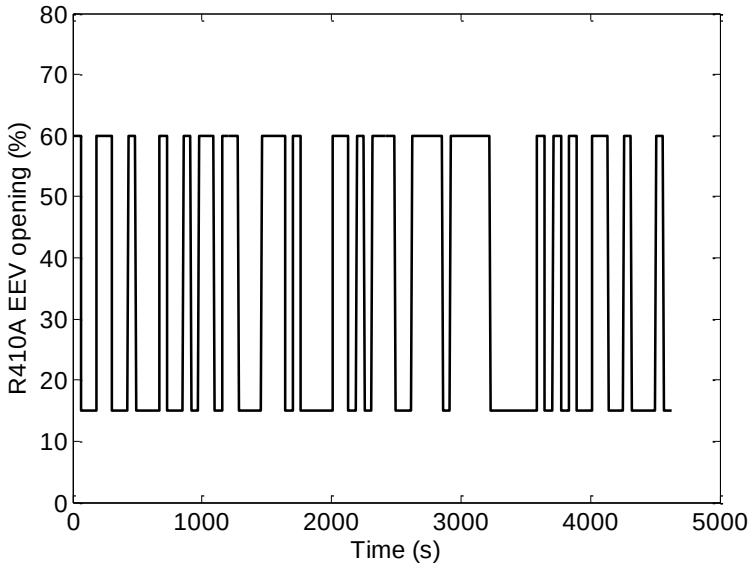

(c) Input signal to R410A expansion valve

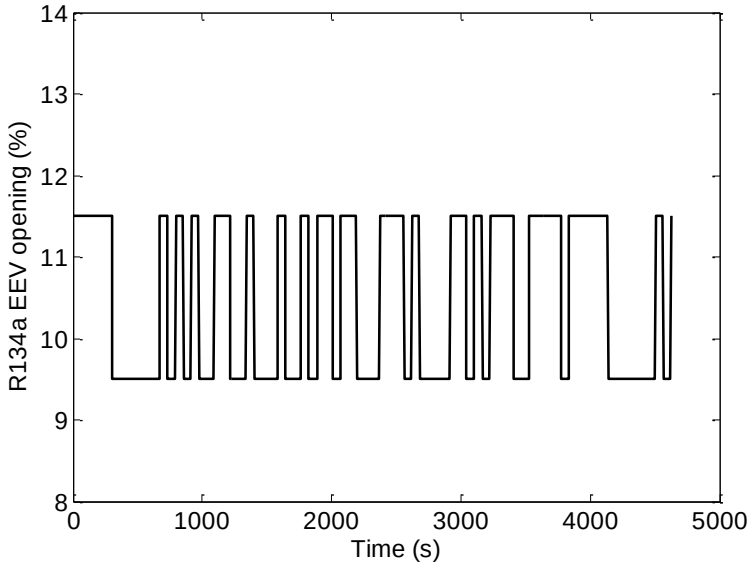

(d) Input signal to R134a expansion valve

Fig. 5.3 System variables variation when the input signals are changed according to PRBS (continued)

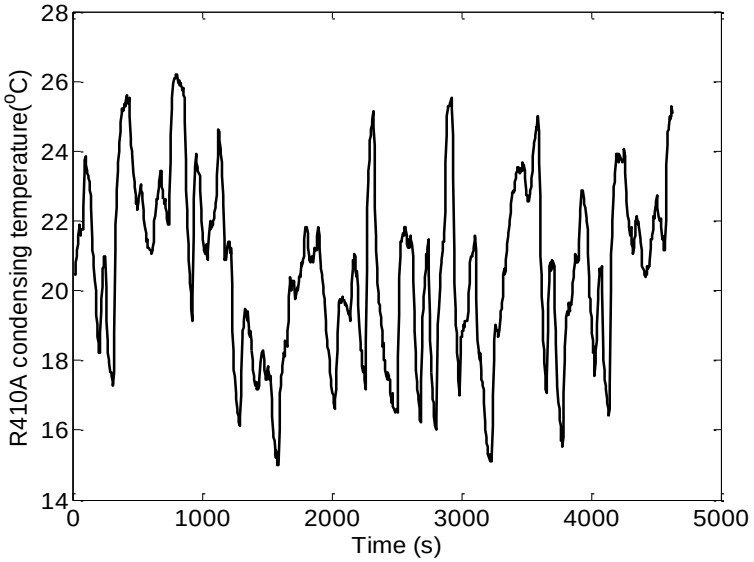

(e) Output signal of R410A condensing temperature

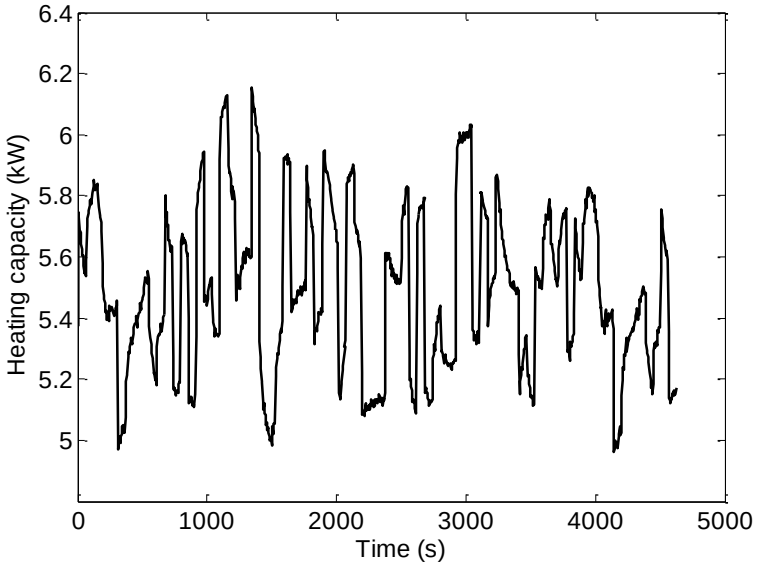

(f) Output signal of heating capacity

Fig. 5.3 System variables variation when the input signals are changed according to PRBS (continued)

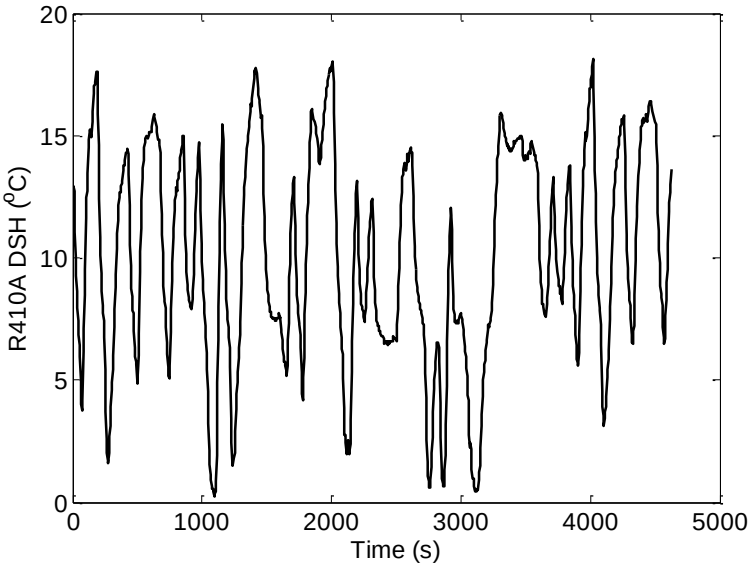

(g) Output signal of R410A degree of superheat

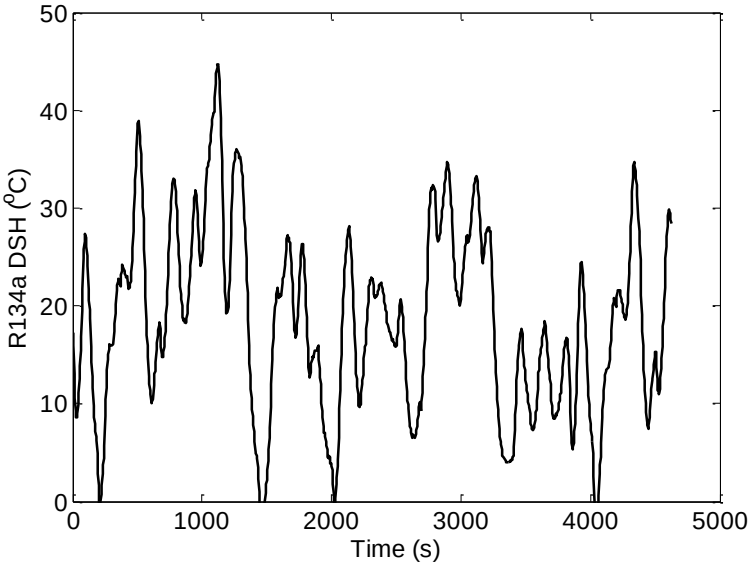

(h) Output signal of R134a degree of superheat

Fig. 5.3 System variables variation when the input signals are changed according to PRBS

5.2.2 System model determination

For the determination of system model, state-space model is adopted. The basic state-space model for the discrete-time is described as shown in Eq. (5.1) and Eq. (5.2).

$$x(t+Ts) = Ax(t) + Bu(t) + Ke(t) \tag{5.1}$$

$$y(t) = Cx(t) + Du(t) + e(t) \tag{5.2}$$

The inputs of this system are compressor speed and expansion valve opeing for high and low stage cycles, and outputs of this system are heating capacity, R410A condensing temperature, R134a and R410A degree of superheats at the compressor inlet. Subspace approach is used for estimating the state-space model parameters using measured input-output data. The aim of the subspace method is the estimation of A, B, C, and D matrixes (Favoreel *et al* (1999)). Firstly, the order of the model is determined from a singular value plot. After the model order has been chosen, a generalized observability matrix is generated in order to estimate the state sequence from the input-output data. Finally, by using the input, output and state sequence, the system matrices are estimated by a linear regression procedure. Matlab 'ident' toolbox which is shown in Fig. 5.4 was used to process the input data. The number of state variable is assumed as 9. The obtained system model is

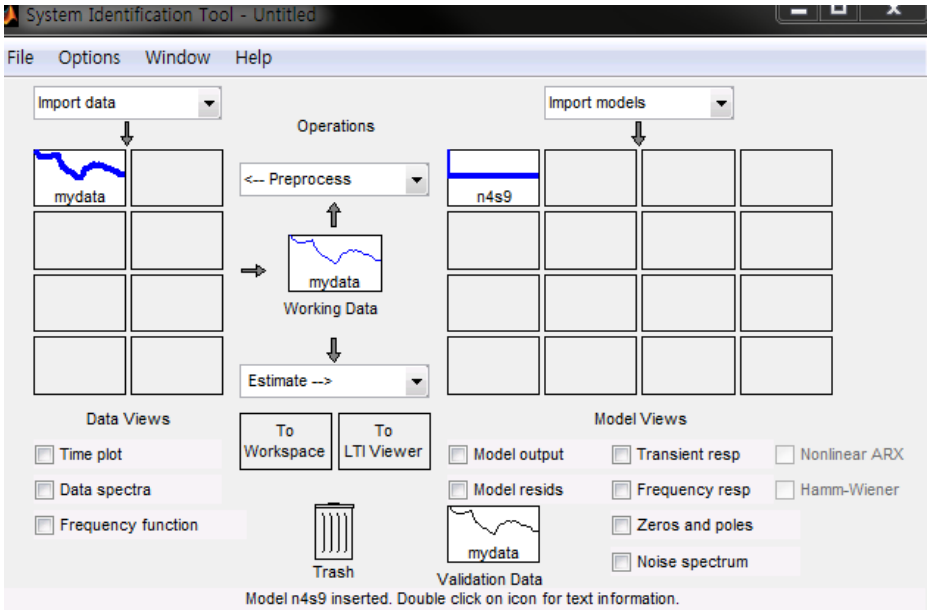

Fig. 5.4 System identification toolbox in Matlab

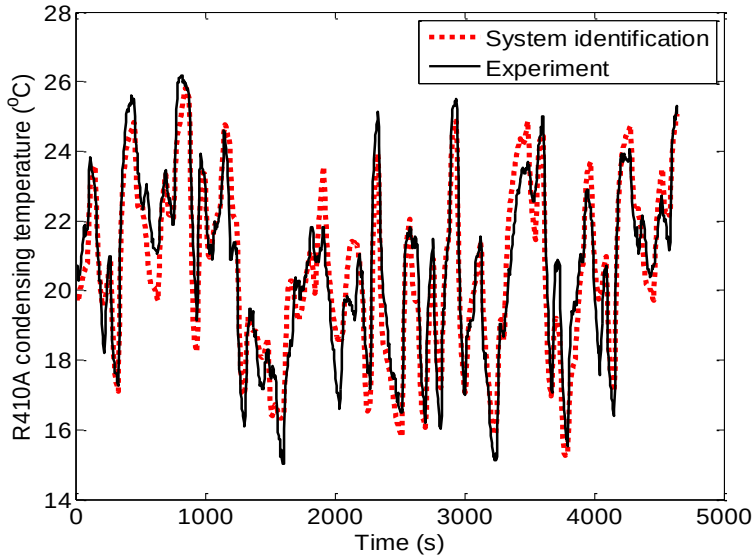

(a) Output signal of R410A compressor

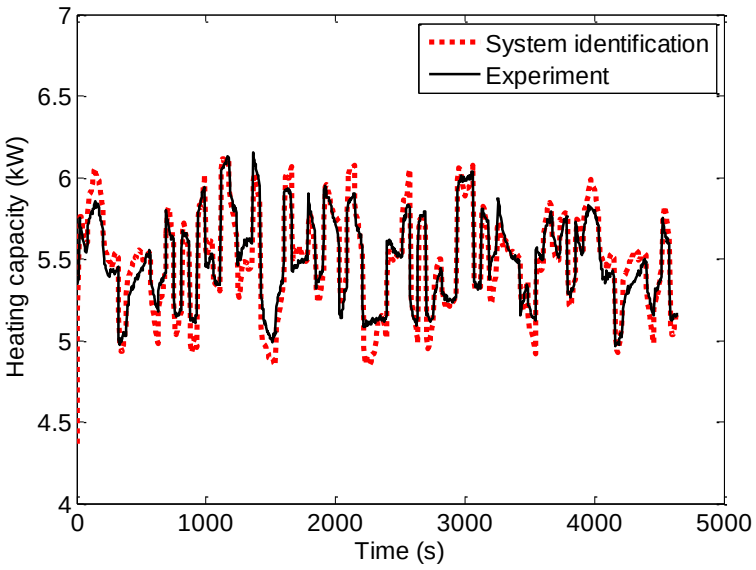

(b) Output signal of R134a compressor

Fig. 5.5 Comparison of system identification results and experiment data (continued)

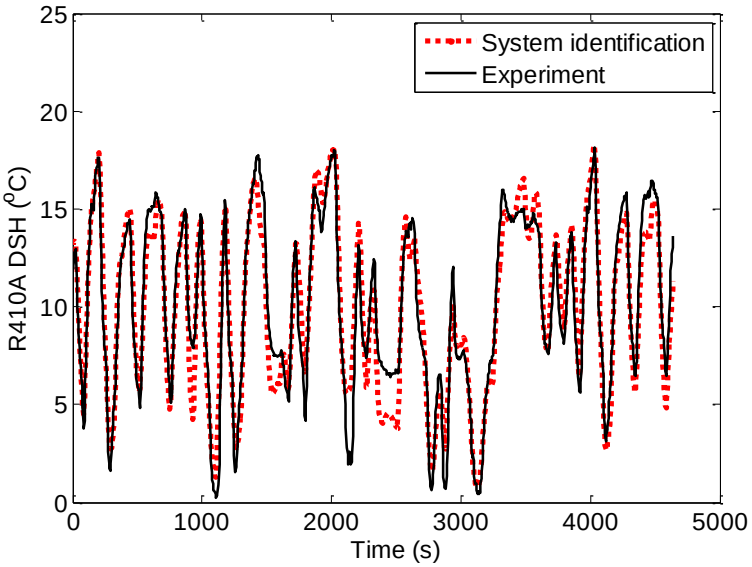

(c) Output signal of R410A expansion valve

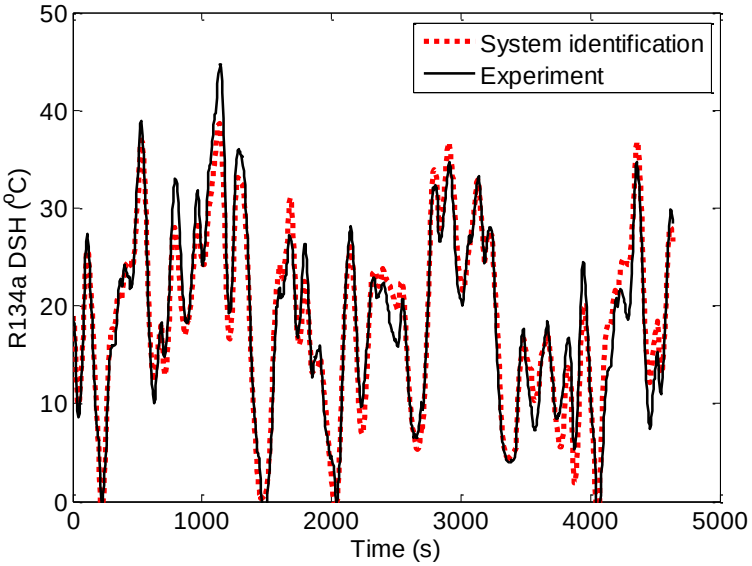

(d) Output signal of R134a expansion valve

Fig. 5.5 Comparison of system identification results and experiment data

controllable and observable system, that is the controllability matrix and observability matrix are full rank. Fig. 5.5 shows comparison of the experimental data and system identification results. The system model simulated by system identification predicts the behavior of real system well.

5.3 Optimization of controller with genetic algorithm

In this study, proportional – integral (PI) control logic is selected for the controller. Control target of cascade heat pump system is to obtain the highest efficiency while desired capacity is satisfied shown in Eq. (5.3).

$$\frac{1}{T}\int_{T}\dot{W}dt = \text{Minimum @ } \dot{Q} = \text{Load required} \tag{5.3}$$

The highest efficiency can be obtained when R410A condensing temperature operated at optimal R410A temperature while satisfying the target heating capacity. The maximum efficiency can be also obtained by regulating the degree of superheat at the evaporator to be zero. As the degree of superheat increase above zero, the power consumption increases due to deteriorated isentropic efficiency. Reversely, if the degree of superheat decreases below zero, the compressor performance will be degraded due to the entrainment of liquid refrigerant into the compressor. To enhance the compressor efficiency and to ensure the safety at the compressor the degree

of superheat should be controlled as low as possible. In this study, the degree of superheat at compressor was controlled about 5 K.

The tuning of controller is essential since system is unstable if proper tuning is no applied. The generic algorithm is used for the optimization of the PI controller.

Genetic algorithm (GA) is a search algorithm based on the mechanics of natural genetics. It uses operation found in natural genetics to guide its track through the search space (Phillips *et al*., 1996). Genetic algorithm searches answer through large spaces of solution quickly, requiring only information on objective function value to guide the search. This is an inviting characteristic since the majority of commonly used search techniques require derivative information, continuity of the search space, or complete knowledge of the objective function to guide their search.

Basic operator of genetic algorithm is cross-over, mutation and selection. Cross-over is mixing operator which mixes two chromosomes to offspring new one. After the evaluation of object function, several possible guesses are selected, and new possible guesses are generated by cross-over with combining superior parts of previous guesses. Mutation is used to introduce a new gene which the parent chromosomes do not have. Mutation operator sometimes can make a more possible solution which is not possible

by only cross-over. The last operator selection process as it implies. Since genetic algorithm is a kind of statistical method, there always exists a possibility to miss a genuine solution by the operation of cross-over and mutation. Thus, unlike other methods such as least square method, the solutions that do not minimized or maximize the object function should be selected sometimes.

The general search step of genetic algorithm is shown in Fig. 5.6. To find a solution, initial guess is necessary at the beginning of calculation. Then, fitness is evaluated by the objective function. Several guesses which have a possibility for genuine solution are selected and new possible guesses are generated by cross-over and mutation. If the value of objective function reaches target value, calculation is terminated. If it is not at optimum, next generation of solution is generated by genetic algorithm operators.

Genetic algorithm was used to find 8 gain values in the PI controller. For the optimization of gain values, objective function is essential. In this study, objective function for the simulation was generated by system identification as described in section 5.2. Simulation program to optimize PI controller is presented in Fig. 5.7. Genetic algorithm finds the solution which minimizes the value of objective function. Objective function which is shown in Eq. (5.4) is defined as integration of difference between target

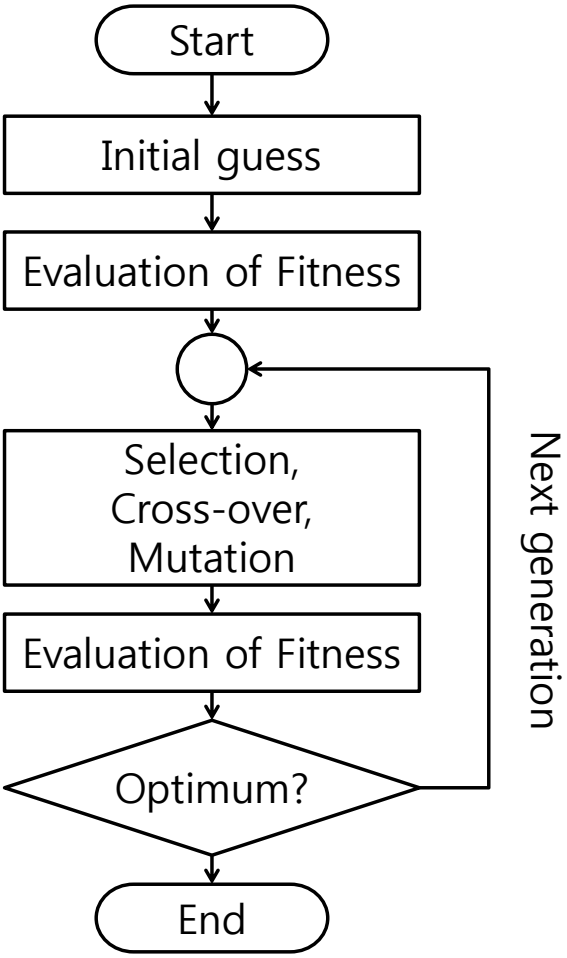

Fig. 5.6 General search steps of the genetic algorithm

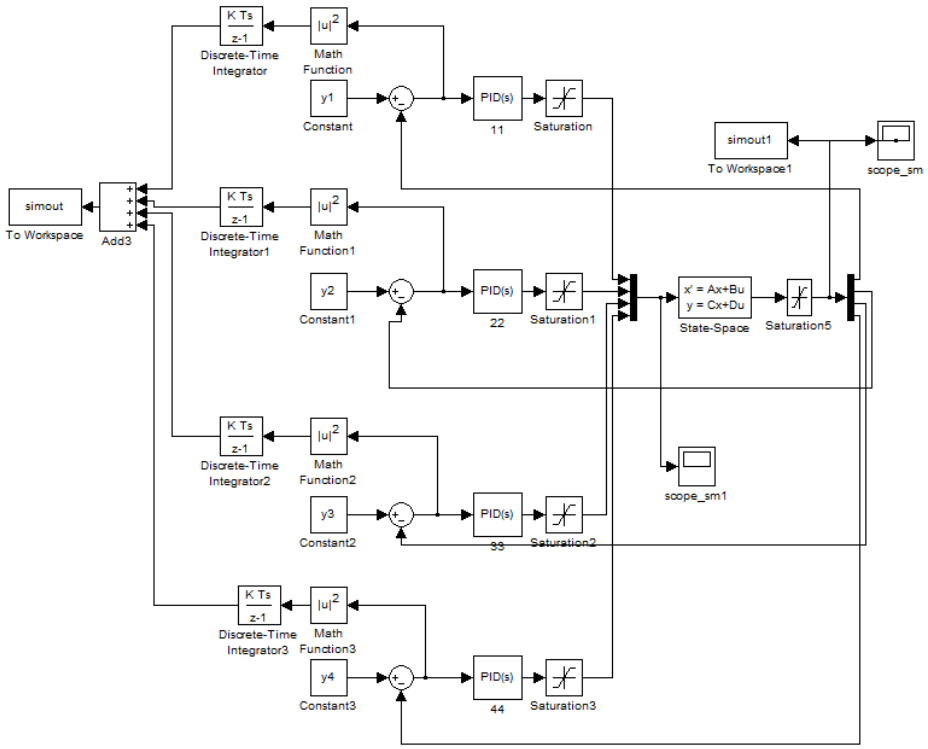

Fig. 5.7 Simulation program for optimization of PI controller

value and current value from t=o to t=2000 sec.

$$f_{object} = \int_{o}^{t_{set}} \left(\left| x_{set} - x_{measured} \right|^2 \right) dt \tag{5.4}$$

The initial population of genetic algorithm is 200, and the calculation was carried out for 200 generation. Evaluated proportional gains and integral gains are shown in Eq. (5.5) and Eq. (5.6), respectively where j means the control target.

$$k_{p-GA,j} = \left[19.54; 8.39; -26.23; -19.02 \right] \tag{5.5}$$

$$k_{i-GA,j} = \left[0.446; 0.259; -0.039; -0.984 \right] \tag{5.6}$$

Control target one to four are the R410A condensing temperatures, heating capacity, R410A degree of superheat and R134a degree of super heat. From Eq.(5.5) and Eq. (5.6), a plus sign gain $k_{1,2}$ mean control inputs should be increased to meet the control target whereas a minus sign gain $k_{3,4}$ mean control input should be decreased to meet the control target. For example, R410A and R134a compressor speed should be increased to increase the R410A condensing temperature and heating capacity, respectively. In contrast, R410A and R134a expansion valve opening should be decreased to increase the degree of superheat at each cycle, respectively.

5.4 Performance of optimized PI controller

5.4.1 Transient performance of cascade heat pump

Transient performance of cascade heat pump when the target heating capacity varies was studied. In order to meet the required heating capacity, the R134a compressor speed was varied. Figs. 5.8 (a) and (b) show the saturation temperature variation when the target heating capacity was increased. To increase the heating capacity, the R134a compressor speed increases and that results higher temperature difference of condensing temperature and evaporating temperature. Since the R134a and R410A cycle is coupled in cascade heat exchanger, the decrease of R134a evaporating temperature brings about decrease of R410A condensing temperature. Then in order to control the optimal intermediate temperature, R410A compressor speed increases. Figs. 5.8 (c) and (d) present the variation of control inputs during the transient performance. EEV opening of each cycle is increased in order to control the DSH since the mass flow rate of each cycle was increased. Fig. 5.9 shows the variation of each cycle saturation temperatures and control inputs when the target heating capacity was decreased. The R134a and R410A compressor speed decreased and the opening of each EEV also decreased in order to control heating capacity and DSH.

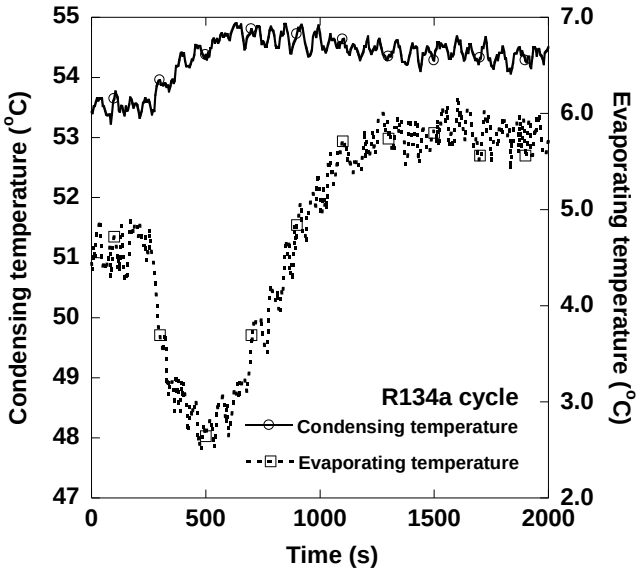

(a) R134a saturation temperature variation

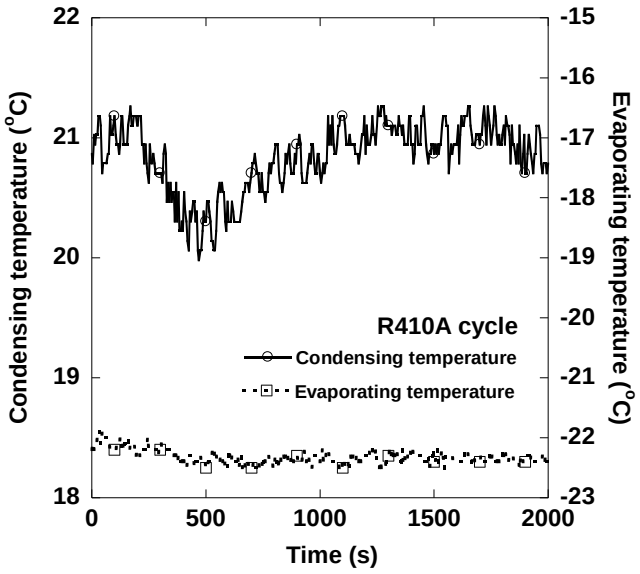

(b) R134a saturation temperature variation

Fig. 5.8 Performance of saturation temperatures and control inputs when target heating capacity increases (continued)

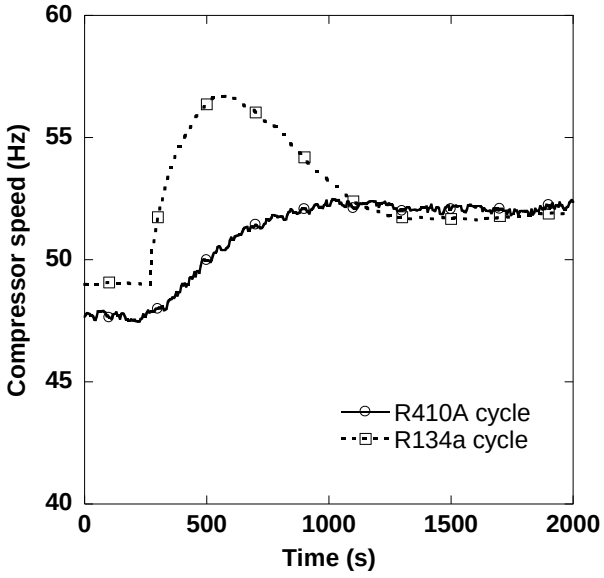

(c) Compressor speed variation

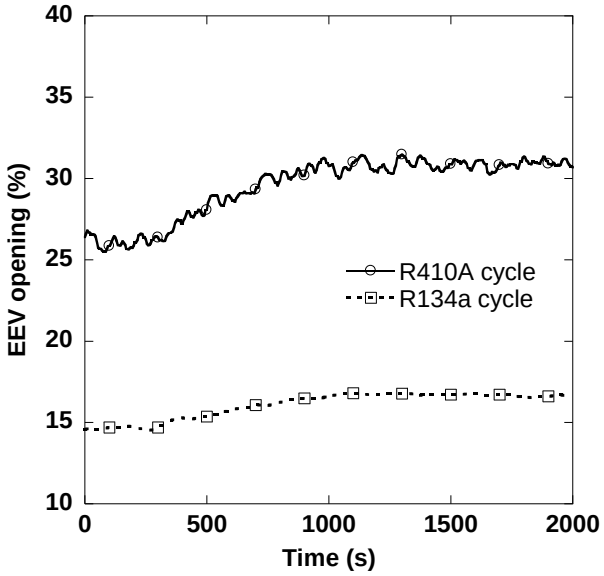

(d) EEV opening variation

Fig. 5.8 Performance of saturation temperatures and control inputs when target heating capacity increases

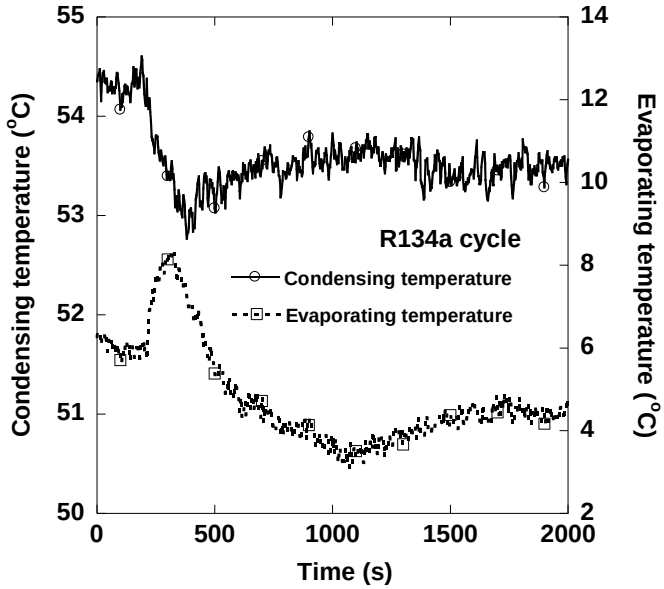

(a) R134a saturation temperature variation

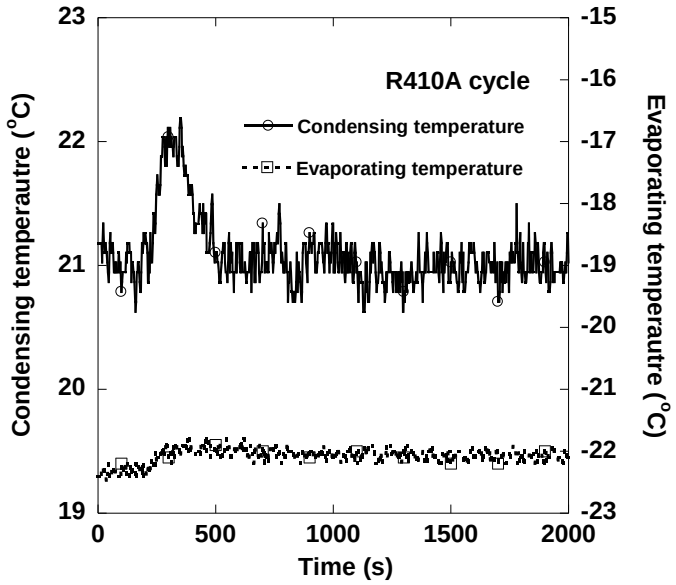

(b) R134a saturation temperature variation

Fig. 5.9 Performance of saturation temperatures and control inputs when target heating capacity decreases (continued)

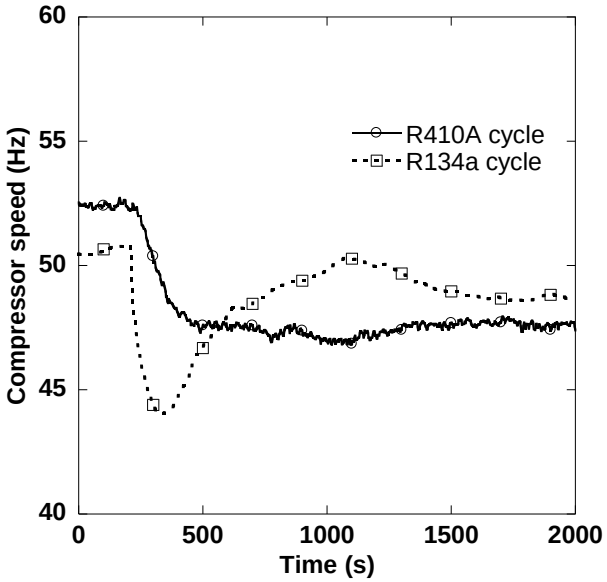

(c) Compressor speed variation

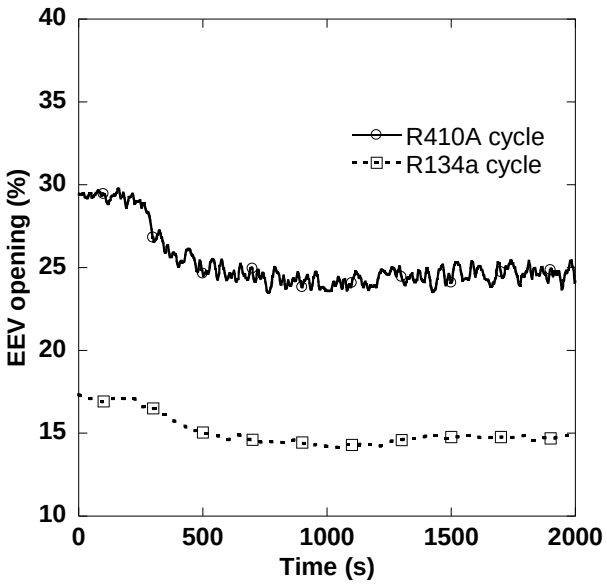

(d) EEV opening variation

Fig. 5.9 Performance of saturation temperatures and control inputs when target heating capacity decreases

5.4.2 Ziegler-Nichols PI controller

The most common classical controller tuning method is the Ziegler-Nichols for PID controller. The Ziegler-Nichols method is a heuristic method of tuning and was developed in 1942. It is performed by setting I and D gains to zero and increases P gains until it reaches the ultimate gain k_{u} at which the output signal oscillates with a constant amplitude. Then, ultimate gain (k_{u}) and oscillation period t_{u} are used to set P, I, D gains depending on the type of controller. The gains for Ziegler-Nichols PI controller is presented in Eq. (5.7).

$$\begin{aligned} k_{p,\mathrm{ZN}} &= 0.5k_u \\ k_{i,\mathrm{ZN}} &= 1.2\frac{k_{p,\mathrm{ZN}}}{t_u} \end{aligned} \tag{5.7}$$

Ziegler-Nichols tuning based controller for cascade heat pump requires four control variables tunings to find optimum gains. Eq. (5.8) and (5.9) shows the obtained gain for cascade heat pump.

$$k_{p-ZN,j} = \left[1.54; 9.21; -3.04; -7.14\right] \tag{5.8}$$

$$k_{i-ZN,j} = \left[0.111; 0.833; -0.041; -0.587\right] \tag{5.9}$$

As previously mentioned, a plus sign gain $k_{1,2}$ mean control inputs should be increased to meet the control target whereas a minus sign gain

$k_{3,4}$ mean control input should be decreased to meet the control target.

5.4.3 Genetic algorithm PI controller

There are two criteria to evaluate the performance of controller. The first one is overshoot. Overshoot is defined as the transitory value of the parameter that exceeds the final (steady state) value during the transition of any parameter from one value to another. If the overshoot is excessive, system takes much time to reach to reach its steady state. Settling time is defined as required time that the transitory value reaches at certain percent compared to steady state value.

Performance test was carried out with ZN controller and GA controller. Fig. 5.10 represents the results of ZN controller and GA controller when the target heating capacity was kept at 5.5 kW initially and at certain time it was set to 6.5 kW. The control variable R134a DSH increases rapidly with the increase of heating capacity and this is due to the decrease of R134a evaporating temperature. Due to the decrease of R134a compressor inlet density, the mass flow rate of R134a decreases and therefore, the DSH increases at a given expansion valve opening. In order to meet the R134a DSH, the opening of R134a EEV increases. The R134a compressor speed increases rapidly to meet the target heating capacity.

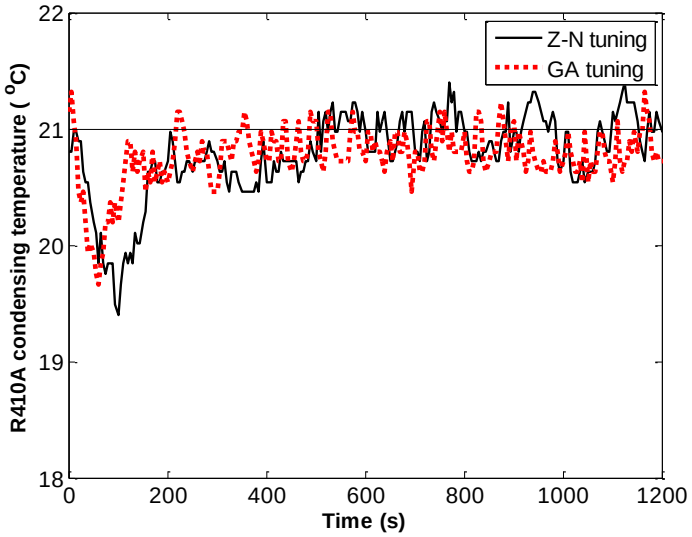

(a) R410A condensing temperature

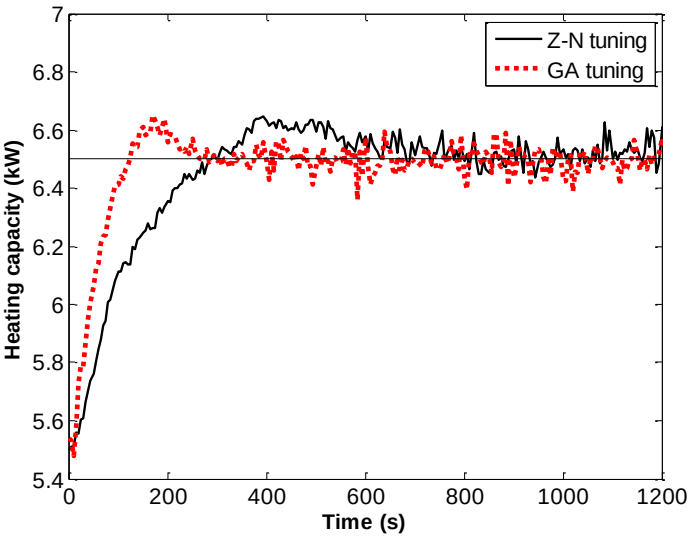

(b) Heating capacity

Fig. 5.10 Variation of system parameter and with ZN and GA controller (Target heating capacity was varied from 5.5 kW to 6.5 kW)

Variation of R410A condensing temperature is shown in Fig. 5.10 (a) and GA control shows the faster behavior compared to ZN control. Small overshoot is observed at R410A condensing temperature around 100 seconds in GA control, but the magnitude is much smaller than that of ZN control. GA control showed the enhanced settling time compared to ZN control. Stability and settling time is improved.

The variation of heating capacity is shown in Fig. 5.10 (b) and the GA control also shows the faster response and reaches the target heating capacity earlier. The settling time decreased about 30% with the use of GA controller. ZN controller takes approximately 835 seconds to reach 97% value of target capacity whereas GA takes quite less time of only 475 seconds.

Fig. 5.11 represents the results of ZN controller and GA controller when the target heating capacity was kept at 6.5 Kw initially and at certain time it was set to 5.5 kW. The variation of R410A condensing temperature (Fig. 5.11 (a)) showed overshoot due to the increase of R134a evaporating temperature and its corresponding results R134a DSH showed undershoot. The variation of heating capacity is shown in Fig. 5.11 (b) and the GA control also shows the enhanced response than ZN tuning and reaches the target heating capacity earlier. The settling time decreased about 30% with the use of GA controller. ZN controller takes approximately 820 seconds to

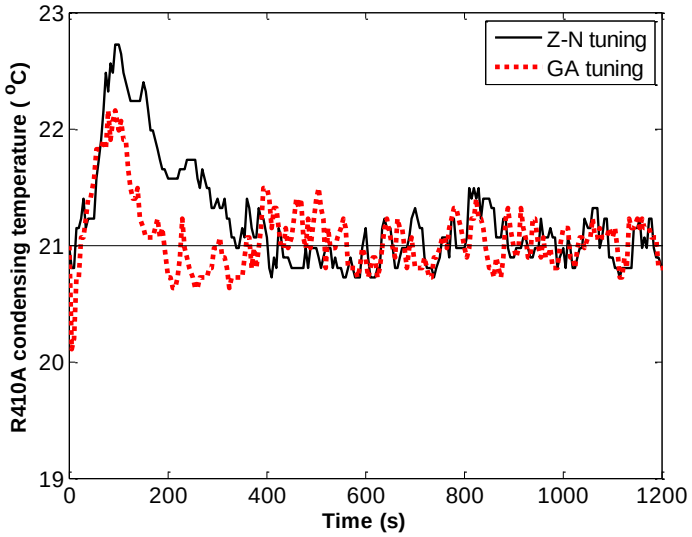

(a) R410A condensing temperature

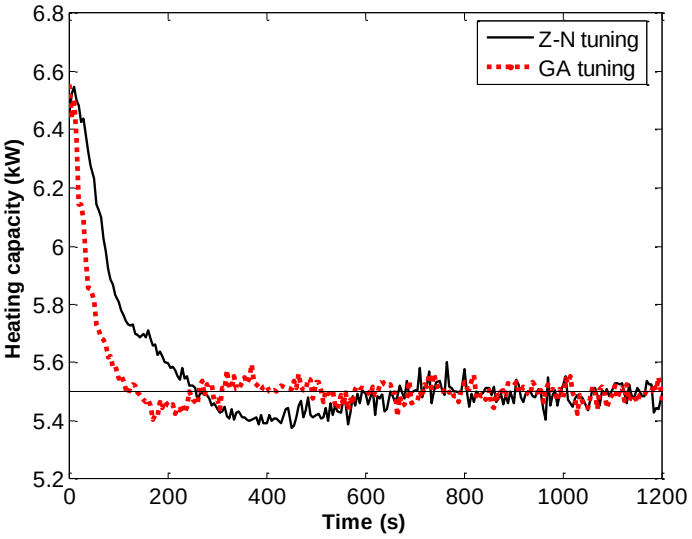

(b) Heating capacity

Fig. 5.11 Variation of system parameter and with ZN and GA controller (Target heating capacity was varied from 6.5 kW to 5.5 kW)

reach 97% value of target capacity whereas GA takes quite less time of only 430 seconds.

5.5 Conclusion

Capacity control for cascade heat pump with PI controller was carried out. R410A condensing temperature, heating capacity and degree of superheat at each cycle were selected as the control variable. For optimal operation, four proportional gains and four integral gains were optimized by genetic algorithm. The general processes to develop controller used in this study is

- Determine the number of state variables and inputs
- Create the signals for input such as pseudo-random binary sequences (PRBS)
- Determine the type of system model such as state-space model
- Obtain the system model using system identification
- Select the control logic for the system (PI controller)
- Perform the system simulation with model using Matlab
- Optimize the controller using genetic algorithm
- Verify the optimized controller in the experiment

Genetic algorithm is the search method based on the mechanics of

natural genetics. PI gains of controller were obtained by genetic algorithm and tested. For the comparison, conventional Ziegler-Nichols controller was also constructed. Experiments were carried out in the various conditions. PI genetic algorithm controller shows a shorter settling time in the experiments, and the settling time was reduced about 30%.

Chapter 6. Concluding remarks

Recent energy crisis and climate change requires a performance enhanced heat pump system. Heat pump is suggested as an alternative of gas boiler; however, conventional heat pump has limited performances such as low water discharge temperature at low ambient temperature regions. In order to increase the water discharge temperature, multi-stage heat pumps have been considered. Among the multi-stage heat pump, cascade heat pump which is composed of separated two single cycles showed best performance at high condensing temperature condition. However, cascade heat pump requires system optimization due to its complexity of configuration and operation.

Determination of refrigerant charge amount at each cycle was conducted by numerical simulation and experiment. The cascade system performance with respect to each charge amount was obtained and the guideline of optimal charge amount on cascade heat pump has been suggested. Optimal degree of subcool at each cycle was proposed with respect to ambient temperature. The optimal degree of subcool at high stage cycle was decreased whereas that of low stage was remained quite constant.

The optimization of cascade intermediate temperature was studied. The

intermediate temperature determines the pressure ratio of each cycle and therefore, the intermediate temperature should be optimized. The reversed-Carnot model was used to develop the intermediate temperature equation and the numerical intermediate temperature was verified by experiments.

The performance characteristics with respect to water temperature lift was conducted experimentally. Despite of several advantages of heat pump than conventional boiler, slower thermal response is the weakness of heat pump water heater. In order to increase the water discharge temperature, mass flow rate of water should be reduced. The performance characteristics of cascade heat pump with respect to water temperature lift was obtained. The heating capacity increases due to the increase of high stage evaporating temperature, whereas the coefficient of performance decreases.

The optimal control logic for cascade heat pump was designed and experimentally verified. The optimized PI controller was designed by genetic algorithm and optimized PI controller showed enhanced performance than conventional Ziegler-Nichols tuning method. The genetic algorithm based PI controller showed less settling time about 30% compared to conventional tuning method.

References

[1] Agrawal, N., Bhattacharyya, S., Sarkar, J., 2007. Optimization of two-stage transcritical carbon dioxide heat pump cycles. International Journal of Thermal Sciences 46, 180-187.

[2] Alberto Dopazo, J., Fernández-Seara, J., Sieres, J., Uhía, F.J., 2009. Theoretical analysis of a CO_2-NH_3 cascade refrigeration system for cooling applications at low temperatures. Applied Thermal Engineering 29, 1577-1583.

[3] Bansal, P., Jain, S., 2007. DA-07-027 Cascade Systems: Past, Present, and Future. Transaction ASHARE 113, 245-252.

[4] Bertsch, S.S., Groll, E.A., 2008. Two-stage air-source heat pump for residential heating and cooling applications in northern US climates. International Journal of Refrigeration 31, 1282-1292.

[5] Bhattacharyya, S., Mukhopadhyay, S., Sarkar, J., 2008. CO_2-C_3H_8 cascade refrigeration-heat pump system: Heat exchanger inventory optimization and its numerical verification. International Journal of Refrigeration 31, 1207-1213.

[6] Bingming, W., Huagen, W., Jianfeng, L., Ziwen, X., 2009. Experimental investigation on the performance of NH_3/CO_2 cascade refrigeration

system with twin-screw compressor. International Journal of Refrigeration 32, 1358-1365.

[7] Cecchinato, L., Chiarello, M., Corradi, M., Fornasieri, E., Minetto, S., Stringari, P., Zilio, C., 2009. Thermodynamic analysis of different two-stage transcritical carbon dioxide cycles. International Journal of Refrigeration 32, 1058-1067.

[8] Chi, J., Didion, D., 1982. A simulation model of the transient performance of a heat pump. International Journal of Refrigeration 5, 176-184.

[9] Cho, H., Baek, C., Park, C., Kim, Y., 2009. Performance evaluation of a two-stage CO_2 cycle with gas injection in the cooling mode operation. International Journal of Refrigeration 32, 40-46.

[10] Cho, H., Ryu, C., Kim, Y., Kim, H.Y., 2005. Effects of refrigerant charge amount on the performance of a transcritical CO_2 heat pump. International Journal of Refrigeration 28, 1266-1273.

[11] Chua, K., Chou, S., Yang, W., 2010. Advances in heat pump systems: A review. Applied Energy 87, 3611-3624.

[12] Corberán, J.M., Martínez-Galván, I., Martínez-Ballester, S., Gonzálvez-Maciá, J., Royo-Pastor, R., 2011. Influence of the source and sink

temperatures on the optimal refrigerant charge of a water-to-water heat pump. International Journal of Refrigeration 34, 881-892.

[13] Corberán, J.M., Martínez, I.O., Gonzálvez, J., 2008. Charge optimisation study of a reversible water-to-water propane heat pump. International Journal of Refrigeration 31, 716-726.

[14] Dopazo, J.A., Fernández-Seara, J., 2011. Experimental evaluation of a cascade refrigeration system prototype with CO_2 and NH_3 for freezing process applications. International Journal of Refrigeration 34, 257-267.

[15] Fernandez, N., Hwang, Y., Radermacher, R., 2010. Comparison of CO_2 heat pump water heater performance with baseline cycle and two high COP cycles. International Journal of Refrigeration 33, 635-644.

[16] Gupta, V., 1986. Optimum design of multi-stage cascaded refrigeration-heat pump system. Journal of heat recovery systems 6, 235-244.

[17] Hamamoto, Y., Amanul Alam, K., Akisawa, A., Kashiwagi, T., 2005. Performance evaluation of a two-stage adsorption refrigeration cycle with different mass ratio. International Journal of Refrigeration 28, 344-352.

[18] Hepbasli, A., Kalinci, Y., 2009. A review of heat pump water heating systems. Renewable and Sustainable Energy Reviews 13, 1211-1229.

[19] Huang, B., Wang, J., Wu, J., Yang, P., 2009. A fast response heat pump water heater using thermostat made from shape memory alloy. Applied Thermal Engineering 29, 56-63.

[20] Jeong, S., Smith, J., 1994. Optimum temperature staging of cryogenic refrigeration system. Cryogenics 34, 929-933.

[21] Ji, J., Chow, T.-t., Pei, G., Dong, J., He, W., 2003. Domestic air-conditioner and integrated water heater for subtropical climate. Applied Thermal Engineering 23, 581-592.

[22] Kilicarslan, A., 2004. An experimental investigation of a different type vapor compression cascade refrigeration system. Applied thermal engineering 24, 2611-2626.

[23] Kim, J.H., Cho, J.M., Lee, I.H., Lee, J.S., Kim, M.S., 2007. Circulation concentration of CO_2/propane mixtures and the effect of their charge on the cooling performance in an air-conditioning system. International Journal of Refrigeration 30, 43-49.

[24] Kim, M., Yoon, S.H., Domanski, P.A., Vance Payne, W., 2008. Design of a steady-state detector for fault detection and diagnosis of a residential air conditioner. International Journal of Refrigeration 31, 790-799.

[25] Kim, S., Kim, M., 2002. Experiment and simulation on the performance of an autocascade refrigeration system using carbon dioxide as a refrigerant. International Journal of Refrigeration 25, 1093-1101.

[26] Kim, W., Braun, J.E., 2012. Evaluation of the impacts of refrigerant charge on air conditioner and heat pump performance. International Journal of Refrigeration.

[27] Lee, T.S., Liu, C.H., Chen, T.W., 2006. Thermodynamic analysis of optimal condensing temperature of cascade-condenser in CO_2/NH_3 cascade refrigeration systems. International Journal of Refrigeration 29, 1100-1108.

[28] Longo, G., Gasparella, A., 2007. Heat transfer and pressure drop during HFC refrigerant vaporisation inside a brazed plate heat exchanger. International journal of heat and mass transfer 50, 5194-5203.

[29] Longo, G.A., 2009. R410A condensation inside a commercial brazed plate heat exchanger. Experimental Thermal and Fluid Science 33, 284-291.

[30] Messineo, A., Panno, D., 2012. Performance evaluation of cascade refrigeration systems using different refrigerants. Int. J. Air-Conditioning Refrigeration. 20, 1250010.

[31] Minetto, S., 2011. Theoretical and experimental analysis of a CO_2 heat pump for domestic hot water. International Journal of Refrigeration 34, 742-751.

[32] Moffat, R.J., 1988. Describing the uncertainties in experimental results. Experimental Thermal and Fluid Science 1, 3-17.

[33] Nekså, P., Rekstad, H., Zakeri, G.R., Schiefloe, P.A., 1998. CO_2 heat pump water heater: characteristics, system design and experimental results. International Journal of Refrigeration 21, 172-179.

[34] Park, N., Woo, H. S., Ha, J. C., Lee, D. H., Chin, S., 2010. On the Optimal Water Discharge Temperature of Air-to-Water Heat Pump for Space Heating and Domestic Hot Water. International Refrigeration and Air Conditioning Conference, 1147

[35] Pettersen, J., Hafner, A., Skaugen, G., Rekstad, H., 1998. Development of compact heat exchangers for CO_2 air-conditioning systems. International Journal of Refrigeration 21, 180-193.

[36] Poggi, F., Macchi-Tejeda, H., Leducq, D., Bontemps, A., 2008. Refrigerant charge in refrigerating systems and strategies of charge reduction. International Journal of Refrigeration 31, 353-370.

[37] Pottker, G., Hrnjak, P., 2012. Effect of Condenser Subcooling of the Performance of Vapor Compression Systems: Experimental and Numerical Investigation.

[38] Stene, J., 2005. Residential CO_2 heat pump system for combined space heating and hot water heating. International Journal of Refrigeration 28, 1259-1265.

[39] Vjacheslav, N., Rozhentsev, A., Wang, C.C., 2001. Rationally based model for evaluating the optimal refrigerant mass charge in refrigerating machines. Energy Conversion and Management 42, 2083-2095.

[40] Wang, C.C., Chi, K.Y., 2000. Heat transfer and friction characteristics of plain fin-and-tube heat exchangers, part I: new experimental data. International journal of heat and mass transfer 43, 2681-2691.

[41] Wang, C.C., Chi, K.Y., Chang, C.J., 2000. Heat transfer and friction characteristics of plain fin-and-tube heat exchangers, part II: Correlation. International journal of heat and mass transfer 43, 2693-2700.

[42] Wang, S., Tuo, H., Cao, F., Xing, Z., 2013. Experimental investigation on air-source transcritical CO_2 heat pump water heater system at a fixed water inlet temperature. International Journal of Refrigeration 36, 701-716.

[43] Wang, W., Ma, Z., Jiang, Y., Yang, Y., Xu, S., Yang, Z., 2005. Field test investigation of a double-stage coupled heat pumps heating system for cold regions. International Journal of Refrigeration 28, 672-679.

[44] Yan, Y.Y., Lin, T.F., 1999. Evaporation heat transfer and pressure drop of refrigerant R-134a in a plate heat exchanger. Journal of heat transfer 121, 118.

[45] Yan, Y.Y., Lio, H.C., Lin, T.F., 1999. Condensation heat transfer and pressure drop of refrigerant R-134a in a plate heat exchanger. International journal of heat and mass transfer 42, 993-1006.

[46] Yokoyama, R., Shimizu, T., Ito, K., Takemura, K., 2007. Influence of ambient temperatures on performance of a CO_2 heat pump water heating system. Energy 32, 388-398.

[47] Zhang, J., Wang, R., Wu, J., 2007. System optimization and experimental research on air source heat pump water heater. Applied Thermal Engineering 27, 1029-1035.

국 문 초 록

본 연구에서는 극 저온 지역에서 난방 및 급탕을 위한 고온수를 생산하는 캐스케이드 히트펌프 시스템의 성능을 향상 시키기 위해서 캐스케이드 시스템 특성 및 최적화에 관한 연구를 수행하였다. 일반적으로 기존의 일단 히트펌프 시스템은 외기 온도가 낮은 지역에서 필요로 하는 난방 부하를 히트펌프가 담당하지 못하는 문제가 발생한다. 극 저온 지역에서 고온수를 생산하기 위해서는 기존의 일단 히트펌프 시스템을 대체하는 캐스케이드 시스템에 대한 연구가 필요하다. 하지만, 캐스케이드 시스템은 기존의 일단 사이클 보다 시스템을 구성하는 요소들이 많아지기 때문에, 성능계수는 일반적으로 낮게 된다. 이를 극복하기 위해서는 캐스케이드 사이클의 최적화가 수행 되어야 한다. 따라서, 본 연구에서는 사이클의 성능 향상을 위해서 냉매 충전량에 관한 연구, 중간 온도에 관한 연구, 고온 수 토출 시 성능에 관한 연구, 제어에 관한 연구를 수행 하였다. 첫째, 캐스케이드 시스템에서 상단 및 하단 사이클의 냉매 충전량에 따른 시스템의 특성을 해석 및 실험적으로 파악하여, 최적의 성능계수를 얻을 수 있는 상단 및 하단 사이클의 과냉도를 제시하였다. 해석적으로 얻은 최적의 과냉도는 실험값과 큰 차이 없이 예측 하였다. 둘째, 열역학적 모델을 통하여 최적 중간 온도의 존재 및 그 값을 제시하였으며, 이를 뒷받침 하기 위해 실험적인 결과를 통하여 검증 하였다. 최적의 중간온도는 상단 및 하단의 열원온도, 상단 및 하단의 카르노 효율, 열교환기 온도차에 관한 식으로 제시가 되었으며, 실험 결과는 이론적인 최적 중간 온도를 잘 예측 하였다. 셋째, 보일러 대비 느린 응답 특성을 일부 해결하기 위한 방안으로 이차 유체 유량을 감소 시키는 방법이 있는데, 이 경우 온수 토출 온도는 증가 하지만 성능이 약화되게 된다. 이때 캐스케이드 히트펌프 시스템의 성능 특성이 어떻게

변화하는지 실험적으로 보여주었다. 마지막으로, 캐스케이드 히트펌프의 제어를 상단 및 하단의 압축기 속도 및 팽창밸브 개도를 제어 입력으로 설정 하였으며, 각각의 입력에 해당하는 중간온도, 난방용량, 각 단의 과열도를 제어변수로 설정하였다. 최적의 운전 및 안정성 확보를 위해 각 단의 과열도를 5 도로 설정 하였으며, 필요한 난방용량을 가장 효율적으로 운전 하기 위하여 중간온도를 제어하였다. 캐스케이드 히트펌프 시스템의 특성을 상태 방정식으로 선형화 시켰으며, 이를 기반으로 최적의 비례 적분 제어기를 개발 하였다. 유전자 알고리즘을 이용하여 비례 적분 제어기의 게인값들을 찾았으며, 최적의 제어기를 실험적으로 증명 하였다. 본 연구를 통하여 극 저온 지역에서의 고온 수를 생산하는 캐스케이드 히트펌프 시스템의 성능을 최적화 하였다.

주요어: 캐스케이드, 히트 펌프, 중간온도, 냉매 충전량, 비례 적분 제어

학 번: 2010-31311

감사의 글

짧지 않은 관악에서의 10 여 년의 시간을 거쳐 이제 박사학위 논문을 완성하고 박사졸업을 앞두고 있습니다. 작은 결실을 얻었지만, 후련함보다는 아쉬움이 남습니다. 하지만, 이 졸업이 학업의 끝이 아닌 공학 연구자로서 첫발을 내딛는 것이라 여기겠습니다. 박사학위가 주는 책임감의 무게를 느끼며, 고마운 분들께 감사의 인사를 드리며 논문을 마무리하고자 합니다.

먼저, 학문적인 내용뿐만 아니라 제자의 생활까지도 걱정해주시고 배려해주신 존경하는 김민수 교수님께 감사 말씀을 전하고 싶습니다. 교수님의 가르침을 평생 가슴에 새기고 바른 인격을 가진 공학자의 삶을 살아가겠습니다.

또한, 부족한 논문을 심사해 주신 송성진 교수님, 송한호 교수님, 고승환 교수님, 그리고 고려대학교의 김용찬 교수님께 깊은 감사를 드립니다.

6년간의 대학원 생활 동안 함께한 실험실의 모든 선배님과 후배님들께 감사를 드립니다. 대학원 생활을 함께 했던 소중한 형님들, 조진민, 최종원, 이재승, 김범준, 한융희, 노철우, 백경돈, 서정훈, 김모세, 김기영, 김성일 형님들에게 감사합니다. 또한, 지금 같이 생활하고 있는 공임모, 김학수, 황성훈, 김영상, 박한샘, 최영욱, 김동규, 정애리, 신창수, 류진우, 신동규, 차상렬, 고재선, 이지성, 강대훈, 김선진, 최은정, 정융, 홍성빈을 포함하여 장지용, 하정훈, 한경호, 조민기에게도 감사를 표하며 회사와 학교를 오가시며 연구

하시는 전상희, 강대경, 권춘규, 이남우 형님들에게 좋은 졸업 논문 쓰시길 기원합니다.

어릴 때부터 우정 잊지 않고 지내는 대포회 친구들, 이강모, 이명국, 이상운, 성우석, 손재명 친구들을 포함하여 대학 동기 40회에도 무한한 감사 드립니다.

지금까지 인내와 사랑으로 저를 키워주시고 이끌어 주신 든든한 지원군 아버지와 어머님께 머리 숙여 감사 드립니다. 두 분께 아들의 학위취득이 작은 기쁨이라도 되었으면 하며, 항상 손자 걱정 해주시는 할머니께도 감사 드립니다. 언제나 가족이라는 울타리 안에서 든든한 힘이 되어준 동생 동훈 에게도 감사 드립니다. 대학원 과정 동안 저의 고충을 이해해주며 항상 곁에서 응원해준 사랑하는 지혜에게 매우 감사 드리며, 이 기쁨을 함께 하고 싶습니다.

2014년 1월 관악에서